EDİTÖRDEN / EDITORIAL

Değerli Meslektaşlar ve Okurlar,

Önümüzdeki Nisan ayında 62. Yaşına giren dergimizin 206. sayısı ile birlikte içeriği bilimsel makalelerden oluşan dergimizin bu sayısında; GMO'nun Aralık 2016'da Gemi Mühendisliği Haftası kutlama etkinlikleri kapsamında düzenlemiş olduğu Yeşil Teknolojiler ana konulu 1. Uluslararası Gemi İnşaatı ve Deniz Teknolojisi Kongresi'nde (GMO SHIPMAR 2016) sunulan pek çok değerli bildiriler arasından, dergimiz Editörler Kurulu tarafından seçilmiş makaleler yayınlanmıştır. Seçilmiş makaleler Gemi İnşaatı, Gemi Hidromekaniği, Gemi Makineleri ve Termodinamik alanlarındadır.

Dergimize uluslararası güçlü katkılar sağlayabilmek adına dergi Editörler Kurulu genişletilmiştir. Bu fırsat ile dergimize yapacakları katkılar için şimdiden tüm kurul üyelerimize teşekkürlerimizi sunarız.

Saygılarımızla.

Prof. Dr. Ahmet Dursun ALKAN
Baş Editör

Distinguished Colleagues and Readers,

With the current issue of our journal entering its 62nd year in April 2017, attained a fully scientific journal status with Issue 206, we present some selected papers scored by the members of the Editorial Board from those presented at the 1st International Congress on Ship and Marine Technology (08-09.12.2016, PRU, Tuzla, Istanbul) organized by Turkish Chamber of Naval Architects and Marine Engineers with special focus on "Green Technologies". The selected papers among a number of invaluable ones cover fields of shipbuilding, marine hydrodynamics, marine engines and thermodynamics.

The Editorial Board of the journal has been expanded to provide strong international contributions. This is the nice opportunity to present our thanks to all our board members in advance for their contributions to our journal.

Best regards,

Prof. Ahmet Dursun Alkan PhD
Editor-in-Chief

Sahibi / Publisher:
TMMOB GEMİ MÜHENDİSLERİ ODASI
UCTEA, The Turkish Chamber of Naval Architects & Marine Engineers

İmtiyaz Sahibi / Owner
İlker CIVELEK

Baş Editör / Editor-in-Chief
Prof. Dr. Ahmet Dursun ALKAN

Yardımcı Editör / Associate Editor
Doç. Dr. Ömer Kemal KINACI

Yayın Komisyonu / Editing Committee
Salih BOSTANCI
Pelin YILMAZCOŞAR
Boran MERT
Çağrı Burak YILDIRIM
Ömer GÜL

Yönetim / Management

TMMOB GMO
Postane Mahallesi, Nil Sokak No: 39
34940 Tuzla, İstanbul, Turkiye
T : +90 216 447 40 30 - 31 -32
F : +90 216 447 40 33
E-Mail: gmo@gmo.org.tr,
GMOShipMar@gmo.org.tr
www.gmo.org.tr

Yayın Türü / Publication Type / Sayı / Number
Süreli Yayın (3 Aylık) / Periodical, 3 months
Sayı / Number : 207

Basıldığı Yer ve Tarih / Printed in / Date
Cenkler Matbaacılık Amb. San. Tic. Ltd. Şti.
İ. Karaoğlanoğlu Cad. Civan Sok. No: 7
Seyrantepe, 4 Levent, Istanbul, Turkiye
T: +90 212 283 02 77 – 264 18 21
F: +90 212 264 05 31
www.cenkler.com

ISSN 1300-1973
Baskı Tarihi / Date of print : Mart 2017
Baskı Sayısı / Number of prints : 500

Editörler Kurulu / Editorial Board

Prof. Dr. Teoman ÖZALP

(14.4.1925 - 19.01.2017)

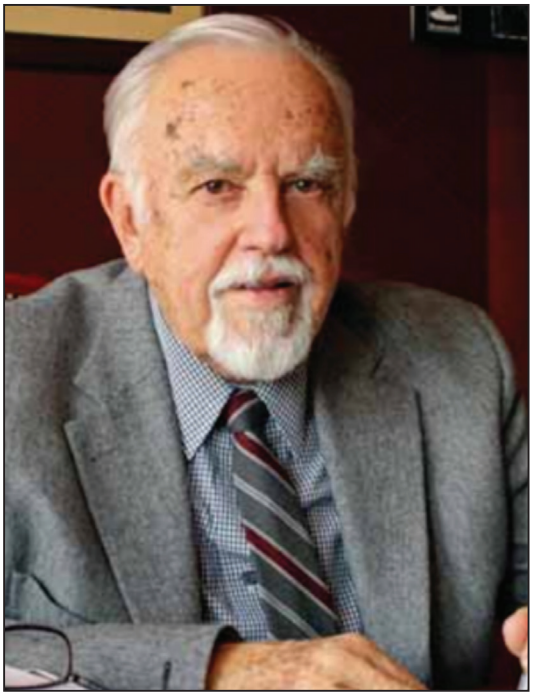

Prof. Dr. Teoman Özalp 14 Nisan 1925 yılında Ankara'da doğdu. Kurtuluş Savaşı'nın önde gelen isimlerinden, Atatürk'ün silah arkadaşı, eski TBMM Başkanı Kazım Özalp'ın oğludur. İlk ve orta öğrenimini Ankara'da tamamlayan Prof. Özalp 1948 yılında İTÜ Makine Fakültesi'nden mezun oldu. Aynı Üniversitede asistan olarak başladığı akademik hayatında 1954 yılında doçent, 1962 yılında profesör oldu. Almanya'da gemi model deneyleri konusunda araştırmalar ve bazı önemli tersanelerde mühendis olarak görevler yaptı. 1962 yılında kurulan Türk Loydu Vakfı'na kurucu Daimi Komite Üyeliğine Teknik Komite Başkanı olarak seçilmiş ve 1962-1964 döneminde İTÜ Makine Fakültesi'nde Dekanlık yaptı. Denizcilik Bankası'nda hükümeti temsilen 6 yıl yönetim kurulu üyeliği yaptı. 1971'de kurucusu olduğu İTÜ Gemi İnşaatı ve Deniz Bilimleri Fakültesi'nde 10 yıl kadar Dekanlık görevinde bulunmuş ve Fakülteyi kapsamlı bir Model Deney Laboratuvarına kavuşturmuştur. Gemi Mühendisleri Odası'nın 25 sicil numaralı üyesi idi. 1966-1973 yılları arası GMO Başkanlığı görevini ifa etti. GMO Gemi Mecmuası dergisinin 1. sayısından 71. sayısına kadar yayın kurulu ve dergi sahibi olarak görevler yaptı. 1962 yılında kurucu heyetinde olduğu Türk Loydu'nun 1978 yılından itibaren 17 yıl yönetim kurulu başkanlığını yaptı. 12 Eylül 1980'den sonra kurulan Danışma Meclisi'nde 2 yıl üyelik yaptı. Sonradan IMAM'a dönüştürülen IMAEM'in (International Maritime Association of East Mediterranean) kuruculuğunu yaptı ve bu akademik teşkilatın 1987 yılına kadar 2. Başkanlığını yaptı. Üniversiteye ve ülkeye yapmış olduğu seçkin katkıları ve hizmetleri onurlandırmak için kendisine 2000 yılında İTÜ Senatosu'nca Fahri Doktor ünvanı ve 2003 yılında TÜBİTAK hizmet ödülü tevdi edilmiş bulunmaktadır. Prof. Dr. Teoman Özalp'ın çok sayıda yayınlanmış makale, kitap, tez çalışmaları, raporları ve dizaynları bulunmaktadır.

Hizmet ve katkıları hiçbir zaman unutulmayacak Prof. Teoman Özalp, 19 Ocak 2017 Perşembe günü aramızdan ayrılmıştır. Denizcilik ve akademik camianın başı sağolsun.

Prof. Dr. Teoman Özalp was born on April 14, 1925 in Ankara. He was the son of Kazım Özalp, who was one of the leading names of the War of Independence, Atatürk's closer friend, and a former Head of Turkish Parliament. Prof. Özalp graduated from Istanbul Technical University, Faculty of Mechanical Engineering in 1948 after completing his primary and secondary education in Ankara. He started his career as an assistant at the same university and became associate professor in 1954 and professor in 1962. He has done research on ship model experiments in Germany and worked as an engineer in some well-known shipyards. He was elected as the Technical Committee Chairman of the Founding Standing Committee of the Turkish Lloyd (Türk Loydu), which was established in 1962, and was the Dean of ITU Mechanical Engineering Faculty between 1962 and 1964. He served as a member of executive board for 6 years on behalf of the government in Denizcilik Bank. He was the founder of the İTÜ Naval Architecture and Ocean Engineering Faculty in 1971, worked as a Dean for about 10 years, and established a comprehensive Model Test Laboratory in the Faculty. He was a member of the Chamber of Turkish Naval Architects and Marine Engineers (GMO) with registration number of 25. Between 1966 and 1973 he served as the GMO President. He worked as a publishing board member and editor of GMO's Journal of Naval Architecture from its first issue, to issue 71. He served as the chairman of the board of Türk Loydu for 17 years starting from 1978. He was a member of the Founding Council established after 12.09.1980 for 2 years. He later became the founder of IMAEM (International Maritime Association of East Mediterranean), which was then transformed into IMAM, and was the co-president of this academic organization until 1987. To honour outstanding contributions and services he has made to university and country, he has been awarded the honorary doctorate of ITU Senate in 2000 and TUBITAK service award in 2003. Prof. Dr. Teoman Özalp has numerous published articles, books, thesis studies, reports and designs.

His service and contributions will never be forgotten. Prof. Teoman Özalp left us on Thursday, January 19, 2017. Our condolences to the maritime and academic community.

İÇİNDEKİLER / CONTENTS

GEMİ ve DENİZ TEKNOLOJİSİ
GMO Journal of Ship and Marine Technology

TMMOB GEMİ MÜHENDİSLERİ ODASI
The Turkish Chamber of Naval Architects and Marine Engineers

BİR AJANDA BİR FİDAN

AN AGENDA A SEEDLING

Aidat borcunu ödeyerek hem çevreye hem odaya katkıda bulunan siz değerli üyelerimize teşekkür ederiz !

Bir ajanda bir fidan kampanyasıyla başlatmış olduğumuz etkinlik sonucu aidatını ödeyen tüm üyelerimiz adına temaya fidan bağışında bulunulmuştur.

We would like to thank our esteemed members who contribute to both the environment and the chamber by paying the dues!

We have donated seedlings to Tema for our members who have paid dues as result of an agenda a seedling campaign.

Effect of Notch Position on Impact Toughness of Friction Stir Processed Low Carbon Steel

Dursun Murat Sekban[1], Semih Mahmut Aktarer[2], Zongyi Ma[3] and Gençağa Pürçek[4]*

purcek@ktu.edu.tr

[1]Department of Naval Architecture and Marine Engineering, Surmene Faculty of Marine Sciences, Karadeniz Technical University, Trabzon, Turkey

[2]Department of Automotive Technology, Recep Tayyip Erdogan University, Rize, Turkey

[3]Shenyang National Laboratory for Materials Science, Institute of Metal Research, Chinese Academy of Sciences, Shenyang, China

[4]Department of Mechanical Engineering, Faculty of Engineering, Karadeniz Technical University, Trabzon, Turkey

Abstract

The effect of single-pass friction stir processing (FSP) on the room temperature impact toughness of a low carbon steel was investigated via Charpy impact test. A fine-grained (FG) microstructure was achieved into the processed zone by large deformation and simultaneous dynamic recrystallization during FSP. The average grain size decreased from 25 µm down to 3.0 µm after FSP. Grain refinement by FSP increased the impact energies as a result of refined grains separated mostly by high-angle of misorientation. Toughness of steel before FSP was about 8.7 J, and it increased up to 11.2 J after processing depending on the notch positions of the samples. The peak impact toughness value of 11.2 J was achieved with the notch position located at top of the surface of processed steel plate.

Keywords*:* Impact toughness, low carbon steel, friction stir processing.

1. Introduction

Low carbon steels are well-known ones among the traditionally employed construction materials. General requirements imposed on such steels are high strength, good corrosion resistance, satisfactory weldability and low susceptibility to cold embrittlement. Grain refinement is known to suppress material susceptibility to cold embrittlement. Grain refinement by severe plastic deformation (SPD) techniques are the promising ones considering their applications and refinement capacity. Among them, friction stir processing (FSP) is one of the best severe plastic deformation (SPD) techniques as considering the processing of large scale plate or sheet type materials (Aktarer et al., 2015). This is a

novel microstructural modification method based on the basic principles of friction stir welding (FSW) (Mishra and Ma, 2005) & (Ma, 2008). In many cases, FSP leads to the transformation of the coarse-grained (CG) initial microstructure into equiaxed fine grained (FG) or even ultrafine-grained (UFG) structures consisting mostly of high angle grain boundaries (HAGBs) (Mishra and Ma, 2005) & (Su et al., 2005) & (Ma et al., 2008).

It is, on the other hand, well known that the mechanical properties are more-or-less depending on the orientation or position of the sample inside the FSPed zone. This effect would be more pronounced considering the notched impact behavior of steels (Ray et al., 1995) & (Joo et al., 2013). Till now, no considerable study has been performed on the impact toughness of FSPed low carbon steels. Also no investigation has been undertaken on the effect of notch position on the impact toughness of FSPed steels. Thus, the main purpose of this study is to investigate the effect of FSP on the room temperature impact toughness of a low carbon steel. Also, the effect of the notch position through the processed zone on the impact toughness of the processed sample was studied.

2. Experimental procedure

A well-known carbon steel sheets initially hot-rolled (0.16 wt % C, 0.18 wt % Si, 0.7 wt % Mn, 0.11 wt % S, 0.18 wt % P, 0.09 wt % Cr , 0.14 wt % Mo, 0.04 wt % Cu, 0.04 wt % V and balance Fe) was used in this study. Samples with the dimensions of 200 mm x 40 mm x 6 mm were cut from the steel plates for performing FSP. FSP was performed with a processing tool having a convex shoulder with the diameter of 18 mm and a cylindrical pin with the diameter and length of 8 mm and 3 mm, respectively. FSP was conducted with a tool rotation of 635 rpm and a traverse speed of 45 mm/min. The shoulder tilt angle was set at 3^0, and the tool plunger downforce was kept constant at 11 kN during process.

Optical microscope (OM) and transmission electron microscope (TEM) were used to observe the microstructure of the samples before and after FSP. The specimens for OM were cross-sectioned on the processed sample perpendicular to the processing direction, polished with standard techniques and then etched with a %3 Nital (3ml. HNO3 + 97 ml. C_2H_6O) for 15 s. The TEM was performed using an FEI Tecnai F20 microscope, operated at a nominal voltage of 200 kV.

The impact toughness of the specimen was evaluated at room temperature by measuring the total absorbed energy using Charpy impact test before and after FSP. The samples with the dimensions of 3 mm x 4 mm x 27 mm with a V-notch depth of 1 mm and a radius of 0.1 mm were cut from the FSPed plate with different notch position (NP) according to DIN50115 (Fig. 1). The fracture surfaces of the fractured specimens were observed using a JEOL 6400 scanning electron microscope (SEM) operated at 15 keV in the secondary electron image mode.

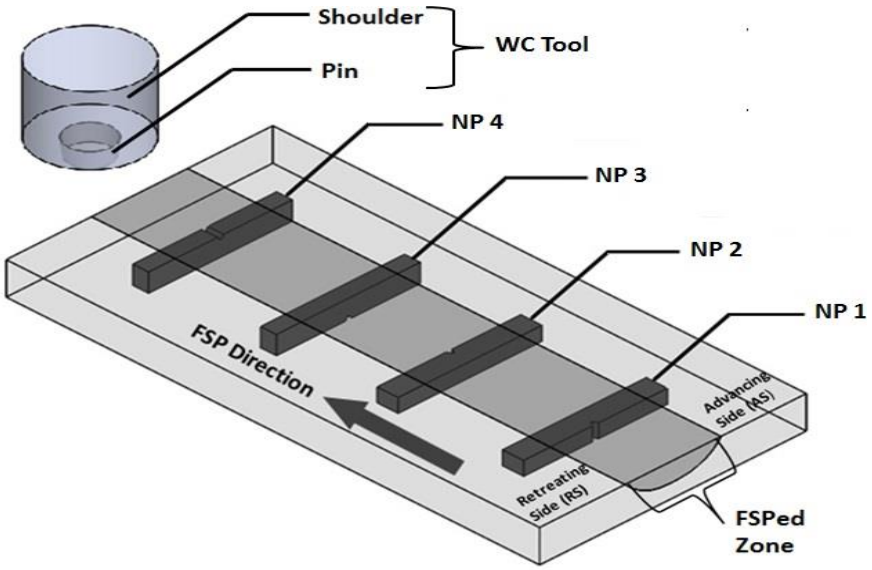

Figure 1. Schematic illustrations showing the FSPed samples and the geometry and position of the impact test specimens inside the processed sample.

3. Results and discussion

3.1. Microstructure

The initial microstructure of base steel plate before FSP is well-known and consists mainly of coarse-grained (CG) ferrite with an average grain size of 25 µm and smaller grains of fine pearlite (Fig. 2(b)). FSP resulted in a considerable refinement in the microstructure of steel inside the processed zone (NZ) (Fig. 2(c)-(f)). A fine-grained (FG) microstructure formed after FSP with decreasing the grain size from 25 µm down to about 3.0 µm in that zone. The coarse ferrite and perlite grains in CG sample were fragmented and refined by the effect of both severe plastic deformation and dynamic recrystallization during FSP (Xue et al., 2013). The microstructure of the stir zone was characterized by the presence of ferrite with aligned and nonaligned second phase of perlite, grain boundary ferrite, and a ferrite/carbide aggregate that appears to be fine pearlite (Lienert et al., 2003). As shown in Fig. 2(e), the top most surface layer just beneath the shoulder has relatively coarser grain size. This may be due to the early recrystallization and grain coarsening effect due to the high pressing effect of shoulder (Prangnell and Heason, 2005). Finer microstructure formed around the pin due to pin's behaves like a forging affect as well as rotation (Fig. 2(f)). From the TEM micrograph (Fig. 2(c)), refined grains are separated mostly by high-angle grain boundaries. TEM micrographs also show that the FG microstructure includes dislocations. However, the dislocations in the microstructures are unevenly distributed in such a way that some grains in their central parts are rather free of dislocations, and most of the dislocations are accumulated and tangled with others around grain boundaries (Fig. 2(e)).

Such distribution of the dislocations is normal, because dynamic recovery and partly recrystallization occurs during deformation, which spreads the trapped lattice dislocations into grain boundaries.

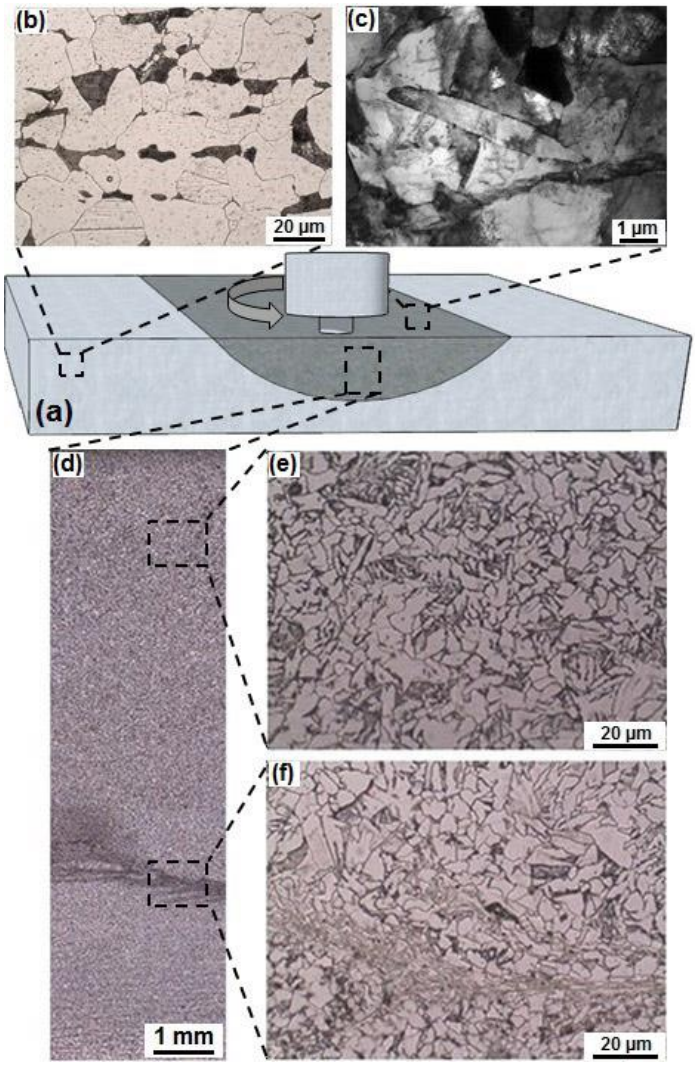

Figure 2. (a) Schematic illustrations of the FSPed plate. (b) Optical micrographs showing the microstructures of un-processed coarse grained steel plate. (c) TEM micrographs showing the microstructures of FG FSPed low carbon steel. (d)-(f) Optical micrographs showing the microstructures of FG FSPed low carbon steel in detail.

3.2. Impact toughness

Room temperature impact toughness values of all specimens before and after FSP are given in Fig. 3. Toughness of the CG steel before FSP is about 8.7 J, and it increased up to 11.2 J after grain refinement by FSP depending on the notch position inside the FSPed sample. The increase in toughness at low temperatures was attributed mainly to the substantial microstructural refinement with grains separated mostly by high angle of misorientation (Saray et al., 2012). The grain refinement from 25 µm down to 3 µm by FSP significantly increased the amount of grain boundaries and brought about an improvement in impact toughness. More grain boundaries mean more barriers in front of the crack propagation. As the cleavage crack propagates along several grains, both the crack tip dislocations and the formation of cleavage facets are interrupted by these boundaries (Song et al., 2005). The peak

impact toughness value of 11.2 J was achieved with the notch position located at top of the surface of processed steel plate (Fig. 3). The other notch positions of NP1 and NP2 (the notch located along the processed directions) gave more or less the same toughness values (10.4 J), while the NP3 (the notch located backside of the processed plate) resulted in a slightly higher value (10.8 J) compared to NP1 and NP2 (Fig. 3). In literature, three basic factors were underlined for clarifying the reasons of toughness anisotropy: non–uniform distribution in the size and shape of inclusions, microstructural anisotropy due to chemical segregation with banding or elongated grain structure and crystallographic texture (Ray et al., 1995) & (Joo et al., 2013). Top-most surface and around of the pin have finer grains compared to other processed regions. This is coming from the effectiveness of the pin and shoulder in that region where both rotation and forging effects are working together leading to more refined microstructure in that zone compared to others. Thus, the specimen with the notch position in NP4 showed the highest toughness among the others. The other specimens followed the same behavior with the change in grain size.

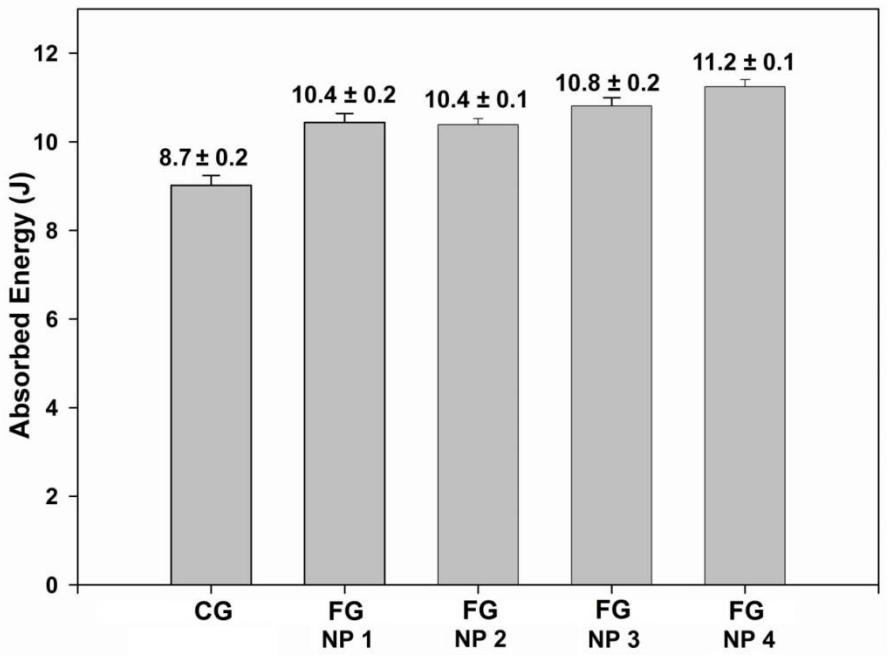

Figure 3. (a) The impact toughness values of both CG and FG specimens. The impact toughness of FG specimens were given depending on notch position inside the friction stir zone.

Morphological features of the fractured surface were also investigated, and representative ones for the specimens before and after FSP were shown in Fig. 4((a)-(b)). In general, a shear-type future morphology without fine dimples is more pronounced in the CG specimens before FSP (Fig. 4(a)). Also, large size voids or fractured valleys is coming from the coarse grained microstructure of initial steel.

FSP changed considerably the fracture surface morphology of the specimen (Fig. 4(b)). As clearly seen, mostly fine dimple-like fracture surface becomes effective due to the more refined microstructure, which also validates relatively high toughness value after FSP.

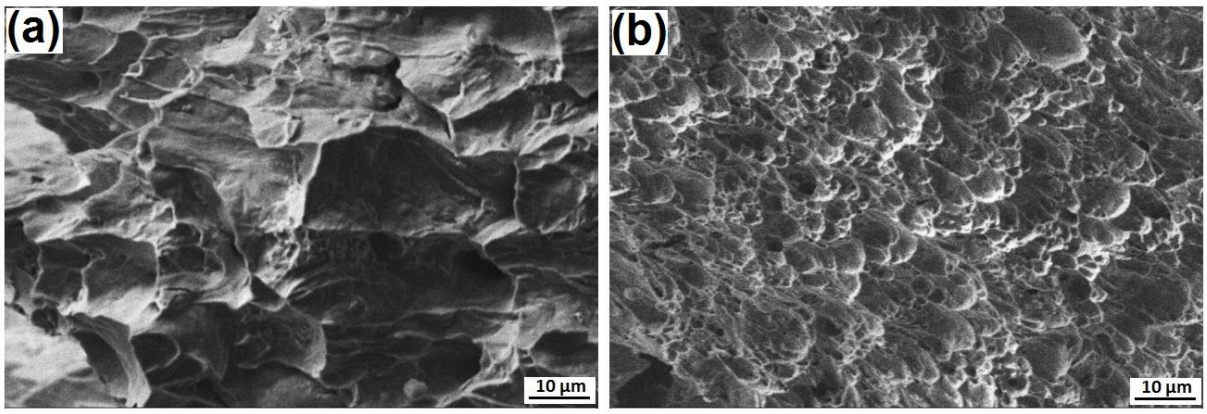

Figure 4. SEM micrographs showing the impacted fracture surfaces of: (a) CG base and (b) FG FSPed steel plates.

4. Conclusions

Room temperature impact toughness of a low carbon steel processed by single-pass FSP was investigated considering the effect of notch position of the samples inside the processed zone. The main results and conclusions of this study can be summarized as follows:

1. A fine-grained (FG) microstructure with an average grain size of about 3 µm was obtained from a coarse grained (25 µm) microstructure of low carbon steel by a single-pass FSP.
2. The microstructural modification by FSP increased room temperature impact toughness of the steel plate at all notch positions. Toughness of CG steel was about 8.7 J before FSP, and it increased up to 11.2 J depending on the notch position. The peak impact toughness was achieved with the notch position located at top of the surface of processed steel plate because of the finest grain size compared to other positions.
3. Ductile fracture mode becomes more effective under impact loading after grain refinement by FSP with decreasing dimple size and increasing amount of the dimples on the fracture surface.

Acknowledgements

Dr. G. Purcek was supported by “The World Academy of Sciences (TWAS)” under the Visiting Researchers Program of TWAS-UNESCO Associateship Scheme. The authors would like to thank Dr. T. Kucukomeroglu for his help on conducting the FSP tests.

References

Aktarer, S.M., Sekban, D.M., Saray, O., Kucukomeroglu,T., Ma, Z.Y., Purcek, G. (2015) Materials Science and Engineering: A, 636 311-319.

Joo, M.S., Suh, D.W., Bhadeshia, H.K.D.H. (2013) Isij Int, 53 1305-1314.

Lienert, B.T.J., Stellwag, J.W.L., Grimmett, B.B., Warke, R.W. (2003) Welding Journal Research Supplement, 82 1-9.

Ma, Z.Y. (2008) Metall Mater Trans A, 39A 642-658.

Ma, Z.Y., Pilchak, A.L., Juhas, M.C., Williams, J.C. (2008) Scripta Mater, 58 361-366.

Mishra, R.S., Ma, Z.Y. (2005) Materials Science and Engineering: R: Reports, 50 1-78.

Prangnell, P.B., Heason, C.P. (2005) Acta Mater, 53 3179-3192.

Ray, A., Paul, S.K., Jha, S. (1995) J Mater Eng Perform, 4 679-688.

Santella, M.L., Engstrom, T., Storjohann, D., Pan, T.Y. (2005) Scripta Mater, 53 201-206.

Saray, O., Purcek, G., Karaman, I., Maier, H.J. (2012) Metall Mater Trans A, 43A 4320-4330.

Song, R., Ponge, D., Raabe, D. (2005) Acta Mater, 53 4881-4892.

Su, J. Q., Nelson, T.W., Sterling, C.J. (2005) Scripta Mater, 52 135-140.

Xue, P., Xiao, B.L., Wang, W.G., Zhang, Q., Wang, D., Wang, Q.Z., Ma, Z.Y. (2013) Mat Sci Eng a-Struct, 575 30-34.

Thermodynamic diesel engine cycle modeling and prediction of engine performance parameters

Mustafa Tuti[1*], Zehra Şahin[2] and Orhan Durgun[3]

mtuti@ktu.edu.tr

[1] *Faculty of Marine Science, Naval Architecture and Marine Eng. Dep., Karadeniz Technical University*

[2] *Faculty of Engineering, Mechanical Eng. Dep., Karadeniz Technical University*

[3] *Faculty of Engineering and Architecture, Mechanical Engineering Dep., Avrasya University*

Abstract

The aim of the present study is to develop a computer code for determining complete cycle, performance parameters and exhaust emissions of diesel engines. For this purpose, a computer program has been used and improved with new assumptions. To compute diesel engine cycle, zero-dimensional intake and exhaust model given by Durgun, zero-dimensional compression, combustion and expansion model given by Ferguson have been used and improved with new assumptions. Using the developed computer program, complete engine cycle, performance parameters and exhaust emissions can be determined easily. The values of the cylinder pressure and engine performance parameters predicted by the presented model matched closely with the other theoretical models and experimental data. Also, this program can be adapted and used practically for various parametric, alternative fuel and water addition studies in diesel engines.

Keywords: Diesel engine cycle, Engine performance characteristics, Simulation Models, Computer Code

1. Introduction

Modern diesel engine cycles can be predicted by applying a variety of simulation models. These models are used for optimization of engine parameters, investigation of control strategies or evaluation phenomena that are difficult to measure. In practice, using engine cycle simulation methods, the number of expensive experiments studies could be reduced and very useful results could be obtained for prediction of engine design parameters in a short time. Thus, these simulation models reduce the cost and time necessitate for engine development. New simulation models are constantly in development and the capabilities of currently available tools are being extended and continually improved. Also, these models are found to be prominent tools for arriving at the optimum designs (Pasternak and Mauss, 2009) & (Shrivastava et al., 2002) & (Bedford et al., 2000).

In the relevant literature, a number of modeling approaches (Pasternak and Mauss, 2009), (Ferguson, 1986) have been proposed and tested with various degrees of success. These models have been classified as phenomenological models and multi-dimensional models or fluid mechanics models (Sahin and Durgun, 2008).Phenomenological models are based on empirical relations to describe or quantify the individual processes that occur in an engine, such as: intake and exhaust, fuel-air mixing, ignition delay, combustion, heat transfer. Furthermore, phenomenological models can be further classified as; single zone, two zone, three zone, and multizone models (Pasternak and Mauss, 2009) , (Sahin and Durgun, 2008). Multidimensional models are based on numerical solution of the fundamental differential equations which govern the fluid motion and the combustion process (Bedford et al., 2000) & (Sindhu et al., 2014). The governing equations are developed and solved for the combustion chamber which is

divided into a fine geometric mesh. Although these models are capable of providing detailed information about both spatial and temporal resolution of the quantities of interest, they require large amounts of computer time and storage capacity (Bedford et al., 2000) & (Sindhu et al., 2014). Thus, if it is desired to examine the effects of all parameters on combustion and pollutant emissions more practical methods such as phenomenological models must be used (Sahin and Durgun, 2008) , (Kökkülünk et al., 2013). Many phenomenological (Sahin and Durgun, 2008), (Kökkülünk et al., 2013), (Qi et al., 2011) and multidimensional model (Tutak and Jamrozik, 2016), (Savioli, 2015) studies on diesel combustion, engine performance parameters and exhaust emission can be found in the literature. Tutak et al. (2016) developed a computational fluid dynamics (CFD) model of a turbocharged diesel engine (1CT107) powered by diesel fuel. In the simulation tests, they analyzed the effects of the ignition timing on the thermodynamic parameters and emissions of toxic components. They verified the model of the test engine and it was then used to optimize the thermodynamics cycle for the test engine. They found that the engine model was at acceptable accuracy and it was suitable for emissions modeling. Savioli (2015) developed a methodology to perform reliable CFD analysis for a 2-Stroke engine, with the support of a conventional steady flow test bench. This methodology is applied to a 2-Stroke engine prototype, for which a comprehensive set of experimental data is available. The achieved good agreement between simulation and experimental data shows the success of the proposed approach. Sahin and Durgun improved a multi-zone combustion model (phenomenological model) to predict the parameters of diesel engine cycles and performance. The values of the cylinder pressure and engine performance parameters predicted by this model matched closely with the other theoretical models and experimental data. Also, this program was adapted and used practically for various parametric and alternative fuel studies (Sahin and Durgun, 2008), (Sahin and Durgun, 2007a), (Sahin and Durgun, 2007b). Qi et al. (2011) proposed a quasi-dimensional combustion model of diesel engine which is based on a new simplified phase-divided spray mixing model. The comparisons with the other methods show that the relative error of effective power and break specific fuel consumption (BSFC) is less than 2.8 % and the relative error of nitric oxide and soot emissions is less than 9.1 % (Qi et al., 2011). Kökkülünk et al. (2013) investigated a thermodynamic simulation model for a steam injected diesel engine for determining of engine characteristics and NO emissions by using zero-dimensional single-zone combustion approximation. By comparing thermodynamic simulation model with experimental data, it can be seen that engine characteristics and NO emissions are closed to actual values at the levels of 1.5 % maximum error (Kökkülünk et al. 2013). Phenomenological and multidimensional modelings are often used to determine the complete engine cycle, engine performance characteristics and exhaust emissions for various engines as well as diesel engines. By this way, very useful results have been obtained for developing diesel engines. For this reason, these models have constantly been developed.

It can be seen from the above summarized relevant publications that many phenomenological and multidimensional model for diesel engines have been developed in the literature. However, further improvements of the complete cycle models for diesel engines is very important. For this purpose, in the present study, a computer code has been used and developed with new assumptions to assess complete cycle, performance parameters and exhaust emissions of diesel engines.

2. Description of the model

2.1. Thermodynamic simulation correlations

2.1.1. Calculation of compression, combustion and expansion strokes

In the present study, a computer program has been used for the prediction of diesel engine cycle and engine performance parameters. For calculation of DI diesel engine cycles, zero dimensional single-zone thermodynamic combustion model developed by Ferguson (1986) has been used and modified with new

assumptions. Here, a brief information about this model has been presented. In a diesel engine, the masses of burned fuel and air has been determined by using the following relations.

$$\frac{dm_a}{d\theta} = \frac{-m_l/\omega}{1+\phi F_s} \quad (1)$$

$$\frac{dm_f}{d\theta} = \frac{1}{\omega}\left(-\frac{m_l \phi F_s}{1+\phi F_s}\right) \quad (2)$$

$$\frac{dm}{d\theta} = -\frac{\dot{m}_l}{\omega} \quad (3)$$

where ω is the angular speed, ϕ is the equivalence ratio, F_s is the stoichiometric fuel-air ratio. Eq. (1, 2) and the following energy equation (4) have been applied to the cylinder contents.

$$\frac{dU}{d\theta} = -\frac{\dot{Q}_l}{\omega} - P\frac{dV}{d\theta} - \frac{\dot{m}_l h_l}{\omega} + \frac{\dot{m}_f h_f}{\omega} \quad (4)$$

In eq. 4, the left hand side terms show heat transfer, work, blowby energy and energy provided by injected fuel, respectively. Some terms in this equation have been expressed as follows.

$$\dot{Q}_l = h\left(\frac{\pi b^2}{2} + \frac{4V}{b}\right)(T - T_w) \quad (5)$$

$$\frac{\dot{m}_{fi}}{m_{fi}} = \frac{\omega}{\theta_d \Gamma(n)}\left(\frac{\theta-\theta_s}{\theta_d}\right)^{n-1} \exp\left[\frac{-(\theta-\theta_s)}{\theta_d}\right] \quad (6)$$

$$\dot{m}_l = \frac{Cm}{\omega} = \frac{C(m_a + m_f)}{\omega} \quad (7)$$

where b is the cylinder bore, T_w is the cylinder wall temperature, θ, θ_s and θ_d are the crank angle, the start of the injection, the injection duration respectively, m_{fi} is the total mass of fuel to be injected per cycle, $\dot{m}_{fi}$ is the mass of injected fuel, c is the blowby coefficient, h is the heat transfer coefficient, V is the volume of cylinder and Γ is the gamma function and it has been determined approximately from the related asymototic formula.

$$\ln\Gamma(n) = \left(n_1 - \frac{1}{2}\right)\ln(n_1) - n_1 + \frac{1}{2}\ln(2\pi) + \frac{1}{12n_1} - \frac{1}{360n_1^3} + \frac{1}{1260n_1^5} - \frac{1}{1680n_1^7} \quad (8)$$

where n_1 is the injection parametre and it could be selected as $1 \le n_1 \le 2$ for open combustion chamber; $3 \le n_1 \le 5$ divided combustion chamber. This value is highly dependent upon the design parameters and the fuel properties. In the present study, n_1 is selected as 1.3 for common-rail direct injection diesel engine. By solving these ordinary differential equations (1), (2) and (4) simultaneously during compression,

combustion and expansion processes by using Runge-Kutta 5 method, V, m_a m_f and U can be calculated. Thus, by using these obtained U, V values and $U = mu(T,P,\phi)$, $V = mv(T,P,\phi)$, cylinder temperature and pressure have been calculated by using Newton-Raphson iteration. For determination of mean gas temperature and pressure values the following relations have been used.

$$T_{i+1} = T_i + \Delta T \tag{9}$$

$$p_{i+1} = p_i + \Delta p \tag{10}$$

$$\Delta T = \frac{-V\left[\dfrac{10\left(\dfrac{du}{d\theta}\right)}{p\dfrac{\partial \ln \upsilon}{\partial \ln p}} + \left(\dfrac{d\upsilon}{d\theta}\right)\left(\dfrac{\partial \ln \upsilon}{\partial \ln T} + \dfrac{\partial \ln \upsilon}{\partial \ln p}\right)\right]}{\dfrac{V^2}{T}\left[\left(-\dfrac{10c_pT}{pV} + \dfrac{\partial \ln \upsilon}{\partial \ln T}\right)\left(-\dfrac{\partial \ln \upsilon}{\partial \ln p}\right) + \dfrac{\partial \ln \upsilon}{\partial \ln T}\left(\dfrac{\partial \ln \upsilon}{\partial \ln T} + \dfrac{\partial \ln \upsilon}{\partial \ln p}\right)\right]} \tag{11}$$

$$\Delta p = \frac{-\dfrac{pV}{T}\left[\dfrac{10c_pT}{pV} - \dfrac{\partial \ln \upsilon}{\partial \ln T}\right]\dfrac{d\upsilon}{d\theta} - \dfrac{10\dfrac{du}{d\theta}\dfrac{\partial \ln \upsilon}{\partial \ln T}}{p}}{\dfrac{V^2}{T}\left[\left(-\dfrac{10c_pT}{pV} + \dfrac{\partial \ln \upsilon}{\partial \ln T}\right)\left(-\dfrac{\partial \ln \upsilon}{\partial \ln p}\right) + \dfrac{\partial \ln \upsilon}{\partial \ln T}\left(\dfrac{\partial \ln \upsilon}{\partial \ln T} + \dfrac{\partial \ln \upsilon}{\partial \ln p}\right)\right]} \tag{12}$$

In relations (11) and (12), thermodynamic properties such as c_p, h etc. have been calculated step by step by using determined pressure and temperature. To compute these properties, combustion products have been determined by Olikara and Borman's method. Here, thermodynamic properties at low and high temperatures have been computed by using FARG and ECP subroutine, which is developed by Ferguson. After determination of combustion products, various thermodynamic properties have been determined. In order to solve the differential equations (1, 2 and 4) given above, the RATES subroutines developed by Ferguson (1986) have been modified and used. To solve temperature and pressure for U, V and f, STATE subroutines developed by Ferguson (1986).

2.1.2. Calculation of intake and exhaust strokes

Intake and exhaust processes are computed by using Durgun's (1991) method in which temperature and pressure at the end of the intake process have been calculated from properties of gas mixtures and Bernoulli equation, respectively, as follows:

$$T_a = \frac{(T_0 + \Delta T + \gamma_r T_r)}{1+\gamma_r} \quad \text{(natural aspirated diesel engine)} \tag{13a}$$

$$T_a = \frac{(T'_c + \Delta T + \gamma_r T_r)}{1+\gamma_r} \quad \text{(turbocharged diesel engine)} \tag{13b}$$

$$p_a = p_0 - \Delta p_a \quad \text{(natural aspirated diesel engine)} \tag{14a}$$

$$p_a = p'_c - \Delta p_a \quad \text{(turbocharged diesel engine)} \tag{14b}$$

$$\Delta p_a = \left(\beta^2 + \xi\right)\frac{V_m^2}{2}\left(\frac{n}{n_N}\right)^2 \rho_a$$

where $(\beta^2+\xi)$ is the total loss coefficient in the intake system, n and n_N are the actual engine speed and nominal engine speed, respectively, V_m is the maximum flow speed in the intake system, ρ_a is the density of air, γ_r is the coefficient of the residual gas, T_0, T_c' and T_r are the surrounding air, the compressor outlet air and residual gas temperatures respectively, and ΔT is the temperature variation of the intake charge flowing through intake channel, p_c' is the compressor outlet air pressure. In the presented study, residual gases which exist in the cylinder have been taken into account by using coefficient of residual gases in the intake process calculations because these gases have an important effect on the intake gas properties. In the presented study, exhaust temperature has been chosen approximately at the beginning of cycle calculations. Then, after cycle calculations are completed, chosen and calculated the exhaust temperatures compared. If the difference ratio between these values is higher than 3%, the final value has been taken as T_r and the cycle calculation is performed again. This calculation procedure has been repeated iteratively until the difference ratio between these values becomes smaller than 3%. Thus, complete cycle control have been performed. Exhaust temperature calculation and this comparison procedure is done by using the following relations:

$$T_r = \frac{T_b}{\sqrt[3]{\frac{p_b}{p_r}}} \tag{15}$$

$$\left|\frac{T_r - T_1}{T_r}\right| \le 3\% \tag{16}$$

where T_r, p_r are the calculated exhaust temperature and pressure values, respectively, T_1 is the selected exhaust gas temperature at the beginning of intake process, T_b, p_b are temperature and pressure values, respectively, at the end of the expansion stroke.

2.1.3 Calculation of engine performance parameters

In the present study, correction factor of indicator diagram ϕ_i has been used to take into account the valve timing, injection advance and ignition delay effects. Thus, indicated work and indicated efficiency obtained from gross cycle simulation have been corrected as follows.

$$\eta_i = \frac{w_i(1+F_s\phi)}{F_s\phi(1\text{-}f)LHV}\varphi_i \tag{17}$$

where η_i is indicated efficiency, w_i is indicated work per unit mass, f is residual mass fraction, LHV is lower heating value of the fuel.

After determining the complete diesel engine cycle, engine performance parameters such as effective power, effective efficiency, and specific fuel consumption are calculated from the relationships given by Heywood (1989) and Durgun (1991). In the presented study, effective engine characteristics have been computed by using the following mean effective pressure relationships given by Durgun (1991), while generally indicated engine performance have been given in the literature.

$$p_{m,m} = 10(a+bV_{p,m})\frac{p_c'}{p_{mi}} \qquad \text{(turbocharged diesel engine)} \tag{18}$$

$$p_{m,e} = p_{m,i} - p_{m,m} \quad (19)$$

For Renault K9K 700 type diesel engine, a and b values are selected as 0.089 and 0.0118, respectively. Eq.(18), $V_{p,m}$ is the mean piston speed and $p_{m,i}$ is the mean indicated pressure.

2.1.4. Calcutation of ignition delay

Ignition delay has been calculated by using Hardenberg and Hase (Sahin et al., 2014) correlation:

$$\theta_{id}(CA) = (0.36 + 0.22 Vpm) \exp\left[E_a \left(\frac{1}{RuT} - \frac{1}{17190} \right) \left(\frac{21.2}{(p - 12.4)} \right)^{0.63} \right] \quad (20)$$

where $V_{p,m}$ (m/sec) is mean piston speed, Ru (kJ/kmole/K) is universal gas constant, p (bar) is cylinder pressure, T (K) is cylinder temperature, E_a (kJkmole) is activation energy. The activation energy E_a is given by E_a = 618,840/(CN-25) where CN is the cetane number of the fuel. The average cetane number for the diesel fuel used for model engine tests is specified to be 45.

3. Accuracy control of the present model with applications for ndf

In the present study, the accuracy of the newly developed model has been controlled comparing with the experimental and theoretical data given in the relevant literature (Kökkülünk et al., 2013), (Qi et al., 2011), (Ottikkutti et al, 1991), (Kızıltan, 1988), (Sahin and Aksu, 2015). For this purpose, numerical results obtained from the presented model are compared with the experimental and the theoretical data of which are accepted to be at sufficient accuracy in the literature. In the comparisons with the experimental ones, Tuti's (2012), Kızıltan's (1988), Kökkülünk's (Kökkülünk et al., 2013) and Kunpeng's (Qi et al., 2011) experiments have been employed. Also, in the comparison with the relevant theoretical study, the results of Ottikkuti's model (Ottikkutti et al, 1991) has been used. The obtained computational results and comparisons have been presented as various tables and figures.

Here, firtsly the accuracy of the newly developed model has been controlled comparing with our experimental studies. These experiments were done in Mechanical Engineering Department KTU. In the experimental study, a turbocharged common-rail DI automotive diesel engine, Renault K9K 700 type, was used. The specifications of the test engine have been given in Table 1. Cylinder gas pressure was measured by using of an AVL GH12P type quartz pressure sensor without cooling (Sahin et al., 2014), (Tuti, 2012). Detailed information about pressure measurment can be found in refs. (Sahin et al., 2014), (Sahin and Aksu, 2015). The cylinder pressure values obtained from the present model have been compared to cylinder pressure values obtained from the experiments in Figs.1. As can be seen in Figs.1., the agreement between the predicted pressure values and the experimental results are generally good.

As shown in Fig.1.(a); the peak pressure for experiment at 2000 rpm is 156.34 bar and it occurs at 10° CA. On the other hand, the peak pressure value obtained from the present model is 157.23 bar and it occurs at 6° CA. It can be seen that the difference between these peak pressure values is 0.57%. The same results have been obtained for the other selected engine speeds. However, the maximum cylinder pressure values obtained from this model was found closely to the experimental results in the range of (0.57-4.5) % error rate at the selected engine speeds. It can be seen in Fig.1.(a) that the peak pressure

angles for predicted model is earlier than that of experiment at 2000 rpm. Possible reasons for this differences can be explained given as follows.

Some working parameters of engine such as ignition advanced (IA), etc. are not known. Actually, this engine has an electronic control unit (ECU). So, there is not constant IA for various engine speeds and diesel fuel injection has been controlled by for considering optimum operating conditions. In the pesent study, IA has been calculated aproximately by using determined experimentally heat release rate diagram (HRR) and relation (20). By using HRR, the crank angle at the the beginning of the combustion (θ_{comb}) has been determined. By taking into account starting point of combustion and relation (20), IA has approximately been computed ($\theta_{inj} = \theta_{comb} - \theta_{id}$).

Renault K9K700 type turbocharged diesel engine has common rail injection system and injectors of this system has five hole. In the present model, this feature of the injection system has not been considered. In the modeling study, it is assumed that the nozzle of the injector has one hole (that is, total injected diesel fuel has been used as input data for develop programme). It is well known that numbers and diameter of the holes of the nozzle are very important to form homogeneous air-fuel mixtures. This effect has not been taken into account in the present model. Also, pilot injection has been applied in the used engine. Here, this effect has not also be taken into account.

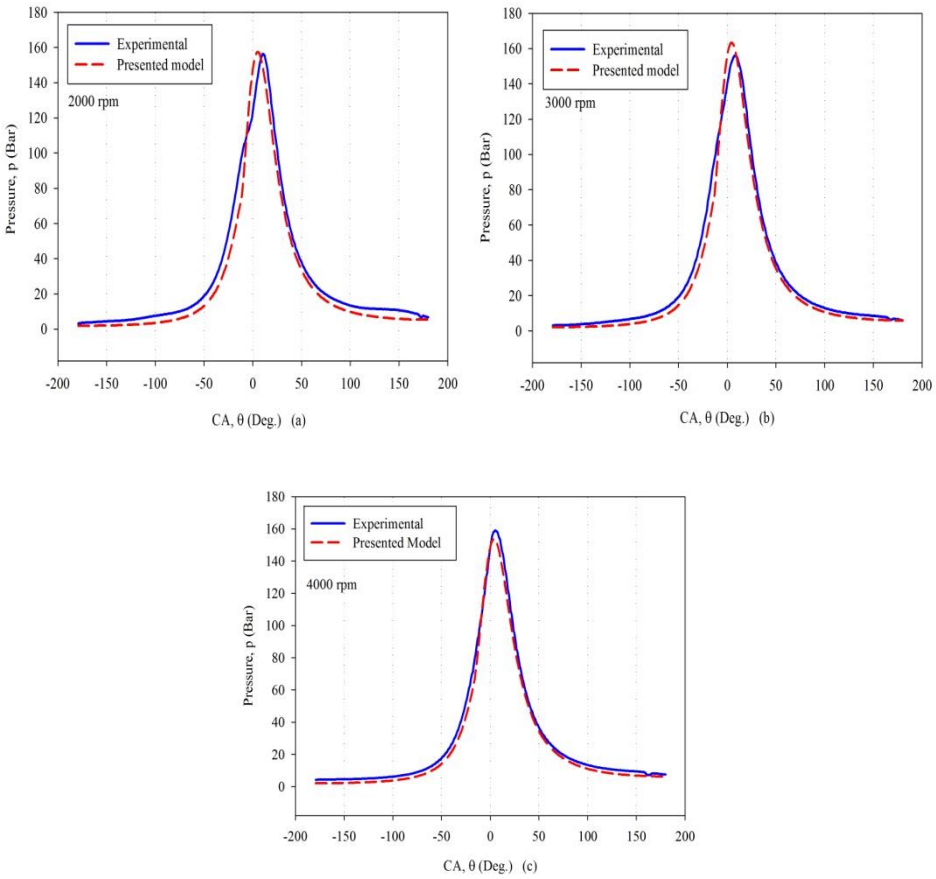

Figure 1. (a), (b) and (c) comparisons of cylinder pressure values obtained from the presented model with the experimental cylinder pressure data for 2000, 3000 and 4000 rpms.

In the present study, effective power and BSFC obtained from the present model have been compared with experimental results at (2000-4000) rpms in Figs.2. Effective power values obtained from the

present model and experiment are 29.13 kW and 31.96 kW respectively at the 2000 rpm. Hence, the difference between the effective powers is 8.8%. BSFC values obtained from present model and experiment are 0.2004 kg/kWh and 0.2205 kg/kWh, respectively at the 2000 rpm. Hence, the difference between these BSFC values is 9.1% at this engine speed. The differences between the present model and experimental data in terms of effective power and BSFC have shown the same variations for the other selected engine speeds. The effective power and BSFC obtained from modelling have approached to experimental data at the range of (0.3-8.8) % and (1.7-9.1) % error rate, respectively at the seleced engine speeds. The reasons for these differences have been given above paragraph. Besides these, the mechanical efficieny of the test engine is also unknown and this has been computed by using the relation (18).

Table 1. Main specifications of the engines used for comparisons of theoretical results with experimental data (n_n is nozzle holes number) [6, 7, 16, 19, 20]

	ε	D(mm)	H(mm)	p_p(bar)	θ_s(°)	d_n(mm)	Z	n_n
Renault K9K	18.25	76	80.5	up to 2000	change	0.12	4	5
Kızıltan	18-24	90	120	90-250	-22	0.36	1	1
Kökkülünk	17	108	100	175	-	-	1	-
Kunpeng	17	135	150	110	-10	0.36	1	4
Ottikkutti	16.8	106.5	127	120-490	-15	0.3	4	4

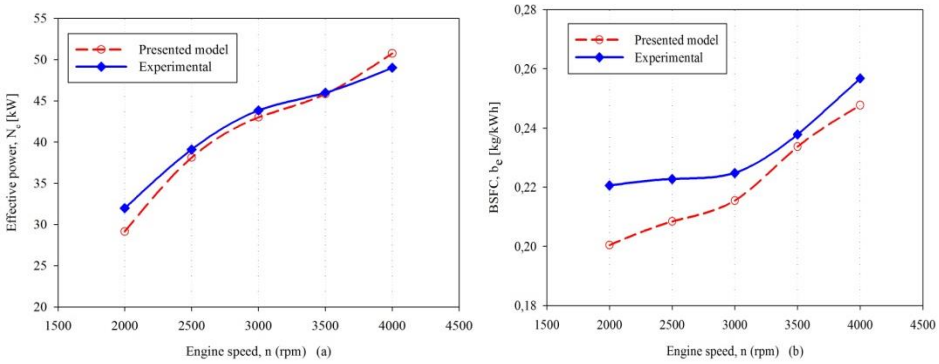

Figure 2. (a) and (b) Comparisons of effective power and BSFC values obtained from the presented model with experimental data

The other comparison has been performed by using Kızıltan's [19] experimental data. In Kızıltan's tests, a single cylinder, four-stroke, water cooled, variable compression ratio experimental engine manufactured by Tecquipment has been used. Main specifications of this test engine are given in Table 1. Comparisons of effective power and BSFC obtained from the presented model and Kızıltan's [19] experimental data have been shown in Figs.3 (a) and (b). As can be seen from these figures, the predicted results agree reasonably with the measured values. At 1300 rpm, the effective power computed by using the developed model for Kızıltan's engine has been obtained as 6.12 kW and the effective power given by Kızıltan was 5.615 kW. Thus, it can be seen that the difference between effective powers is 8.9 % at 1300 rpm. Also, BSFC values obtained from present model and experiment are 0.2647 kg/kWh and 0.281 kg/kWh respectively at the 1300 rpm. Hence, the difference between these BSFC values is 5.77%. For

different speeds, the maximum error rate between effective power and BSFC was found to be approximately 11%. This could be attributed to not knowning some parameters of the engine and selecting these parameters approximately and using an insufficient relation of mechanical losses and mechanical efficieny originally given for multi cylinder vehicle engine. This relation may not be suitable for the used engine. Similar error rates were observed in Şahin's multi-zone thermodynamic model for Kızıltan's experimental results (Sahin and Durgun, 2008).

In another comparison, experimental results given by Kökkülünk et al. have been used. Kökkülünk et al. were used a single cylinder, four-stroke, DI diesel engine in their experimental study (Kökkülünk et al., 2013). Table 1. shows the specifications of this engine. Fig.4 shows the comparison of cylinder pressure values obtained from the presented model with that of Kökkülünk's experimental data at 2200 rpm. As shown in Fig.4, the peak pressure for Kökkülünk's experiment at 2200 rpm is 68.13 bar and it occurs at 4° CA. On the other hand, the peak pressure value obtained from the present model is 67.74 bar and it occurs at 6° CA. It can be seen that the difference between these peak pressure values is 0.57 at this engine speed. Thus, a satisfactory conformity can be observed in Fig.4.

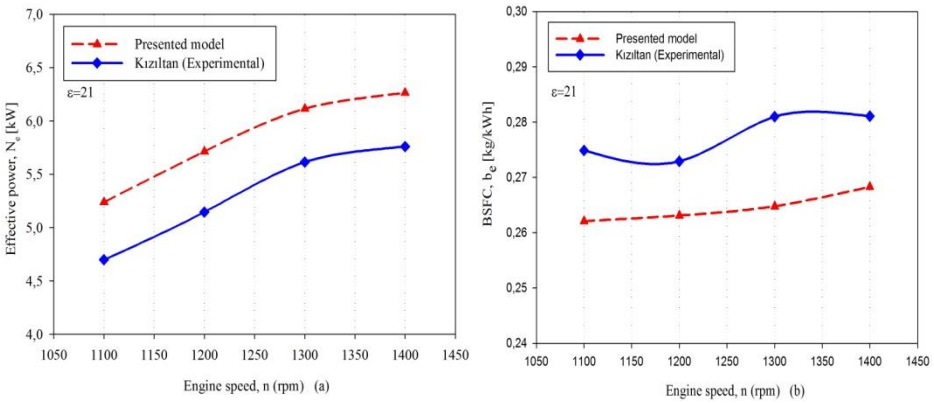

Figure 3. (a) and (b) Comparison of effective power and BSFC values obtained from the presented model and Kızıltan's experimental data

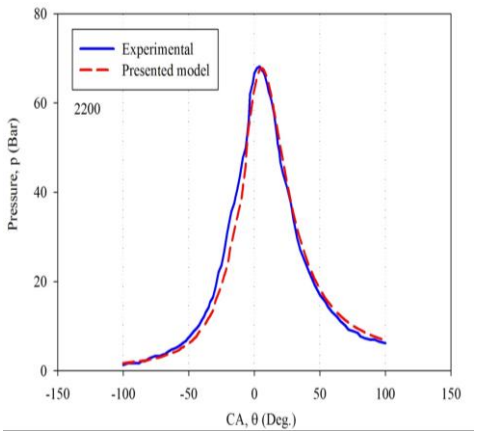

Figure 4. Comparisons of cylinder pressure values obtained from the presented model with the Kökkülünk's experimental data as a function of crank angle

Furthermore, effective power and BSFC obtained from the present model have been compared with Kökkülünk's data at (1700-2300) rpms in Figs.5. Effective power values obtained from the present model and experiment are 11.57 kW and 12.13 kW respectively at the 2000 rpm. Hence, the difference between these effective power values is 4.64%. The difference between the present model results and the

experimental data in terms of effective power shows the same variation for all selected engine speeds. BSFC values obtained from present model and experiment are 0.2672 kg/kWh and 0.2827 kg/kWh respectively at the 2000 rpm. Hence, the difference between these BSFC values is 5.48%. The difference ratios of BSFC according to the engine speeds obtained from the presented model were at levels of (3-11) % error. It can be seen In Fig. 5(a) that, difference between BSFC values obtained from the presented model and Kökkülünk's experimental data increase while engine speeds are increasing. This can be attributed to being used an empirical mean pressure of the mechanical losses relation originally developed for vehicle diesel engines as stated above. This equation may not be suitable for the used Kökkülünk's test engine.

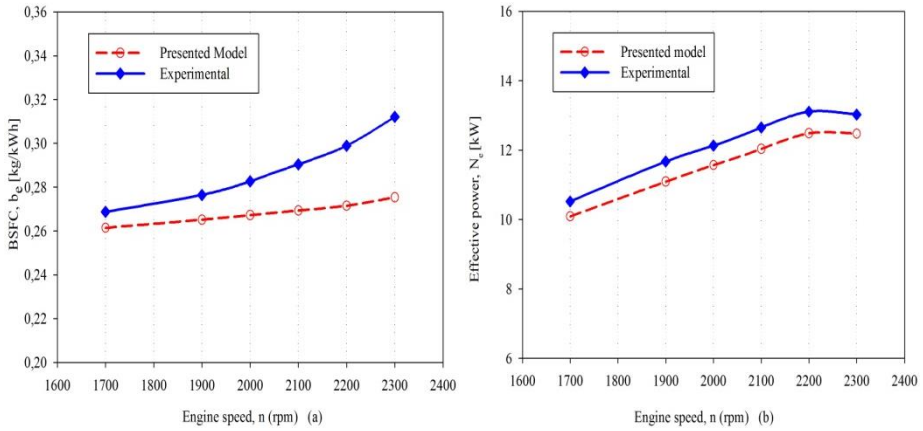

Figure 5. (a) and (b)Comparison of BSFC and effective power values obtained from the presented model and Kökkülünk's experimental data

Also, accuracy control of the present model have been performed by using Kunpeng's experimental data (Qi et al., 2011). In the Kunpeng's experimental study, a single cylinder, four-stroke, and water cooled, 1135 naturally aspirated diesel engine were used. Main specifications of this test engine are given in Table 1. In Fig.6 cylinder pressure values obtained from present model have been compared with Kunpeng's experimental data for 1500 rpm. As shown in Fig.6, at 1500 rpm, the peak pressure of Kunpeng's is 69.6 bar and it occurs at 13°CA, while in the presented model peak pressure is 70.8 bar and it occurs at 6°CA. Also, at 1500 rpm, the effective power and BSFC computed from the presented model are 13.496 kW and 256 g/kWh respectively. The effective power and BSFC values given by Kunpeng's experimental results are 14.7 kW and 245 g/kWh respectively. Thus, it can be seen that the difference effective power and BSFC values are 8.2 % and 4.5 % respectively. This could be attributed to not knowning some parameters of Kunpeng's test engine and selecting approximately these parameters. Injection pressure and IA have also been selected approximately and these parameters affects cylinder presure values. Also, injection strategy of the Kunpeng's test engine is not completely comply with gamma function used in present model ore injection parameter n_1 of this function may not be chosen well.

In the comparison with the relevant theoretical study, the results of Ottikkuti's model has also been used (Ottikkutti et al., 1991). The numerical results obtained from the presented model are compared with the theoretical results of Ottikkuti. In this theoretical study, Ottikkuti was used a 4 cylinder, four-stroke and turbocharged diesel engine. Main specifications of this test engine are given in Table 1. Effective power, the mean indicated pressure ($p_{m,i}$) and indicated thermal efficiency (η_i) values obtained from the

present model are compared with that of Ottikkutti's model. Effective power values obtained from the present model and Ottikkutti's model are 56.6 kW and 54.24 kW respectively at the 1500 rpm. Hence, the difference between these effective power values is 4.16 %. $p_{m,i}$ values obtained from the present model and Ottikkutti's model are 10.46 bar and 11.22 bar respectively at the 1500 rpm. Hence, the difference between these $p_{m,i}$ values is 7.27 %. η_i values attained from the present model and Ottikkutti's model are 0.459 and 0.497 respectively at this engine speed. These parameters show similar differences for 2100 rpm. Generally, effective power, $p_{m,i}$ and η_i values obtained from the present model showed maximum differences at the level of 9 % with Ottikkutti's model.

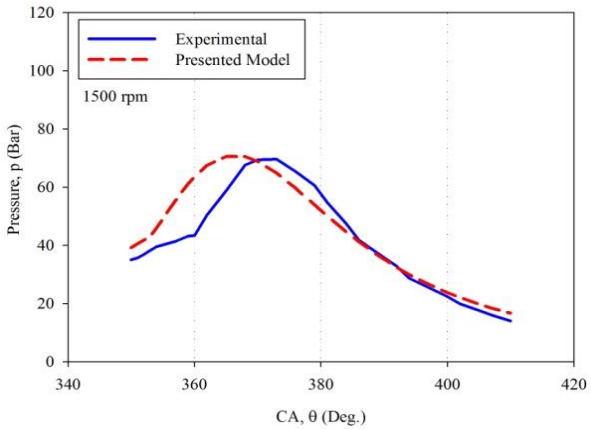

Figure 6. Comparisons of cylinder pressure values obtained from the presented model with Kunpeng's experimental cylinder pressure data as a function of crank angle

4. Conclusions

Results obtained from the development and verification studies and various applications of the presented diesel engine cycle model can be briefly summarized as follows:

1. The present model is able to predict the diesel engine cycles for neat diesel fuel. The model can predict the cylinder pressure and engine characteristics in good agreement with experimental and theoretical results and it can be applied easily and the run time is sufficiently low. Thus, it can be used effectively in various engine development and parametric studies.

2. Engine performance parameters and cylinder pressure values for only neat diesel fuel has been examined using present model. Actually, in the next studies we aimed to investigate the effect of addition of water to the intake air manifold in diesel engines by using this cycle model. Thus, this model will be adapted to addition of water to the intake air manifold of diesel engine in the near future. The theoretical studies on water addition have been started.

References

Bedford, F., Rutland, C., Dittrich P., Raab A., Wirbelit F. (2000). Effects of Direct Water Injection on DI Diesel Engine Combustion, SAE J. Automot. Eng., 01-2938.

Durgun, O. (1991). A Practical Method for Calculation Engine Cycles, Union of Chambers of Turkish Eng. And Arc., Chamber of Mech. Eng., 383,18-29.

Durgun, O., Sahin, Z. (2009). Theoretical Investigation of Heat Balance in Direct Injection (DI) Diesel Engines for Neat Diesel Fuel and Gasoline Fumigation, Energy Conversion and Management, 50, 43-51.

Ferguson, R. (1986). Internal Combustion Engines-Applied Thermody, John Wiley & Sons, New York.

Hardenberg, H.O., Hase, F.W. (1979). An Empirical Formula for Computing the Pressure Rise Delay of a Fuel from its Cetane Number and from the Relevant Parameters of Direct Injection Diesel Engines, SAE Paper 790493.

Heywood, J.B. (1989). Internal Combustion Engines Fundamentals, McGraw Hill Book Company, New York.

Kızıltan, E. (1988). Effect of Alcohol Addition to Motor Fuels on Engine Performance, Master Thesis, KTU Graduate School of Natural and Applied Sciences, Trabzon, [in Turkish].

Kökkülünk, G., Gonca, G., Ayhan, V., Cesur, I., Parlak, A. (2013). Theoretical and Experimental Investigation of Diesel Engine with Steam Injection System on Performance and Emission Parameters, Applied Thermal Eng., 54, 161-170.

Ottikkutti, P., Gerpen, JV., Cui, KR. (1991). Multi-zone Modeling of a Fumigated Diesel Engine, SAE, 910076:1–21.

Pasternak, M., Mauss, F. (2009). Diesel Engine Cycle Simulation with a Reduced Set of Modeling Parameters Based on Detailed Kinetics, SAE, 01-0676.

Qi, K., Feng, L., Leng, X., Du, B., Long, W. (2011). Simulation of quasi-dimensional combustion model for predicting diesel engine perf., Appl. Math. Model., 35, 930-40.

Sahin, Z., Aksu, O. (2015). Experimental investigation of the effects of using low ratio n-butanol/diesel fuel blends on engine performance and exhaust emissions in a turbocharged DI diesel engine, Renewable Energy, 77, (279-290).

Sahin, Z., Durgun, O. (2007a). High speed direct injection (DI) light-fuel (gasoline) fumigated vehicle diesel engine, Fuel, 86:388–99. 597.

Sahin, Z., Durgun, O. (2007b). Theoretical investigation of effects of light fuel fumigation on Diesel engine performance and emissions, Energy Conversion & Management, 48, 1952–64.

Sahin, Z., Durgun, O. (2008). Multi-zone Combustion Modeling for the Prediction of Diesel Engine Cycles and Engine Perf. Par., Appl. Therm. Eng., 28, 2245-2256.

Sahin, Z., Tuti, M., Durgun, O. (2014). Experimental Investigation of the Effects of Water Adding to the Intake Air on the Engine Performance and Exhaust Emissions in a DI Automotive Diesel Engine, Fuel, 115:884-895.

Savioli, T. (2015). CFD Analysis of 2-Stroke Engines, Energy Procedia, 81, 723-31.
Shrivastava, R., Hessel, R., Reitz, R.D. (2002). CFD Optimization of DI Diesel Engine Performance and Emissions Using Variable Intake Valve Actuation with Boost Pressure, EGR and Multiple Injections, SAE, 2002-01-0959.

Sindhu, R., Amba Prasad Rao, G., Madhu Murthy, K. (2014). Thermodynamic Modelling of Diesel Engine Processes for Predicting Engine Performance, International Journal of Applied Engineering and Technology, Vol. 4 (2).

Tutak, W., Jamrozik, A. (2016). Validation and optimization of the thermal cycle for a diesel engine by computational fluid dynamics modeling, Appl. Math. Model., 40, 6293–6309.

Tuti, M. (2012). Experimental Investigation of the Effects of Water Adding to the Intake Air on Engine Performance and Exhaust Emissions in Diesel Engines, Master Thesis, KTU Institute of Science, Trabzon, Turkey [in Turkish].

Tip Vortex Index (TVI) Technique for Inboard Propeller Noise Estimation

Savaş Sezen[1], Ali Dogrul[2], Şakir Bal[3]

[1]ssezen@yildiz.edu.tr, [2] adogrul@yildiz.edu.tr, [3] sbal@itu.edu.tr

[1,2] Department of Naval Architecture and Marine Engineering, Naval Architecture and Maritime Faculty, Yildiz Technical University, Istanbul, Turkey

[3] Department of Naval Architecture and Marine Engineering, Faculty of Naval Architecture and Ocean Engineering, Istanbul Technical University, Istanbul, Turkey

Abstract

Cavitating marine propeller is one of the most dominant noise sources in marine vessels. The aim of this study is to examine the cavitating propeller noise induced by tip vortices for twin screw passenger vessels. To determine the noise level inboard, tip vortex index (TVI) technique has been used. This technique is an approximate method based on numerical and experimental data. In this study, it is aimed to predict the underwater noise of a marine propeller by applying TVI technique for two bladed and three bladed propellers. The hydrodynamic performance of cavitating propeller has been calculated by a potential flow code based on lifting surface method. The effect of cavitation number and propeller rotation speed on sound pressure level has been discussed.

Keywords: Acoustic, Lifting Surface Method, Underwater Noise, Tip Vortex Index

Nomenclature

Symbol	Description
$\vec{\upsilon}_\Gamma$	velocity vector by unit strength vortex element
$\vec{\upsilon}_Q$	velocity vector by unit strength source element
Q_B	line source for blade thickness source strength
Q_C	line source for cavity source strength
$\vec{n}_m$	unit vector normal
Γ	circulation
k_{tbl}	thrust coefficient per blade
k_{tip}	tip loading factor
Z	number of blades
σ	cavitation number
P_{atm}	atmospheric pressure
h	operating depth of the propeller

ρ	fluid density
g	gravitational acceleration
P_v	saturation pressure
n	propeller rotation speed
D	propeller diameter
dB	decibel
J	advance ratio

1. Introduction

Underwater noise has become a growing concern in view of its significant effect on marine environment although underwater radiated noise is a main interest for submarines, naval vessels, fishing vessels and research vessels traditionally. Underwater radiated noise is mostly caused by shipping activities which masks the natural background noise and communication network between marine animals. International Maritime Organization (IMO) recently has investigated to reduce underwater noise from shipping activities.

Underwater radiated noise sources on marine vessels are mainly divided into three different categories: engine noise, flow noise and propeller noise (Carlton, 1994). To reduce the engine noise, isolation equipment can be applied and also engine foundation has to be resiliently mounted instead of rigidly mounted (Wittekind, 2014). Ship hull design should also be proper to decrease the hydrodynamic noise which is caused by the flow. Marine propellers on the other hand, are one of the most important noise sources on marine vessels. Reducing the propeller noise is especially important for detection of vessel position and velocity. Due to this reason, not only hydrodynamic properties but also acoustic performance should also be taken into consideration for propeller design. Therefore, accurate calculation of the marine propeller noise is considerable subject in maritime industry.

Propeller noise can be mainly divided to two sub-categories: cavitation noise and non-cavitation noise. The cavitation is one of the main sources of underwater radiated noise. Cavitation noise is especially inevitable for high speed vessels. Because of sudden changes of cavitation phenomenon on propeller blades, cavitation noise prediction is a difficult task. Empirical calculations based on full or model-scale measurements and theoretical estimations can be applied. To predict the propeller cavitation noise, acoustic analogy methods are also used. As the first step of the analogy, the strength of noise source can be solved by numerical methods such as CFD (Computational Fluid Dynamics), LSM (Lifting Surface Method) and so on. The sound field is then calculated by the helping of Ffowcs-Williams Hawkings (FW-H) equation (Zhang and Xiong, 2011).

In the past, Seol and Lee (Seol and Lee, 2002) have investigated non-cavitation and cavitation noise of propeller numerically. The non-cavitation noise has been predicted using time-domain acoustic analogy and boundary element method. Additionally, they have developed computational methods for the analysis of the propeller surface cavitation noise. The flow field has been analyzed with potential based panel method and then the time-dependent pressure datum has been used as the input for Ffowcs-Williams Hawkings formulation to estimate far field acoustics. Ekinci et al. (2010) have investigated hydrodynamic features of model propeller and noise prediction has been made by empirical formulations which are improved for low frequency. Hydrodynamic characteristics of DTMB 4119 propeller and Seiun-Maru HSP

propeller have been compared with both potential based LSM (Lifting Surface Method) and CFD code. Noise based on propeller blade sheet cavitation has been investigated with empirical formulations. In addition, this method has been applied under uniform and non-uniform flow conditions. Lidtke et al. (2016) have investigated propeller noise which belongs to commercial vessel and cavitation has been modeled with Schnerr-Sauer model. For cavitation condition, time-dependent change in URANS model could not have been predicted totally and cavitation at the tip vortex area could not have been observed as well. Therefore, it has been stated that LES method is more suitable for observing cavitation. Salvatore and Ianniello (2003) have studied on theoretical prediction of the acoustic pressure field induced by marine propellers with a coupled hydrodynamics and hydroacoustic analysis based on boundary element method. The hydroacoustic FW-H model has been coupled with an inviscid-flow unsteady cavitation hydrodynamics calculation based on boundary element method. Numerical predictions of the propeller noise by using FW-H equation have been compared by a classical Bernoulli equation. Propeller noise has been predicted for non-uniform inflow conditions under non-cavitating and cavitating flows. Kim et al. (2016) have developed a numerical method to predict propeller tonal noise whereas contributor of the broadband noise has been investigated experimentally. Propeller tonal noise has been calculated by taking into account of cavitation volume variation on propeller blades. Broadband noise calculations have been done in water tunnel and onboard measurements in the real ship. Tonal noise acoustic results have been validated in water tunnel experiments. The semi-empirical formula based on experimental results for tip vortex cavitation noise has been developed. Lafeber et al. (2015) have investigated propeller cavitation noise via both computational and experimental methods. Three different propellers have been used for acoustic calculations. The unsteady flow around the propeller has been calculated by PROCAL method. ETV noise model based on TVI technique has been used for prediction of cavitating vortex noise. Matusiak and Brown's model has been calculated in terms of the sheet cavitation noise. Szantyr et al. (2012) have studied on tip vortex cavitation. The main aim of the study is to develop a reliable method for numerical prediction of tip vortex cavitation. The calculations were based on both experiments and numerical calculations. The experimental study on tip vortex cavitation behind the hydrofoil has been done in a cavitation tunnel and flow around the hydrofoil has been calculated by particle image velocimetry (PIV) method. For numerical calculations, Fluent and CFX commercial CFD codes have been used. It was shown that experimental and numerical results have been in a good agreement with each other. Jeung-Hoon et al. (2013) have studied on detecting the inception of tip vortex cavitation. Short-Time Fourier Transform (STFT) analysis and Envelope Modulation On Noise (DEMON) spectrum analysis have been applied to determine the tip vortex cavitation noise. The scope of the study was to compare the applicability to the detection of cavitation inception. Wijgaarden et al. (2005) have studied the broadband inboard noise and vibration on passenger vessels between 20-70 Hz frequency ranges. Especially, hydroacoustic calculations involving tip vortex cavitation has been investigated both by sea trials and model experiments. Sezen et al. (2016b) have applied TVI technique for prediction of inboard noise level of a three bladed DTMB 4119 model propeller without taking the thickness effect into account.

In this paper, it is aimed to carry out some calculations using an empirical method considering that the propeller noise is caused by the tip vortices of the propeller blades. An acoustic study has been performed for a twin screw passenger vessel. The propeller has been considered as the noise source and acoustic results have been carried out at three decks above propeller and aft perpendicular. DTMB 4119 propeller has been investigated by means of hydrodynamic performance via lifting surface method under cavitating condition considering that the blade number is 2 and 3, respectively. The results have been discussed depending on advance ratio and cavitation number using tip vortex index (TVI) technique. This paper is

the extended version of the study (Sezen et al., 2016b) presented in the symposium organized by Turkish Chamber of Naval Architects.

2. Mathematical model

2.1. Lifting surface method

A lifting surface method was applied to calculate the propulsive performance and induced velocities due to the propeller, similar to the one given (Bal, 2011b) & (Bal, 2011a) & (Kerwin, 2001) & (Bal and Güner, 2009). The lifting surface method (propeller analysis code) models the 3-dimensional unsteady cavitating flow around a propeller by representing the blade and wake as a discrete set of vortices and sources, which are conveniently located on the blade mean camber surface and wake surface. In particular, the 3 components of the discretization are as follows:

i) A vortex lattice on the blade mean camber surface and wake surface to represent the blade loading and trailing vorticity in the wake.

ii) A source lattice on the blade mean camber surface to represent blade thickness.

iii) A source lattice throughout the cavity extent to represent cavity thickness.

The sources representing blade thickness are line sources along the spanwise direction. The strengths of the line sources are given in terms of derivatives of the thickness in the chordwise direction and are independent of time. The unknown bound vortices on the blade and the unknown cavity sources are determined by applying the kinematic boundary condition and the dynamic boundary condition.

In this method, a discretized version of the kinematic boundary condition can be employed as:

$$\sum_{\Gamma} \Gamma \vec{\upsilon}_{\Gamma} . \vec{n}_m = -\vec{\upsilon}_{in} . \vec{n}_m - \sum_{Q_B} Q_B \vec{\upsilon}_Q . \vec{n}_m - \sum_{Q_C} Q_C \vec{\upsilon}_Q . \vec{n}_m \qquad (1)$$

where $\vec{\upsilon}_{\Gamma}$ the velocity vector is induced by each unit strength vortex element, $\vec{\upsilon}_Q$ is the velocity vector induced by each unit strength source element, and $\vec{n}_m$ is the unit vector normal to the mean camber line or trailing wake surface. Q_B and Q_C represent the magnitude of the line sources that model the blade thickness and cavity source strengths, respectively. The kinematic boundary condition must be satisfied at certain control points located on the blade mean camber surface. The kinematic boundary condition requires that the sum of the influences for all of the vortices' sources and the inflow normal to a particular control point on the blade is equal to zero. Another way to explain this is that the kinematic boundary condition requires the flow to be tangential to the surface. Other assumptions employed throughout the method include:

i) The cavity thickness varies linearly across panels in the chordwise direction and is piecewise constant across panels in the spanwise direction.

ii) There are no spanwise flow effects in the cavity closure condition.

iii) Viscous force is calculated by applying a uniform frictional drag coefficient, C_f , on the wetted regions of the blade.

The details of the method can be found in (Bal, 2011b) & (Bal, 2011a) & (Bal and Güner, 2009).

2.2. TVI technique

Tip vortex index (TVI) technique has been developed by Det Norske Veritas (DNV GL) in order to estimate inboard noise caused by marine propeller. The technique consists of several empirical formulations based on experimental studies. Experimental studies have been conducted for 15 ships including cruise liners and ferries. In this method, the propeller itself is considered as the source of transmitting the noise to the ship hull while the hull is the receiver of the pressure fluctuations (Raestad, 1996).
TVI has been used to predict the inboard noise level in a location at three decks above the propeller and aft perpendicular. It is the non-dimensional factor expressing the pressure field from the tip vortices.

$$TVI=\left(k_{tbl}.k_{tip}\right)^2 Z^{0.5}/\sigma \qquad (2)$$

This technique considers that the noise is caused by the tip vortices of the propeller blades in a cavitating condition. k_{tip} is for the relative tip loading factor. This factor is nearly constant for a wide range of speed in fixed pitch propellers while it is dependent on the pitch settings for controllable pitch propeller.
Here, Z is the blade number and σ is the cavitation number.

$$\sigma=\frac{P_{atm}+\rho gh-P_v}{0.5\rho\left(nD\right)^2} \qquad (3)$$

Cavitation number is calculated by considering the operating depth of the propeller (h) is 5 meters while the saturation pressure (P_v) is taken as 2000.7 Pa. The propeller rotating speed (n) is derived from the non-dimensional cavitation number.

$$k_{tip}=\left(\Gamma_{tip}/k_{tbl}\right)/\left(\Gamma_{tip}/k_{tbl}\right)_{ref} \qquad (4)$$

The circulation distribution on the propeller blades is significant in calculating the tip vortex index. Thrust force per blade is represented by k_{tbl} while Γ_{tip} is the circulation at the propeller blade. The optimum circulation distribution can be observed by taking k_{tip} as 1.

$$dB_{ref}=20\log\left(TVI.n^2D^2\right)+80 \qquad (5)$$

It is assumed that the noise level is directly related to the sound pressure level at any selected position. Detailed information about TVI technique can be found in (Raestad, 1996).

3. Results and discussions

DTMB 4119 model propeller has been chosen for the investigation of flow and prediction of acoustical performance. Geometrical properties of the model propellers have been presented in Table 1. 3-D view of the DTMB 4119 model propellers have been shown Fig. 1.

Table 1. DTMB 4119 main particulars

DTMB 4119 Model Propeller	
D (m)	0.3048
Z	2 - 3
Skew (°)	0
Rake (°)	0
Blade section	NACA66 a=0.8
Rotation direction	Right

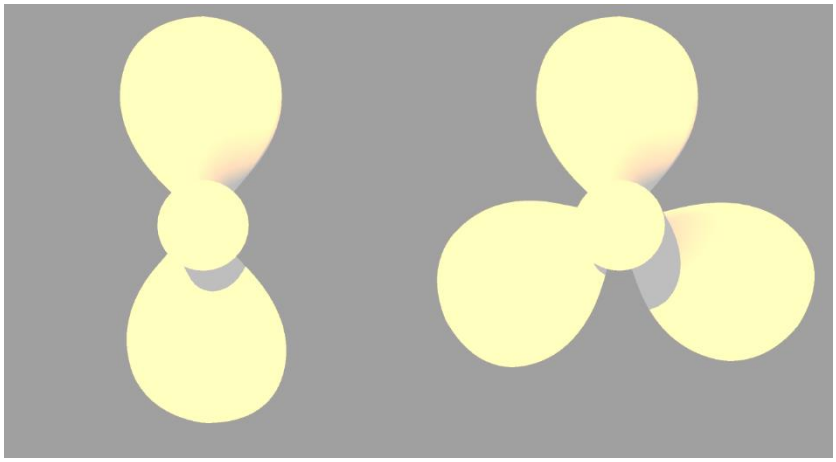

Figure 1. 3-D models of DTMB 4119

The flow around the model propeller has been solved by lifting surface method. The code has been applied in order to predict the hydrodynamic performance of the propeller by means of circulation distribution per blade. Hydrodynamic results have been derived for different cavitation numbers and advance ratios. In Fig. 2, the elements used are shown with wakes.

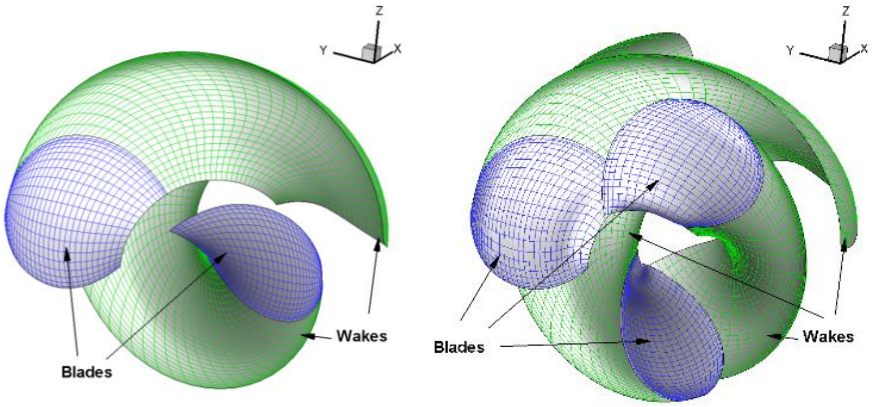

Figure 2. Perspective view of DTMB 4119 propeller blades and wakes

In Fig. 3, the cavity pattern on the blades is shown at critical cavitation numbers for both two and three bladed propellers. One can see from fig. 3 that the cavity patterns are quite similar for both model propellers.

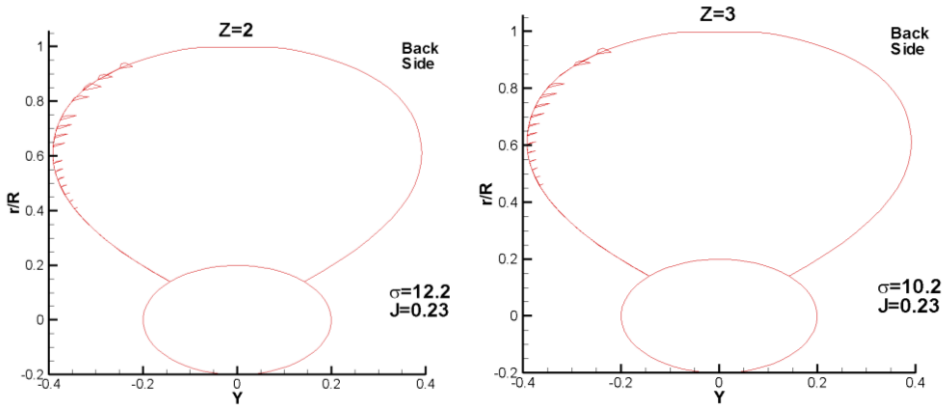

Figure 3. Comparison of cavity pattern of DTMB 4119 propeller

The circulation distribution on the propeller blades have been given in Fig. 4 for different advance ratios by means of blade numbers. As expected, the blade loading is decreasing with the increasing advance ratio. In addition, it has been observed that the blade loading is decreasing while the blade number is increasing.

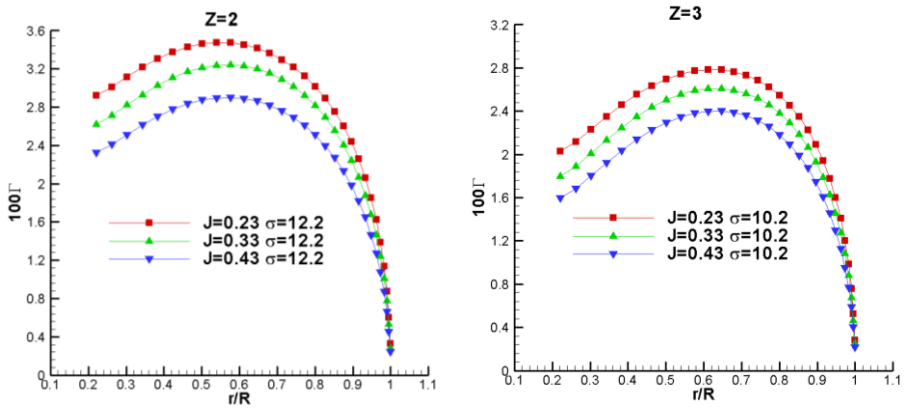

Figure 4. Circulation distribution on the blades for different blade numbers

Fig. 5 gives the performance characteristics of the model propeller DTMB 4119 at critical cavitation numbers of two and three bladed model propellers. The propeller performance has been observed in an operating range with high propulsive efficiency both in hydrodynamic and hydroacoustic manner. As can be seen from the figs. 4-5, higher circulation distribution has been obtained from two-bladed propeller which provides higher efficiency.

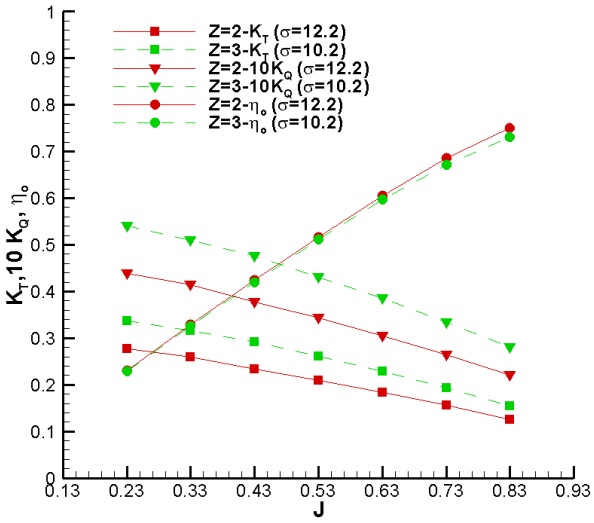

Figure 5. Hydrodynamic performance characteristics of DTMB 4119 at a constant cavitation number for different blade numbers

Tip vortex has a significant effect on underwater propeller noise. The vorticity on the propeller blade tips trigger the noise level even inboard the ship (Sezen, 2016), (Sezen et al., 2016a). The tip loading factor is crucial in the calculation of TVI. This factor has been calculated by using the circulation on the tip and the maximum circulation of the blade as reference value. TVI has been used for the estimation of sound pressure level at the reference location inboard the ship.

For observing the effect of cavitation phenomenon on the propeller noise, TVI method has been used for different cavitation numbers at a constant advance ratio. The results have been presented in Fig. 6. It is obvious that the sound pressure level decreases while the cavitation number increases for both blade numbers. This is because the cavitation risk also decreases with an increase in the cavitation number. It is observed that sound pressure level for two bladed propeller is more than that of for three bladed propeller. In accordance with the cavity patterns given in fig. 6, it is obvious that the cavitation phenomenon is more dominant than the blade number by means of sound pressure level.

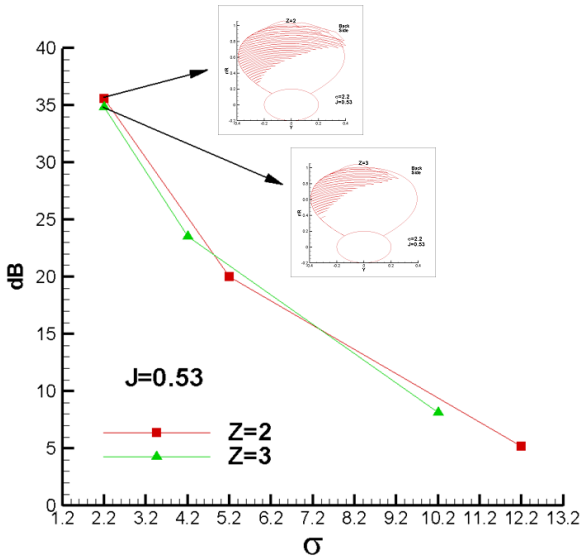

Figure 6. Sound pressure level distribution for different cavitation numbers at a constant advance ratio for different blade numbers

Fig. 7 shows the relation between the propeller rotation speed and the sound pressure level for both blade numbers. The noise level has an increasing trend with the propeller rotation speed. This can be explained that the higher propeller rotation speed increases the cavitation risk so the noise level. The main highlight of Fig. 7 is that the sound pressure level increases with the decreasing cavitation number. Note that the critical cavitation numbers are σ=12.2 and σ=10.2 for two and three bladed propellers, respectively. One can observe that the sound pressure level decreases with the decreasing blade number.

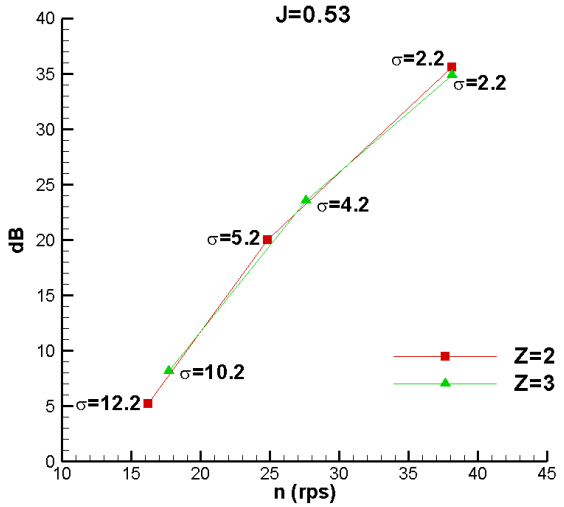

Figure 7. Sound pressure level distribution for different propeller rotation speeds and blade numbers

Fig. 8 is given for the observation of effect of advance ratio on sound pressure level at the critical cavitation number. As can be seen in Fig. 8, sound pressure level shows a decreasing behavior with the increase in advance ratio, as expected. This is because that the cavitation occurs only at J=0.23 for the critical cavitation number while there is no cavitation behavior in the other advance ratios for three bladed propeller.

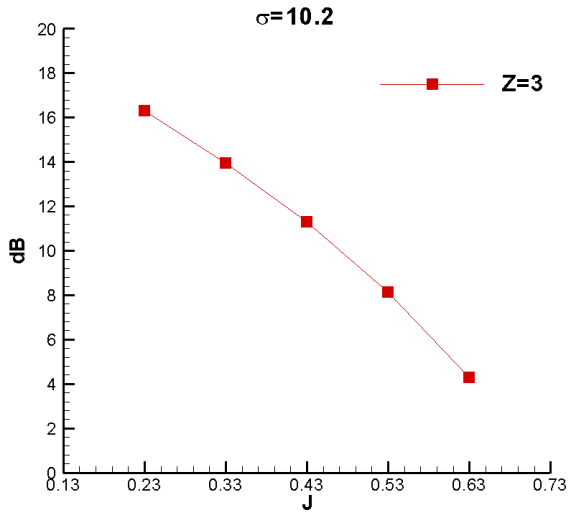

Figure 8. Sound pressure level distribution for different advance ratios at a constant cavitation number for three bladed propeller

Tip loading factor has been chosen as another parameter affecting the hydroacoustic performance empirically. As seen Table 2, three different cavitation numbers have been investigated via two different

tip loading factors for three-bladed propeller at a constant advance ratio. k_{tip}=1 is the case which the propeller has the optimum circulation distribution. Table 2 also shows the cavitation effect on propeller noise clearly.

Table 2. Sound pressure level results at different tip loading factors for three bladed propeller

σ	J	k_{tip}	dB
10.2	0.53	0.082	8.13
10.2	0.53	1.000	51.46
4.2	0.53	0.082	23.54
4.2	0.53	1.000	66.87
2.2	0.53	0.082	34.84
2.2	0.53	1.000	78.17

4. Conclusions

Two main arguments have been obtained in this study:

- Effect of tip loading factor has shown that hydrodynamically optimum propeller design does not have the optimum hydroacoustic performance.
- Under critical cavitation number, the cavitation phenomenon triggers the underwater noise. This means that the cavitation affects not only the hydrodynamic performance but also hydroacoustic performance.

Some future works have been planned:

- Tip vortex index (TVI) method will be applied to a four bladed DTMB 4119 model propeller in order to predict the noise level.

References

Bal, S. (2011a). A method for optimum cavitating ship propellers. Turkish Journal of Engineering and Environmental Sciences, Vol. 35, pp. 139-158.

Bal, S. Güner, M. (2009). Performance analysis of podded propulsors. Ocean Engineering, Vol. 36, pp: 556-563.

Bal, S. (2011b). Practical technique for improvement of open water propeller performance. Proceedings of the Institution of Mechanical Engineers, Part M, Journal of Engineering for the Maritime Environment, Vol. 225, Issue 4, pp: 375-386.

Carlton, J. S. (1994). Marine propellers and propulsion. Butterworth Heinemann, London.

Ekinci, S., Celik, F. and Guner, M. (2010). A practical noise prediction method for cavitating marine propellers. Brodogradnja 61 (4): 359–66.

Jeung-Hoon, L., Jae-Moon, H., Hyung-Gil, P. and Jong-Soo, S. (2013). Application of signal processing techniques to the detection of tip vortex cavitation noise in marine propeller. J. Hydrodyn. Ser B, vol. 25, no. 3, pp. 440–449.

Kerwin, J.E. (2001). Hydrofoils and propellers. Lecture Notes, Department of Ocean Engineering, Massachusetts Institute of Technology, USA.

Kim, T., Jeon, J., Chu, S., Kim, S. and Joo, W. (2016). Numerical and experimental prediction methods of cavitation noise radiated by underwater propellers. International Congress on Acoustics, Buenos Aires.

Lafeber, F.H., Bosschers, J. and Wijngaarden, E. van. (2015). Computational and experimental prediction of propeller cavitation noise. OCEANS 2015, Genova

Lidtke, A.K., Humphrey, V.F. and Turnock, S.R. (2016). Feasibility study into a computational approach for marine propeller noise and cavitation modelling. Ocean Engineering.

Raestad, A.E. (1996). Tip Vortex Index-an engineering approach to propeller noise prediction.The Naval Architect.

Salvatore, F. and Ianniello, S., (2003). Preliminary results on acoustic modelling of cavitating propellers. Comput. Mech., vol. 32, no. 4–6, pp. 291–300.

Seol, H. and Lee, S. (2002). Numerical analysis of underwater propeller noise. The 2002 International Congress and Exposition on Noise Control Engineering Dearborn, MI, USA.

Sezen, S., Dogrul, A. and Bal, S. (2016a). Investigation of marine propeller noise for steady and transient flow. The Second International Conference on Global International on Innovation in Marine Technology and The Future of Maritime Transportation (GMC 2016), Bodrum, Turkey.

Sezen, S. (2016). Numerical investigation of ship propeller hydro-acoustics performance. MSc Thesis, Istanbul Technical University, Istanbul.

Sezen, S., Dogrul, A. and Bal, S. (2016b). Tip Vortex Index (TVI) technique for inboard propeller noise estimation. Proceedings of the 1st International Congress on Ship and Marine Technology.

Szantyr, J.A., Flaszyński, P., Tesch, K., Suchecki, W. and Alabrudziński, S. (2012). An experimental and numerical study of tip vortex cavitation. Pol. Marit. Res., vol. 18, no. 4, pp. 14–22.

Wittekind, D. K., (2014). A simple model for the underwater noise source level of ships. Journal of Ship Production and Design, Vol.30, No.1, pp. 7 -14.

Wijngaarden, E.v., Bosschers, J. and Kuiper, G. (2005). Aspects of the cavitating propeller tip vortex as a source of inboard noise and vibration. ASME 2005 Fluids Engineering Division Summer Meeting, 2005.

Zhang, Y. K. and Xiong, Y. (2011). Numerical method for predicting ship propeller cavitation noise. 30th Chinese Control Conference (CCC), pp. 5722–5726.

A Critical Assessment of Measures to Improve Energy Efficiency in Containerships

Volker Bertram[1] , **Ahmet Taşdemir**[2]

volker.bertram@dnvgl.com, atasdemir@pirireis.edu.tr

[1]*DNV GL, Hamburg, Germany*
[2] *Pîrî Reis University, Istanbul, Turkey*

Abstract

Containership operators are confronted with a multitude of proposals for fuel saving measures and even more promises. Actual savings are generally much lower than quoted numbers in advertisement material and even scientific publications. Reasons for discrepancies are discussed and some guidelines for selecting suitable measures are given. There are options with significant fuel savings false promises that result in zero savings or even losses.

Keywords: Energy Efficiency, Fuel Saving, CO2, Container Ships

1. Introduction

Increasing fuel prices and legislation concerning CO2 emissions (respectively energy efficiency) have made fuel efficiency a key topic in our industry. While new designs offer much larger potential gains in energy efficiency, refit and operational measures may in- crease fuel efficiency for the fleet in service, and some of these measures offer attractively short payback times. Bulhaug et al. (2009), OCIMF (2011) and Bertram (2011) give over- views of such measures.

The relative importance of these measures depends on many factors, including ship type. For example, trim optimization is more attractive than hull maintenance for container ships, Fig. 1, Köpke & Sames (2011a). But for large tankers, OCIMF (2011) rates the fuel saving potential of hull maintenance (listed as CBM = condition-based maintenance) higher than trim optimization (listed as trim assistant), namely 2.0% versus 0.3%.

Sometimes the saving potential of an option depends on individual ship hull and propeller characteristics, giving large scatter in reported savings even for same ship type. Modern computer simulations offer substantial progress in assessing saving potential of many de- vices, allowing case-by-case assessment. For example, CFD (computational fluid dynamics) allows quantifying the effect of a propulsion improving device and gives insight ex- plaining why devices are effective in one case and counterproductive in another.

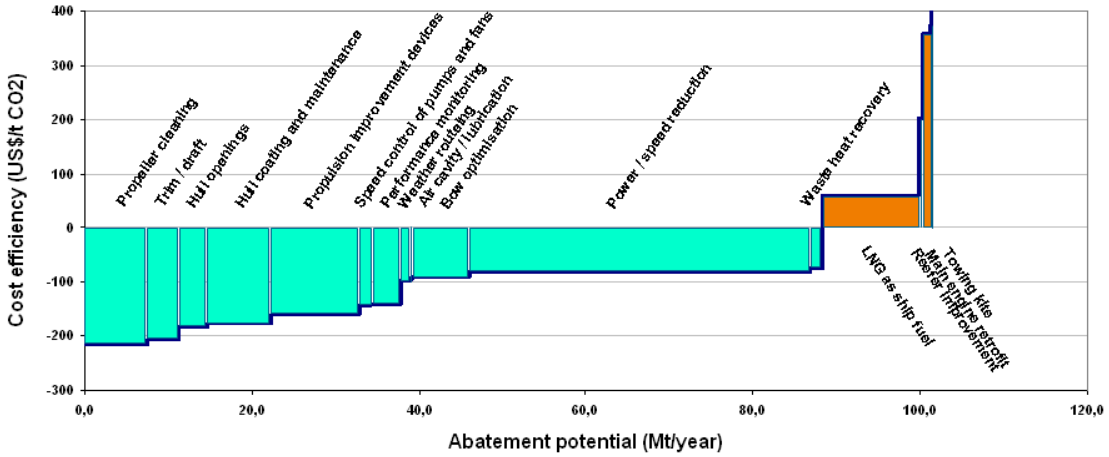

Figure 1. Marginal abatement cost curve for container ship fleet

Many publications give unrealistically optimistic potential for fuel savings. There are various reasons for this:

- The published savings are often for the best case. Quoted savings may be valid for

initially bad designs, whereas hydrodynamically optimized designs would never reach these savings. This is best illustrated in a concrete example: DNV GL Mari- time Advisory Services looked at its hull optimization projects in early 2012. The achieved improvements for all projects until that date were collected in a histogram, Fig. 2.

The statistical distribution may be described in various ways:

- Hull optimization may improve the fuel efficiency of a ship by up to 20%.
- Hull optimization improves the fuel efficiency of a ship by 7% on average.
- Hull optimization improves the fuel efficiency of a ship in most projects by 4-6%.

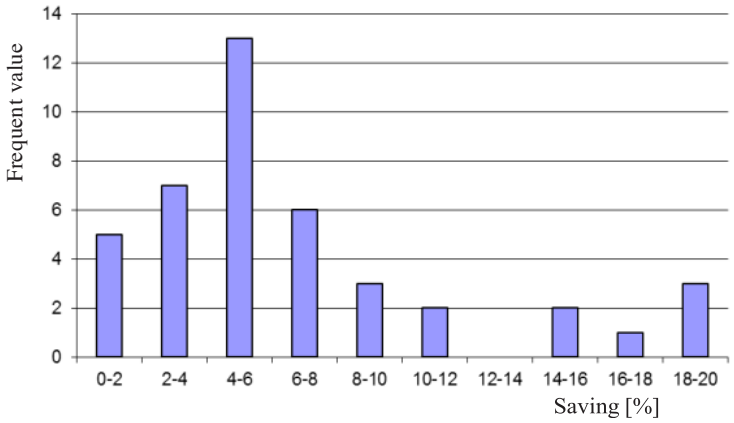

Figure 2. The potential of hull optimization varies. Gains in actual projects show a wide spectrum with 4-6% improvement as most frequent value until end of 2011

All statements are correct. However, “up to X%” is often quoted as “X%” as saving potential in subsequent reports or surveys. Generally, companies do not publish statistical distributions of savings achieved by their products. Instead, marketing strategies promote “up to” numbers which invariably lead to unrealistic expectations and subsequent disillusion.

- Numbers valid for one ship type (say bulk carriers) are taken for other ships (say containerships), where they do not apply.
- Numbers are taken for design speed and draft. Frequently encountered off-design conditions are ignored. Utilization of a fuel saving device is often incorrectly assumed to be 100% of the time at sea for a ship and 100% over fleets for global estimates.
- Saving potential may be measured for calm-water resistance, but real fuel savings apply to total fuel consumption (including added resistance in service and on-board energy consumption). Relating saving to smaller reference numbers gives higher percentage figures. Ideally all savings should be related to (an estimated) total yearly fuel consumption.
- For propulsion improving devices, published savings are based on a comparison of power requirement measured before and after conversion. Sometimes, measurements are not corrected for hull and propeller roughness, while ship and propeller were cleaned during the refit, sea state and loading condition. If measured values are corrected for a "neutral condition", the correction procedure in itself may still have an uncertainty of 2-3%.
- Saving potential is quoted based on model tests and questionable extrapolation to full scale. Model tests violate Reynolds similarity; hence boundary layers and flows at appendages in the boundary layer are not similar. Most quoted figures are based on publications (and model tests) of the 1970s and 1980s. Usually, there is no documentation on how figures were derived. In our experience, re-analyses and detailed full-scale measurements with today's technology showed always substantially lower figures.

2. Some options to improve fuel efficiency of containerships

DNV GL looked into fuel saving options for containerships, with particular focus on fleet in service. The most attractive options are identified in Sames and Köpke (2010), Köpke and Sames (2011a, b). These are discussed in the following in the order of expected payback, see Fig. 1:

a. Propeller cleaning

Propeller roughness increases in time due to cavitation, impingement and fouling. Propeller cleaning intervals should be based on performance monitoring.

b. Trim (optimization)

The wave resistance reacts very sensitively to local changes in the hull geometry. Trim optimization software, e.g. Hochkirch and Mallol (2013), can lead to significant improvement for most ship types, but particularly for container ships. Trim software based on "numerical sea trials" (viscous CFD simulation of ship with propeller at full-scale Reynolds numbers) is our recommended approach, Bertram (2014).

c. Hull openings

Bow thrusters and inlets (e.g. sea chests) may be designed better, again by using CFD. Knowledge about achievable savings is at best anecdotal. The 2nd IMO Green- house Gas study, Buhaug et al. (2009), gives 0.9-4.2% without differentiation for ship type and based on vendor information. The actual saving potential may be lower than 0.9% for many container ships. Large scatter in saving

potential is expected, as losses (and thus improvement potential) will depend on local flow details. CFD analyses are recommended for assessment and guidance in re-design.

d. Hull coating and maintenance

The frictional resistance depends on the area and roughness of the wetted surface. The surface roughness is influenced by the choice of coating and appropriate hull management over the life-time of the ship. Some coatings perform very well initially and then degrade rapidly. Hull performance monitoring has evolved dynamically over the past few years, e.g. Bertram and Lampropoulos (2014). The evolving ISO 19030 (Measurement of changes in hull and propeller performance) is expected to contribute to wider use of hull (and propeller) performance monitoring and management. Hull performance monitoring requires assorted corrections (a.k.a. normalization). Corrections for actual draft and trim are very important for containerships. Simple interpolations between model test predictions give unacceptably high errors for containerships (around 10%), Krapp and Bertram (2015). Instead, extensive CFD simulations are required to give dense interpolation matrices covering the complete operation spectrum for speeds, drafts and trims. Here synergies with trim optimization software should be used.

e. Propulsion improvement devices (PIDs)

Opinions on PIDs scatter widely, from negative effects (increasing fuel consumption) to more than 10% improvements. Indeed, the effectiveness depends on local flow details (such as the strength and position of the bilge vortex in the propeller plane). The effectiveness of PIDs should be assessed on an individual case base, using full-scale CFD simulations, Hochkirch and Mallol (2013). Wake-equalizing ducts are generally not suitable for containerships, as these have already more homogeneous wakes than bulker and tankers. Pre-swirl devices can give improvements typically in the range of 1-4% based on our CFD studies.

f. Speed control of pumps and fans

Speed-controlled (a.k.a. frequency-controlled) of pumps instead of fixed rpm pumps (for cooling water and other systems with high utilization rate) decrease energy consumption for the pumps typically by 25%. The measure has attractive payback periods, but the overall saving potential is relatively small, estimated 0.1 -0.6%.

g. (Engine) Performance monitoring

Engine performance monitoring based on simulation models has developed very dynamically over the past 5 years, e.g. Freund (2012), Lampe et al. (2015). This threshold technology is expected to gain in importance and acceptance in the industry. One of the expected effects is increased awareness leading to more fuel efficient operation by the crew.

h. Weather routing

Realistic estimates for the saving potential of weather routing range from 0.1% to 1.5%, falling significantly short of vendors' claims. The added resistance in waves can be predicted only with uncertainties, which are much larger than the claimed savings due to route optimization, Bertram and Couser (2014). This renders weather routing as a most questionable option for fuel savings. Solid arguments for weather routing are rather safety of cargo and crew.

i. Air lubrication

Air lubrication has attracted considerable media and industry attention. The basic idea is that a layer of air (on part of the hull) reduces the frictional resistance. There is no consensus on the saving potential and, at present, we have no reliable third- party evaluation. Venture capital and entrepreneurial spirit are required to invest into air lubrication.

j. Bow optimization

Hull optimization has progressed over the decades from research applications to state of the art in modern ship design, Hochkirch and Bertram (2012). Modern optimization projects employ numerical sea trials (as for trim optimization), Hochkirch and Mallol (2013), looking at 10-20 thousands of variants. It is becoming common to look at spectra of operational conditions (draft-speed combinations) in the optimization. More recently, bulbous bow refit has been adopted as an attractive option to re- duce fuel consumption, Hochkirch and Bertram (2009, 2013), Hahn and Bertram (2014). It is recommended to explore fuel savings for different operational spectra before deciding on the new bow design.

k. Speed reduction (slow steaming)

Speed reduction is a very effective way to improve fuel efficiency. A 10% lower de- sign speed saves an estimated 23-25% fuel for constant delivery capacity (i.e. increased size of ship or fleet to transport the same amount of cargo per year). Slow steaming is less effective than designing for lower speed as hull, propeller and engine operate in off-design conditions and thus at lower efficiencies. Often refit measures for hull (bow refit), propeller and machinery (e.g. de-rating) are then advisable.

l. Waste heat recovery

The amount of energy that may be recovered from exhaust gas losses depends on the engines used, the exhaust gas temperature and the sulphur content in the fuel. In an expert survey, the saving potential in using heat recovery was estimated to be 2 -7% for ships without power take-in. Many ships already employ this option. Lower installed power and slow steaming reduce the potential for waste heat recovery. Refit- ting waste heat recovery is problematic due to the additional space requirements for the equipment and the already cramped conditions in most engine rooms.

3. Case studies

In following, three case studies will highlight applications of fuel saving measures in practice. The selected case studies from our project experience are “typical”, representative for several projects with savings obtained ranging in the most common group
rather than the “up to” extremes.

3.1 Case study 1: Hull optimization

Ship operator Hamburg-Süd wanted the lines of a new 9600 TEU containership design optimized for fuel consumption, Hochkirch et al. (2013). Hamburg-Süd supplied records of actual operational

data for a fleet of similar-sized containerships for a whole year. This database of speeds and drafts was condensed to four representative clusters of speed-draft combinations with associated weights ranging between 20 and 30%. The objective was then to reduce the combine fuel consumptions for these four operational states, considering their time share in yearly operation. A global hull optimization was performed using a fast, simplified hydrodynamic assessment of the generated hull variants. In a refinement of the hull optimization, the hydrodynamic assessment used a high-fidelity CFD code, solving the Reynolds-averaged Navier-Stokes equations (RANSE), thus capturing viscous effects directly in the simulation.

Fig. 3 compares for one operational condition the computed wave patterns of the baseline design and our optimized design. The relatively small differences in wave patterns translate into significant fuel savings. For this particular operational condition, the required power for the optimized hull was 6.5% lower than for the baseline. For final validation, model tests were conducted at Hamburg Ship Model Basin (HSVA). The baseline design and DNV GL's optimized design were tested under same conditions and full-scale predictions followed the general guidelines. The model tests confirmed that DNV GL's optimized de- sign outperformed the baseline design on all conditions of the operational profile, with expected yearly fuel savings just short of 4%.

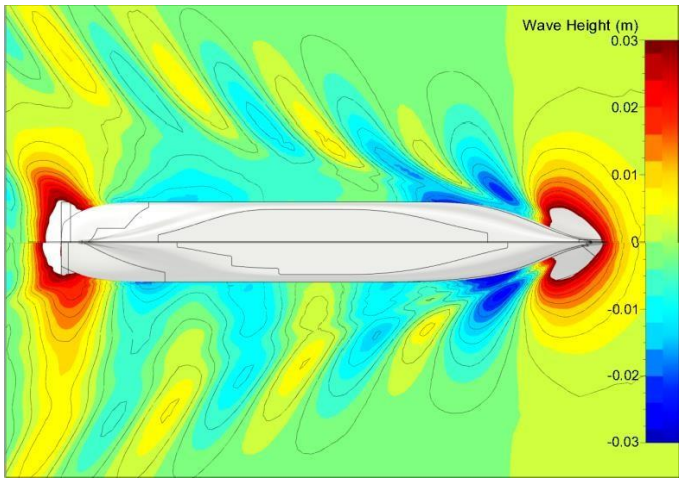

Figure 3. Wave patterns for one operational condition; baseline (top) and optimized design (bottom)

3.2 Case study 2: Bulbous row refit

While obtainable fuel savings are significantly larger for complete hull optimizations, optimization of the bulbous bow region alone offers still potentially very attractive fuel efficiency gains, especially for high powered large containerships which now operate in off- design conditions (slow steaming and partially loaded). State-of-the-art optimization for a realistic operational profile rather than a single design point opens the door to significant further fuel savings, also for refits. This was demonstrated by Hochkirch and Bertram (2013).

The ship owner realized the opportunities of a bulbous bow refit for his fleet of 13000 TEU ships.

The task was now to find the best solution. Qualitatively, the larger the cut-out is chosen, the higher are the cost for the refit, but also the potential gains. In this particular case, there were two general options for such a refit:

- Option 1: Larger cut-out covering the ship below the waterline and before the collision bulkhead
- Option 2: Smaller cut-out below the waterline and before the forward perpendicular

The ship owner supplied records of actual operational data for the ship for a whole year. This database of speeds and drafts was condensed to eight representative clusters of speed- draft combinations with associated weights ranging between 10 and 25%. The objective was then to reduce the combined fuel consumptions for these eight operational states, considering their time share in yearly operation.

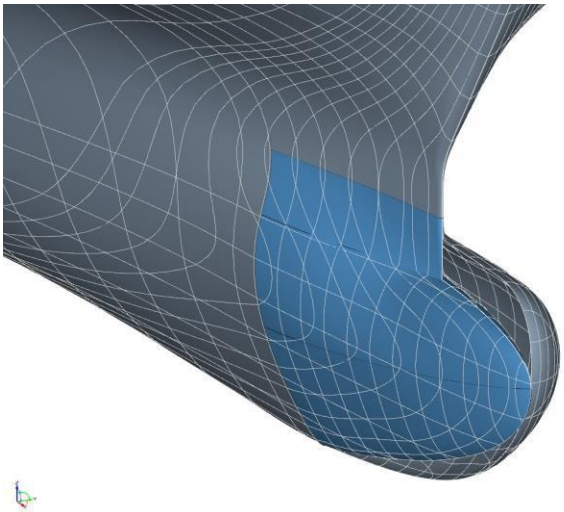

Figure 4. Original hull (port) and re-design alternative (starboard)

A parametric model was set up for the bow section, employing 26 free parameters. The high number of parameters ensured that a vast number of possible bow shapes could be created. In any case, a harmonious fit with the rest of the hull was ensured by suitable constraints on the hull-bow intersection. Roughly 20000 bow variants were investigated. Two final hull shapes were identified featuring optimal performance measures across the operational profile. As expected, the larger flexibility of Option 1 resulted also in larger possible fuel savings. Option 1 had expected gains in off-design conditions of up to 11%, yielding expected yearly fuel savings of ~3.5% for the actual operational profile. Option 2 had expected gains in off-design conditions of up to 6%, yielding expected yearly fuel savings of ~1.8% for the actual operational profile. Results were validated by “numerical sea trials” (high-fidelity CFD simulations for full-scale ship) and model tests.

Depending on size of fleet, employed repair yard and assumed fuel oil price, there are variations in payback times, but all realistic scenarios show payback times between 2 and 8 months, making this refit a good business decision by anybody’s standards.

The biggest issue in many of these projects remains the definition of the operational profile. AIS analyses for own or competitor's fleets can only reflect the past. But frequently questions concern the future and changing market conditions: What if I operate at other conditions some day? Can we change the operational profile once more?

DNV GL has developed a new tool to support better decisions in this situation. First, 5000 - 10000 vessel-specific bow designs are created and assessed for all operational conditions using CFD ("numerical towing tank"). An interactive excel-based tool allows then easy and immediate exploration of "what-if" scenarios for changing operational profiles.

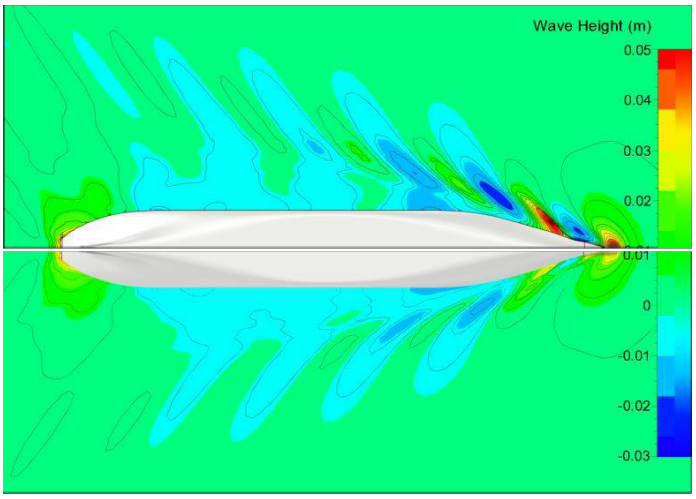

Figure 5. Off-design condition: original hull (top) and optimized Option 1 (bottom)

The input consists of the design operational profile (expressed by a matrix of 4 speeds and 3 drafts with associated relative time spent on each speed-draft combination) for which the bulbous bow shall be optimized, optional performance constraints (e.g. must reach design speed at 85% engine power), and an alternative profile (again 4 x 3 matrix of speed and draft). The tool then immediately displays estimated savings (in USD/year and % power) and payback time for the best bulbous bow for the design operational profile and the corresponding values for the alternative profile. The payback time calculation takes aspects like fleet size, conversion costs and fuel price into account. When changing input data, savings are re-computed instantaneously.

The tool allows insight into available savings for each operational condition, Fig. 6, and implications of constraints. A relaxation of required by power at design speed by 1 percent point often results in higher overall savings. It is only after seeing the achievable effect that ship operators start thinking about margins which are often unnecessarily high. Of course, the tool cannot change the volatility of the market, but it can quantify performance for a bandwidth of scenarios from worst-case to best-case scenarios, supporting more informed business decisions.

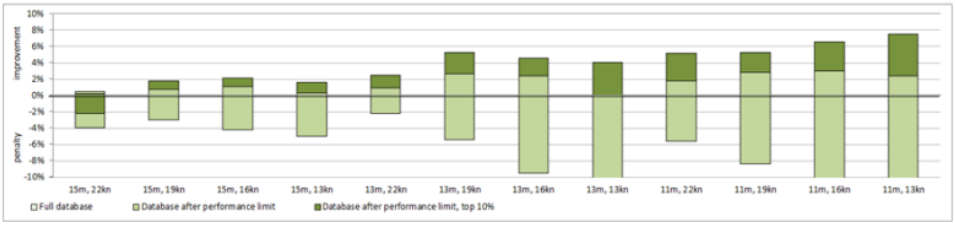

Figure 6. Relative power savings compared to reference design

3.3 Case study 3: Trim optimization

There is no single trim for a vessel that is optimum for all speeds, displacements and water depths, leave alone an optimum single-value for all ships. Finding the optimum trim for a ship is a non-trivial task. There are several commercial trim optimization tools on the market to help with this task. These vary in price, user-friendliness, fundamental approach and performance.

Compared to sensor-based trim assistance tools, CFD-based trim advisory systems do not require interfacing with on-board systems and sensors to monitor operational parameters. DNV GL's ECO-Assistant, Hansen and Hochkirch (2013), can be installed on any computer on the vessel, which makes the installation much more cost effective than sensor-based trim optimization tools. The hydrodynamic database for trim optimization is based solely on CFD simulations. The CFD simulations cover a dense matrix of speed, trim and draft values. The discrete simulation data sets are connected by a multidimensional response sur- face, i.e. a sophisticated interpolation scheme. This allows consistent interpolation for arbitrary input values within the simulated range.

The GUI (graphical user interface) is kept simple with a minimum of input: speed, (zero- speed) drafts aft and fore, and optional extra ballast. The tool then displays optimum trim, regions of good trim (in green), regions of satisfactory trim (in yellow) and regions of poor trim (in red), Fig. 7. In addition, the savings (as compared to even trim) in required power and tons of fuel and CO_2 per day are displayed. Practical constraints such as bending moment and stability are checked by other software tools. To support efficient cross-referencing, the ECO-Assistant can be integrated into a vessel's loading computer and cargo planning system.

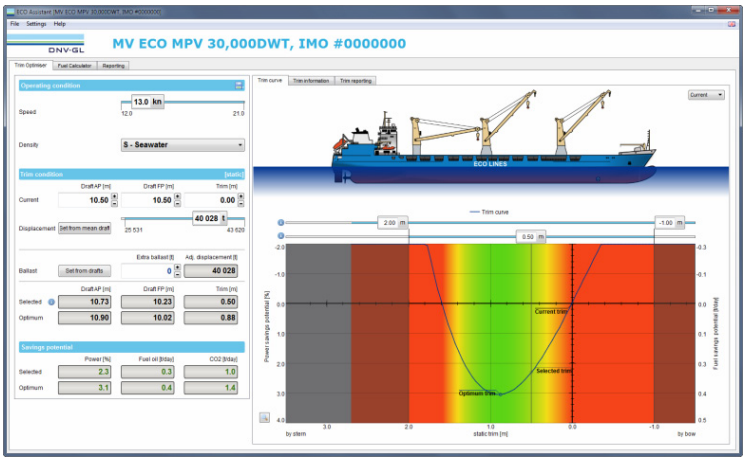

Figure 7. The easy-to-use interface has become a trademark of ECO-Assistant. Speed, displacement (or current drafts) and optional extra ballast is all that is needed to get the best trim displayed.

The effectiveness of trim optimization systems is best assessed sea trials. Trim trials are variations of classical sea trials. Typically, two conditions are tested: One trim with relatively high fuel consumption and another trim with lower fuel consumption. Sea trials on opposite course and for different main engine rpm yield speed-power curves for both trim conditions. By comparison, the fuel savings due to trim are identified. Such trials were completed successfully by China Shipping for a 14000 TEU containership. For a trim change of 1.8 m, fuel savings of more than 10% were found in line with ECO-Assistant's prediction. Such large trim adjustments are not always possible in actual operation. However, China Ship- ping reported in long-term performance monitoring fuel savings up to 8%; typically 3-4% savings were reported.

4. Conclusions

Our experience shows that potential for fuel savings is often over-estimated, but sometimes also underestimated. Frequently, modern simulation technology can guide us:

a. Virtual try-outs are highly recommended before committing to any large investment in propulsion improving devices. CFD simulations give a solid ground for assessing the fuel saving potential of a device and hence the basis for an investment decision.
b. Optimization is a mature and powerful tool in fuel efficient designs and operation. It is mainly up to the ship operators to employ this tool to achieve major savings at relatively little expense.
c. Refitting optimized bows on containerships operating now with much lower speeds than their original design speeds is an attractive option.
d. Trim optimization is attractive for most ship types, especially large container ships. The recommended approach is using CFD for full-scale conditions to create the required hydrodynamic knowledge base.
e. CFD-based knowledge bases for trim optimization should be reused for hull performance management.

References

Bertram, V. (2011). Practical ship hydrodynamics. 2nd Ed. Oxford: Butterworth and Heinemann.

Bertram, V. (2013). Trim optimization meets hull performance monitoring. Lloyd's Maritime Academy Seminar "Hull Management and Performance", London.

Bertram, V. (2014). Trim optimization – Don't blind me with science. The Naval Architect, September, pp.66-68.

Bertram, V. and Couser, P. (2014). Computational methods for seakeeping and added resistance in waves. 13th Conf. Computer and IT Applications in the Maritime Industries (COMPIT), Redworth, pp.8-18.

Bertram, V. and Lampropoulos, V. (2014). A model for hull performance monitoring in ship operation, European Conf. Production Technologies in Shipbuilding (ECPTS), Hamburg.

Buhaug, Ø., Corbett, J.J., Endresen, Ø., Eyring, V., Faber, J., Hanayama, S., Lee, D.S., Lee, D., Lindstad, H., Markowska, A.Z., Mjelde, A., Nelissen, D., Nilsen, J., Pålsson, C., Winebrake, J.J., Wu,

W.Q., Yoshida, K. (2009). Second IMO GHG study 2009. International Maritime Organization (IMO), London.

Freund, M. (2012). Holistic analysis of on-board consumption and efficiency of the energy systems of ships. PhD Thesis, Univ. Federal Armed Forces, Hamburg.

Hahn, C. and Bertram, V. (2014). Bulbous bow refits – The industry catches on. The Naval Architect, June.

Hansen, H. and Hochkirch, K. (2013). Lean ECO-Assistant production for trim optimization. 12th Conf. Computer and IT Applications in the Maritime Industries (COMPIT), Cortona, pp.76-84.

Hochkirch, K. and Bertram, V. (2009). Slow steaming bulbous bow optimization for a large containership. 10th Conf. Computer and IT Applications in the Maritime Indus- tries (COMPIT), Budapest, pp.390-398.

Hochkirch, K. and Bertram, V. (2012). Hull optimization for fuel efficiency – Past, present and future. 11th Conf. Computer and IT Applications in the Maritime Industries (COMPIT), Liege, pp.39-49.

Hochkirch, K. and Bertram, V. (2013). Bulbous bow refits – A little-known goldmine. Hansa 150/11, pp.27-29.

Hochkirch, K., Heimann, J., Bertram, V. (2013). Hull optimization for operational pro- file – The next game level. 5th Int. Conf. on Computational Methods in Marine Engineering (MARINE), Hamburg.

Hochkirch, K. and Mallol, B. (2013). On the importance of full-scale CFD simulations for ships, 12th Conf. Computer and IT Applications in the Maritime Industries (COM- PIT), Cortona, pp.85-95.

Köpke, M. and Sames, P. (2011a). Outlook on CO_2 emissions of the container world fleet and possible reduction targets. 8th Annual Green Ship Conf., Copenhagen.

Köpke, M. and Sames, P. (2011b). Outlook on CO_2 emissions of the worldwide containership fleet and possible reduction targets. Nonsto 2/2011, Germanischer Lloyd.

Krapp, A. and Bertram, V. (2015). Hull performance monitoring – Combining big data and simulation. 14th Conf. Computer and IT Applications in the Maritime Industries (COMPIT), Ulrichshusen, pp.57-63.

Lampe, J., Magdanz, A., Ginnetti, A. (2015). Energy simulation for waste heat recovery systems. 17th Int. Conf. Computer Applications in Shipbuilding (ICCAS), Bremen.

OCIMF (2011). GHG emission-mitigating measures for oil tankers – Part A: Review of reduction potential. Oil Companies International Marine Forum, London.

Sames, P. and Köpke, M. (2010). Future required energy efficiency of container vessels. 32nd Motorship Propulsion & Emissions Conf., Hamburg.

An Alternative Superior Combustion Mechanism that can Convert Domestic Production Marine Diesel Engines to 100% Natural Gas Fuels

Rafig Mehdiyev[1], Ahmet Dursun Alkan[2*], Mustafa Ünar[3], Ömür Karataş[4]
alkanad@yildiz.edu.tr

[1] Department of Mechanical Engineering , Gebze Technical University, Kocaeli, Turkey
[2]Department of Naval Architecture and Marine Engineering, Naval Architecture and Maritime Faculty, Yıldız Technical University, Istanbul, Turkey
[3]Nurdeniz Denizcilik San. Ltd. Şti., Istanbul, Turkey
[4]ORTECH Marine A.Ş., Istanbul, Turkey

Abstract

In this article some industrial application results of a novel combustion mechanism so-called MR-Process developed by R. Mehdiyev have been reported. The MR-Process combustion mechanism realised in a twin turbulence swirl combustion environment gives the opportunity to combine advantages of both Diesel and Otto cycles in a single structure. In addition, the current status of the heavy duty diesel engine TLM16V185, a product of TÜLOMSAŞ A.Ş., in terms of efficiency and emission, the advantages of MR-Process combustion mechanism allowing to use CNG and LNG fuels as being primary fuel of the near future. A brief information on the development of innovative and competitive domestic brand engines with 6-8-12-16 cylinders ranging from 500 to 2800 kW for various possible applications from civil to defence ships, locomotives, work machines, generators and power plants being adoptable for local and global market.

Keywords: Heavy duty engine, "MR-Process" combustion mechanism, Diesel and Otto, NOx Emission, CNG / LNG fuel.

Yerli Üretim Gemi Dizel Motorlarının %100 Doğal Gaz Yakıtına Dönüşümünü Gerçekleştirebilen Alternatif Üstün Bir Yanma Mekanizması

Rafig Mehdiyev[1], Ahmet Dursun Alkan[2*], Mustafa Ünar[3], Ömer Karataş[4]
alkanad@yildiz.edu.tr

[1] Department of Mechanical Engineering , Gebze Technical University, Kocaeli, Turkey
[2]Department of Naval Architecture and Marine Engineering, Naval Architecture and Maritime Faculty, Yıldız Technical University, Istanbul, Turkey
[3]Nurdeniz Denizcilik San. Ltd. Şti., Istanbul, Turkey
[4]ORTECH Marine A.Ş., Istanbul, Turkey

Özet

Makalede R. Mehdiyev tarafından geliştirilmiş ve Türkiye yerli motor üretici firmalarla yapılan ortak Ar-Ge projeleri ile kanıtlanmış Çift Türbülanslı Döngü ortamında gerçekleştirilen yeni MR-Process yanma mekanizmasının özellikleri, aynı konstrüksiyon yapıda Dizel ve Otto çevrimlerinin gerçekleştirilmesine imkan veren yeni tasarım MR-2 yanma odası hakkında bilgiler sunulmaktadır. Ayrıca, TÜLOMSAŞ A.Ş. üretimi TLM16V185 tipi ağır dizel motorunun verim ve emisyon açısından mevcut durumu, günümüz en etkin alternatif teknoloji olarak daha verimli ve düşük emisyonlu, yakın geleceğin ana yakıtı olarak CNG ve LNG doğal gazlarla çalışma imkânı veren "MR-Process" yanma mekanizması kullanılarak, bu motor bazında ülkemizde ve dünyada kabul edilebilir, Sivil ve Askeri amaçlı gemiler, lokomotifler, iş makineleri, jeneratörler ve enerji santralleri için gücü 500 - 2800 kW arasında değişen, 6-8-12-16 silindirli Yenilikçi ve Rekabetçi Yerli Marka motorların geliştirilmesi hakkında özetle bilgiler de sunulmaktadır.

Anahtar kelimeler: Ağır Dizel motorları, "MR-Process" Yanma Mekanizması, Dizel ve Otto çevrimleri, NOx Emisyonu, CNG/LNG yakıtları.

1. Giriş

Dünya ticaret taşımacılığının yaklaşık % 70'nı gerçekleştiren Gemilerde ürettiği güç başına daha az ve nispeten ucuz yakıt kullanıldığı için esasen Dizel motor kullanılmaktadır. Denizler ülkesi ve denizci ülke Türkiye'nin gemi sanayi sektörü, katma değeri ve istihdam sağlama açısından öncü konumdadır. Öncülüğü daha da ileri götürmek için yurtdışına bağımlılık oranını düşürmeye ihtiyaç vardır. Bilim, Sanayi ve Teknoloji Bakanlığımız, Türkiye'nin yıllık 3 milyar dolar dış ticaret açığına sebep olan Ağır Dizel Motorlarına ihtiyacının ve yerli üretimle onun karşılanmasının önemli olduğunu açıklamıştır (Dünya gazetesi, 11.03.2015). Bu bakımdan Eskişehir'deki TÜLOMSAŞ Lokomotif ve Motor A.Ş.'de yerli marka olarak üretilmekte olan TLM16V185 tipi ağır dizel motorların performans ve verim açısından, özel olarak ise kirletici egzoz gaz emisyonları açısından uluslararası

günümüz taleplerine uygun hale getirilerek Güncel İpek Yolu'nun kara ve deniz güzergâhlarında kullanılması önem arz etmektedir.

Son yıllarda İçten Yanmalı Motorlar (İYM) üzerinde yapılan çalışmaların büyük bir kısmı, mevcut motorları emisyon standartlarına uyacak şekilde elden geçirme ve yenilerini bu standartları sağlayacak şekilde üretme üzerinedir. Standartlar daha da sıkılaştıkça Partikül Filtreler ve AdBlue, ya da SCR gibi yeni teknolojiler motorlara eklenmeye başlanmıştır. Bütün bu teknolojik gelişmeler emisyon hedeflerini karşılasa da, motor yapımını karmaşıklaştırmış, Enerji Verimini kötüleştirmiş ve gerek ilk yatırım, gerekse de işletme maliyetlerini fark edilecek derecede artırmıştır. Bu durum, dizel motorları ile donatılmış şehir içi ulaşım araçları gibi, Lokomotif, Gemi ve Jeneratör motorların da çevreci ve ucuz olan CNG ve LNG gibi %100 Doğal Gaz (NG) yakıtlarına dönüştürülmesini gündeme getirmiştir. IMO MEPC'nin son günlerde aldığı karara göre 2020 yılına dek Gemi motorların egzoz gazlarıyla sülfür - SO_2 salımı da %0.5'i aşmamalıdır. Bunun üçün ise en etkin yol olarak Gemi motorların %100 NG yakıtına dönüşümü öngörülmektedir.

Hâlihazırda bu amaçla yaygın olarak motorun Dizel çevriminden Otto çevrimine dönüştürülme (buji ile tutuşma) yöntemi kullanılmaktadır. Lakin yüksek sıkıştırma oranına sahip olan (>14:1) mevcut dizel motorun %100 NG yakıtına dönüştürüldüğünde vuruntu olayı meydana çıkmasın diye, motorun pistonu üzerindeki açık yanma odası hacmini artırarak sıkıştırma oranını 10,5:1 ve 11:1 seviyelerine dek düşürmek zorunluluğunu meydana getirmiştir. Silindirik geometriye sahip olan bu tip yanma odalı pistonların (Şekil 1.) sıfırdan üretilmesini gerektirmektedir. Bu ise mevcut dizellerin NG yakıtlarına dönüştürülme işlemlerini zorlaştırmakta, maliyetini ise önemli ölçüde artırmaktadır. Diğer taraftan, sıkıştırma oranının düşürülmesi bu motorların orijinal halindekine nispeten daha düşük performans ve verimlilikle çalışmasına neden olmaktadır. Bu yüzden motorun performansını fazla düşürmemek ve buji ile tutuşmanın istikrarlı bir şekilde gerçekleşmesini sağlamak için hava fazlalık katsayısını λ=0,90-1,05 değerlerinde tutmayı gerektirmektedir. Bu durumda, Dizel Çevriminde olduğu gibi, NOx emisyonunun artışı kaçınılmaz olmuştur. Bu ise EGR ve AdBlue gibi ek emisyon düşürücü sistemler kullanmağı mecburi hale getirmiştir´(Vesttergard, 2014). Bundan başka, %100 NG yakıtına dönüştürülen motorun dizel çevrimi ile mukayesede daha zengin karışımlarla çalıştırılma gereği (λ>1.5'e karşın λ=0.90-1.05), Küresel ısınma probleminin çözümüne ters olarak, sera etkili karbon dioksit - CO_2 emisyonun da ek olarak %8-%10 civarında artışına sebep olmuştur (Dinc ve diğerleri, 2009).

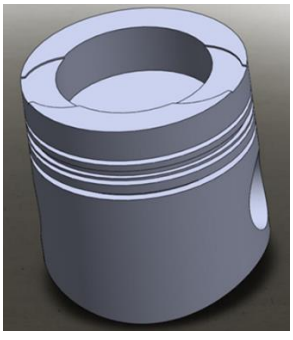

Şekil 1. Günümüz dizel motorların Otto çevrimi ile %100 NG yakıtına dönüştürmek için kullanılan konvansiyonel yanma odası.

Makalede Dizel ve Otto çevrimlerini aynı konstrüksiyon yapıda gerçekleştirebilmesini sağlayan, bununla da yapısal değişikler yapılmadan, dizelin mevcut sıkıştırma oranı ve yanma odasını koruyarak %100 NG yakıtına dönüşümüne imkan veren MR-Process Yeni Yanma Mekanizması ve bu mekanizmanın farklı motorlar üzerinde uygulama çalışmaları hakkında bilgiler sunulmaktadır. Ayrıca, TÜLOMSAŞ A.Ş. üretimi TLM16V185

tipi ağır dizel motorunun verim ve emisyon açısından mevcut durumu, günümüz en etkin alternatif teknoloji olarak daha verimli ve düşük emisyonlu, yakın geleceğin ana yakıtı olarak NG yakıtla çalışma imkânı veren MR-Process yanma mekanizması kullanılarak, bu motor bazında ülkemizde ve dünyada kabul edilebilir, Sivil ve Askeri amaçlı gemiler, lokomotifler, iş makineleri, jeneratörler ve enerji santralleri için gücü 500 - 2800 kW arasında değişen, 6-8-12-16 silindirli Yenilikçi ve Rekabetçi Yerli Marka motorların geliştirilmesi hakkında özetle bilgiler de sunulmaktadır.

2. MR-Process yanma mekanizmasının özellikleri

Azerbaycan Teknik Üniversitesinde (AzTÜ, Azerbaycan) Rusya Bilimsel Akademisinin N. Semyonov adına Kimyasal Fizik Enstitüsü (IXF, Moskova) ve Varşova Teknik Üniversitesi (WP, Polonya) ile işbirliği kapsamında kademeli dolgulu motorlarda yanma sürecinin özellikleri çeşitli fiziksel modeller (“bomba”), hassas basınç kaptörleri ve osiloskop, alev cephesini görüntüleyen Şileren hızlı fotoğraf cihazı vb. kullanılarak detaylı bir şekilde incelenmiştir (Mehdiyev ve diğerleri, 1978) & (Mehdiyev, 1983) & (Mehdiyev ve Wolanski, 2000). Bu çalışmalarla zengin karışımın YO'da kapsadığı hacim oranının, başka bir deyişle karışımın kademelenme derecesinin yanma hızı ve basınç artışına, kirletici emisyonların miktarına etkisini belirleyebilecek bir dizi deneyler yapılmıştır. Bir örnek olarak Şekil 2'de kademelenme derecesinin yanma hızı ve basınç artışına etkisini açıklayan

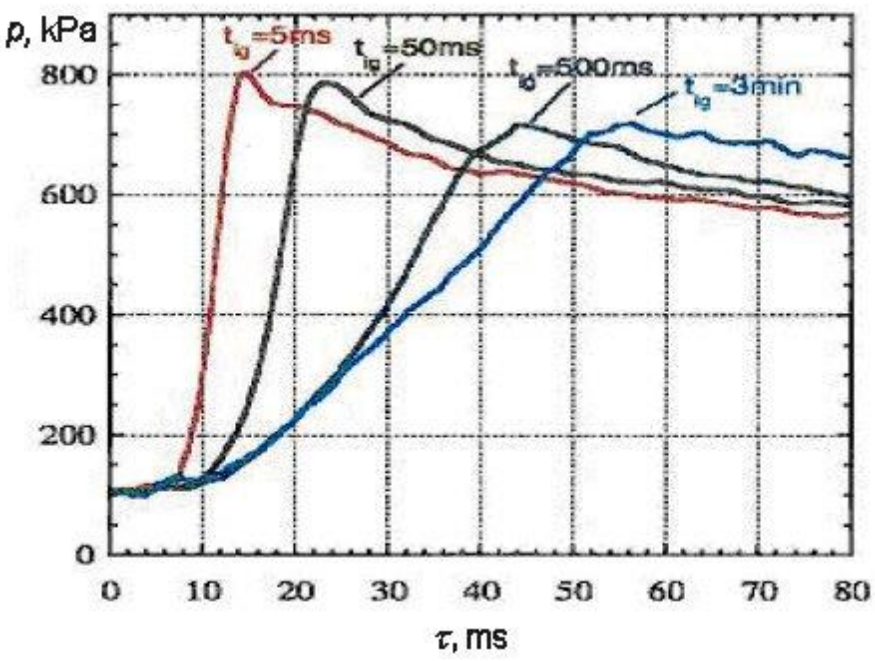

Şekil 2. C_3H_8/hava karışımın kademelenme derecesinin yanma süresi ve basınç artışına etkisi.

grafikler gösterilmiştir. Bu deneylerde karışımın çeşitli kademelenme derecesi YO'nın fiziksel modeline önceden doldurulmuş hava içerisine zengin bileşimli (λ_1=0,6) propan (C_3H_8) + hava karışımını püskürttükten sonra bujiden ateşleme (kıvılcımın verilme) zamanını değiştirmekle elde edilmiştir. Şekildeki yanma basıncının artış grafikleri t_{ig}=5, 50, 500 *ms* ve 3 *min (dak)* ile gösterilmiş ateşleme zamanlarıyla dört kademelenme derecesine sahip genel bileşimi λ=1 olan karışımın yakılmasıyla elde edilmiştir. Ateşleme geciktirildikçe (t_{ig} arttıkça) zengin karışımın hava ile karışma zamanı arttığından dolayı karışımın kademelenme derecesi azalarak homojen yapıya sahip olmaktadır. Şekilde t_{ig}=5 *ms* olduğunda en yüksek derecede kademelenmiş karışımın

yanması, t_{ig}=3 *min* olduğunda ise kademelenmesi sona ermiş homojen karışımın yanması ile elde olunan basınç artış grafikleri gösterilmiştir. t_{ig}'nin ara değerlerinde basıncın değişme grafikleri kademelenme derecesinin de ara değerlerinde elde edilmiştir. Şekilden görüldüğü gibi, karışımın kademelenme derecesi arttıkça (t_{ig} küçüldükçe) yanma, hız kazanarak basıncın maksimum değerini artırmaktadır. Örneğin, homojen karışım (t_{ig}=3 *min)* yandığında basınç, maksimum değerine (710 *kPa*) τ=55 *ms* geçtikten sonra ulaşmasına rağmen, en yüksek derecede kademelenmiş karışım (t_{ig}=5 *ms)* yandığında yanma süresi τ=14 *ms* olmakta (yani yanma hızı 3,9 kat artmakta), yanma basıncı ise 800 *kPa* değerine ulaşmaktadır (%12 artmaktadır).

Fiziksel modelde elde edilmiş pozitif sonuçların sebebini açıklamak için özel matematik modeller kullanılarak incelemeler esasında tespit edilmiştir ki (Mehdiyev, 1983) & (Mehdiyev ve Wolanski, 2000), birinci aşamada zengin karışımın (λ_1=0,6-0,8) yanmasıyla oluşan eksik yanma ürünleri olan karbon monoksit (CO) ve serbest hidrojen (H_2), ikinci aşamada hava ile karışarak yanma işlemini hızla sona erdirmektedirler. Birinci aşamada hava yetersizliği yüzünden oluşabilen $2C+O_2=2CO$ stokiyometrik reaksiyonunda C'nin CO'ya dek oksitleşmesi için bir mol O_2 tüketilirken, iki mol CO oluşturulmaktadır. Böylece bu reaksiyonla karbon, içerdiği ısı enerjisini tam olarak açığa çıkaramamış olsa bile, sabit hacimde CO'nun mol sayısının aynı karbon (C) ile elde edilebilecek CO_2 mol sayısına kıyasla iki kat artması yanma basıncını yükseltmektedir. H_2'nin etkisiyle aşırı hızla gerçekleşen yanma işleminin ikinci aşaması su buharının (H_2O) katkısı ile CO'nun da hızla yanıp bitmesine, böylece C'nin geriye kalmış enerjisinin de tam olarak açığa çıkmasına sebep olmaktadır. Bununla da aynı genel yakıt/hava oranında kademelenmiş karışımın iki aşamalı yanma mekanizması ile yakılmasının yanma hızı ve basıncın yükseltilmesi bakımından daha avantajlı olduğu gözlenmiştir. Ayrıca, bu durumda NO_x emisyonu artmamakta, tam aksine, oluşan NO_x miktarı, aynı bileşimli homojen karışımın yanmasıyla oluşan NO_x miktarına göre iki-üç kat düşmektedir. Bunun sebebi, yanma sürecinin birinci aşamasında NOx oluşumu için HC'ların yanma reaksiyonları bittikten sonra geriye oksijenin kalmaması, ikinci aşamasında ise yanma hızının yüksek olmasından dolayı NOx oluşumu için yeterli zamanın olmamasıdır. Bu çalışmalarla kademelenmiş karışım kullanıldığında CO ve HC emisyonlarının da büyük bir miktarda düşmesi gözlenmiştir (Mehdiyev ve Wolanski, 2000).

Fiziksel modeller ve farklı boyutlu motorlar üzerinde yapılan bir dizi deneysel çalışmaların sonuçlarına dayanarak Prof. R. Mehdiyev tarafından, sembolik olarak "MR-Process" adlandırdığı İki Aşamalı Yanma Mekanizmasını Çift Türbülanslı Döngü ortamında gerçekleştirebilen MR-2 Yanma Odası geometrisi teklif edilmiştir. Ayrıntılı bilgiler (Mehdiyev, 1983) & (Mehdiyev ve Wolanski, 2000)'de verilmiş bu Yanma Odasının seması ve yanma sürecinin fiziksel modelde gerçekleştirilen anlık fotoğrafları Şekil 3'te gösterilmiştir. Şekilde görüldüğü gibi, Yanma Odasının özelliği, geometrisinin "8"e benzeyen iki eşit bölgeye ayrılmasıdır. Emme ve sıkıştırma süreçlerinde yanma odasının bu bölgelerinde farklı yöntemlerle birbirinin tersine aynı hızda dönen iki türbülanslı döngü hareketi oluşturulur. Yanma Odasının buji yerleşen bölgesinde bileşimi λ=0,6...0,9 arasında değişen zengin karışım, diğer bölgesinde ise sadece hava yer almaktadır. Her iki döngü aynı hız ve momentuma sahip olduğundan dolayı, iki bölgedeki dolgu ateşleme anına dek birbirleriyle karışamamakta ve böylece motorun tüm çalışma rejimlerinde yakıt-hava karışımı kademelenmiş şeklini korumaktadır. Döngüler emme zamanından itibaren gerçekleştirildiği için yakıt-hava karışımını da bu süreçte silindirin dışında (manifoltta) oluşturmak ve günümüzde seri üretimi yaygınlaşmış elektronik sıvı ve gaz yakıtları püskürtme sisteminden (hatta karbüratör veya gaz karıştırıcısından) yararlanmak mümkündür.

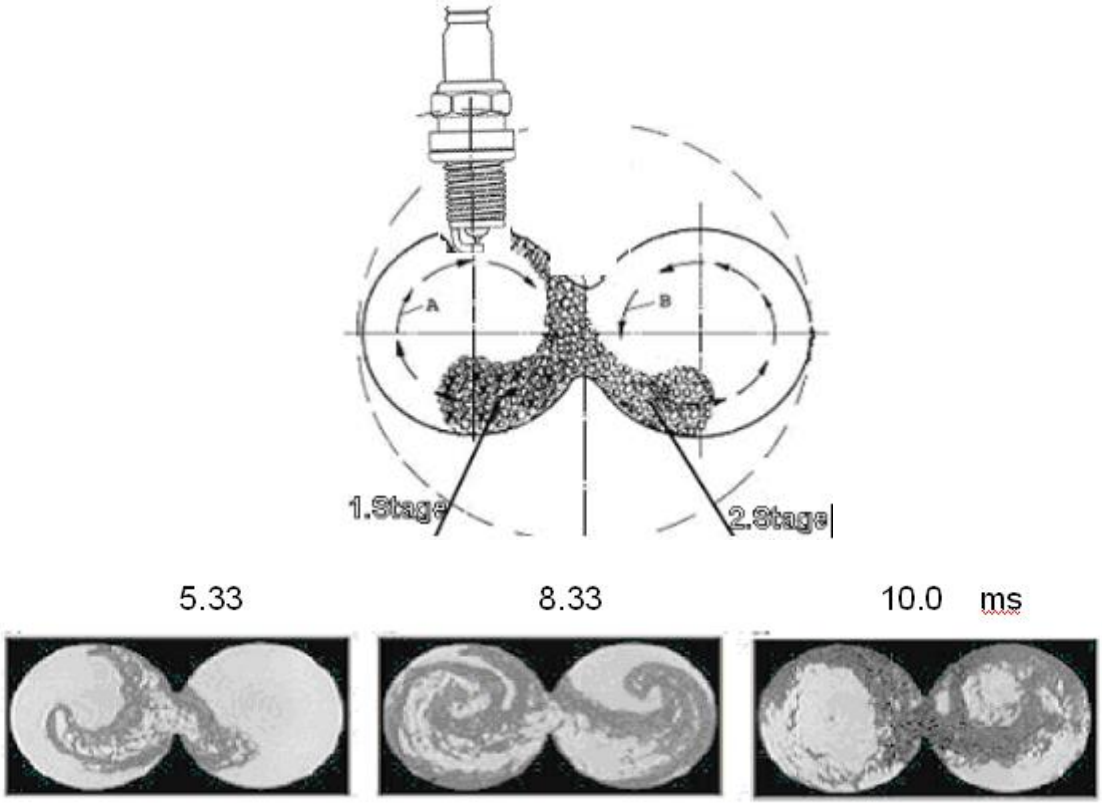

Şekil 3. Çift döngülü MR-2 Yanma Odasının şeması
ve fiziksel modelde yanma sürecinin anlık fotoğrafları (Mehdiyev, 1983).

MR-2 YO'sının diğer bir avantajı, sıkıştırma oranını vuruntu oluşturmadan optimum seviyelerine dek (ε=14-17) yükseltme imkanının olmasıdır. Odanın bir bölgesinde zengin karışımın (λ=0,6-0,9) yakılması ile oluşan eksik yanma ürünlerin (*CO* ve H_2), ikinci bölgesinde ise hızla dönen türbülanslı ortamda yanabilmesi nedeniyle vuruntu olayı önlenmektedir. YO'nın diğer bir avantajı, konvansiyonel YO'larında soğuk cidarlarda kaçınılmaz olan alev cephesinin sönme olayının önlene bilinmesidir. Bunun sebebi, Şekil 3'ten de görüldüğü gibi, yanma sürecinin birbirinin tersine dönen türbülanslı ortamda gerçekleştirilmesiyle alev cephesi YO'nın sağ ve sol cidarlarından yanmamış karışımı sıyırıp odanın merkezine – en sıcak bölgesine sürükleyerek oksitlenme reaksiyonların alev sönmesi olmadan devam edebilmesidir. Böylece, söz konusu YO bir taraftan motorun tüm yük rejimlerinde genel bileşimi fakir olan (λ =1,3...2,0) en yüksek derecede kademelenmiş yakıt-hava karışımın İki Aşamada Yanma Mekanizması ile yakılması, diğer taraftan yüksek sıkıştırma oranının (ε=14...17) kullanıla bilinmesi ve alev cephesinin sönme olayının önlenmesi gibi temel şartların sağlana bilinmesi sayesinde, farklı boyutlu motorlar üzerinde yapılan testlerle de kanıtlanmış, verimli ve düşük emisyonlu motor geliştirmeyin mümkün olduğunu göstermektedir (Dinc ve diğerleri, 2009) & (Mehdiyev ve Wolanski, 2000) & (Mehdiyev ve diğerleri, 2009).

3. MR-Process yanma mekanizması ile çalışan dizel motoru

Çift Türbülanslı Döngü ortamında gerçekleşen MR-Process Yanma Mekanizması, sıkıştırma oranını yükseltmek imkanı verdiği için Kendinden Tutuşma Prensibi ile, başka bir değişle, Dizel Prensibi ile çalışabilen motorun geliştirilmesine de vesile olmuştur. Dizel Çevrimi ile çalıştırılması öngörülen motorun Çift Döngülü MR-2 yanma odalı pistonu ve yanma sürecinin simülasyon resmi Şekil 4'de gösterilmiştir.

Göründüğü gibi, MR-2 YO piston üzerinde sekize benzer şekilde tasarlanmıştır. YO oyuğunda yanma işleminden önce birbiriyle aynı hızda ve ters yönde dönen çift hava döngüleri oluşturulmaktadır. Yakıt, iki delikli enjektörün yardımıyla düşük basınçta (<350 *bar*) çift hava döngüleri yönünde teğet olarak püskürtülerek, yaklaşık %95'e varan miktarı duvara sıvanmakta ve mikro kalınlıkta bir tabaka (film) oluşturmaktadır. Yakıt tabakasının duvarla doğrudan temasta olması ısı transfer katsayısının kat kat artışına sebep olmakta ve sıkıştırılmış hava sıcaklığına nispeten duvarın yaklaşık 2 kat düşük sıcaklıkta olmasına rağmen (< 400 ^{o}C), yakıtın yeterince çabuk buharlaşması gerçekleşmektedir.

Buharlaşma düşük sıcaklık ortamında gerçekleştiği için yakıt, tutuşmadan önce doğal hidrokarbon yapısını korumakta ve klasik homojen karıştırma yönteminden farklı olarak, piroliz prosesine (CH'nin C *ve* H'ya parçalanmasına) maruz kalmamaktadır. Sonuçta, eksik yanma ürünleri olan C veya PM- partikül madde emisyonu epey azalmaktadır. Yanma sürecinin ters yönlü türbülanslı hava döngüleri ortamında gerçekleşmesi ise, alev cephesinin nispeten soğuk cidarlarda sönmesini engelleyerek, CO ve HC'in de azalmasına, böylece yanma veriminin yükselmesine sebep olmaktadır. Ayrıca, yanma süreci yakıtın buharlaşma sürecini takip ettiği için yanma sırasındaki basınç artış hızı azalmaktadır. Bu durumda "Mach etkisi" ile yanmış ürünlerin sıcaklığının ilaveten artırılması önlenerek, NOx ve Gürültü emisyonları da azaltılmakta ve böylece optimum hızla gerçekleşen yanma süreci elde edilmektedir.

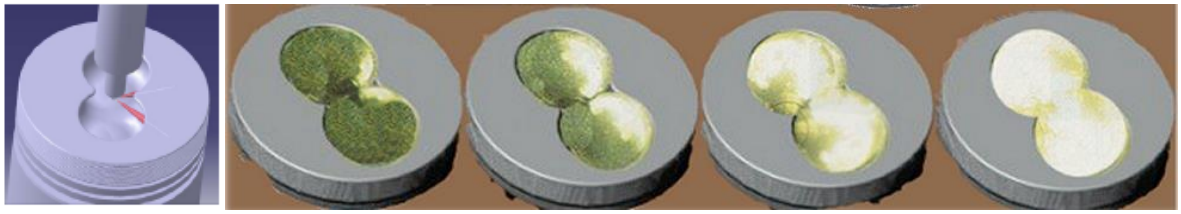

Şekil 4. Çift Döngülü MR-2 yanma odasında "MR-Process" Yanma Mekanizmasının Dizel Prensibi ile gerçekleştirilme şeması.

Teorik olarak öngörülen bu beklentileri deneysel olarak kanıtlamak için İstanbul Teknik Üniversitesi Motorlar ve Taşıtlar Laboratuvarında özel olarak tasarlanan tek silindirli bir model dizel motor (S/D=95/85 *mm*) bazında deney düzeneği yapılandırılmıştır. Şekil 5'de dört supaplı model motorun çiftleştirilmiş emme ve egzoz portları ve yakıt püskürtme enjektörü ile bir arada üç boyutlu montaj resmi gösterilmiştir. Piston üzerindeki 8'e benzer yanma odasında emme sürecinden başlayarak oluşturulan çift hava döngüleri, birbirinin tersine helisel çıkışları olan çiftleştirilmiş emme portunun (2) araçlığı ile elde edilmektedir.

Farklı yük ve hız rejimlerinde deney motorun ayarlama, performans ve emisyon testleri esnasında indikatör diyagramları çıkarılmış ve yanma analizi yapılmıştır. Şekil 6'da motorun farklı yanma odaları ile çalıştığında yakıt püskürtme avansının (θ) optimum değerlerinde çıkarılmış indikatör diyagramları karşılaştırılmıştır. Buradan görüldüğü gibi, her iki halde yakıt püskürtme basıncının maksimum değeri yaklaşık aynı - p_y= 220-230 *bar* seviyesinde, yanma basınçların maksimum değeri (p_z) ve oluşma zamanları ise birbirinden farklıdır.

Konvansiyonel yanma odası kullanıldığında optimum yakıt püskürtme avansı $\theta = 15^0$ *CA* olduğu için tutuşma, ÜÖN (TDC)'den 5^0 önce – $\varphi = 355^0$'de gerçekleşmiştir. Bu anda silindir içinde basınç p_c=45

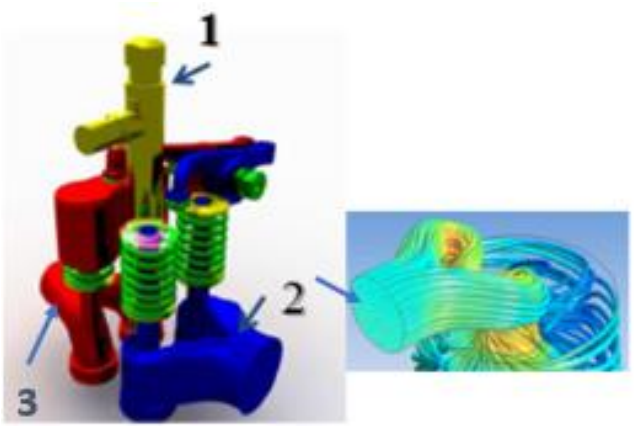

Şekil 5. Tek silindirli model deney motorunun (S/D=95/85 *mm*) yakıt püskürtme enjektörü (1), çiftleştirilmiş emme (2) ve egzoz (3) portları ile bir arada üç boyutlu montaj resmi.

bar değerinde olmuştur. Yanma süreci, $\varphi = 12^0$ KMA'a eşit zaman içinde (φ =367-355=12^0) gerçekleşerek, yanma basıncını maksimum değerine (p_z=80 *bar*) TDC'den φ =7° geçtikten sonra ulaştırmıştır. Bu durumda ortalama basınç artış oranı $\Delta p/\Delta\varphi$ =(80-45)/12=2,91 $bar/1^0\varphi$ değerinde olmakla, en yüksek performans ve verim elde edilmiş, lakin NO emisyonu da maksimum – NO=1100 *ppm* seviyesine ulaşmıştır.

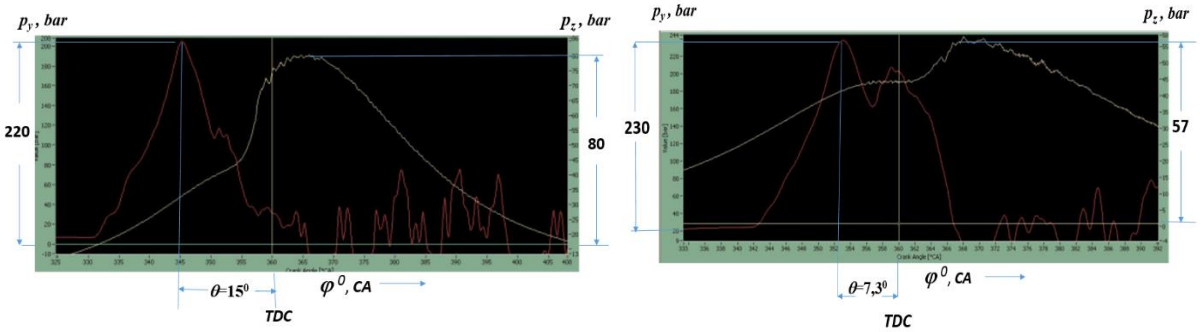

a) b)

a) Konvansiyonel YO: θ=15^0 *CA*, p_{me}=0,653 *MPa*, b_e=204 *g/BGh*, *k*=2,52 *1/m*, *NO*=1100 *ppm*

b) MR-2 YO: θ=$7,3^0$ *CA*, p_{me}= 0,662 *MPa*, b_e=197 *g/BGh*, *k* =2,53 *1/m*, *NO* = 302 *ppm*

Şekil 6. Tek Silindirli model deney motorunun farklı yanma odaları ile çalıştığında çıkarılan indikatör diyagramları.

Motor, MR-2 YO ile çalıştığında yakıt püskürtme avansı düşük olduğu için (θ =15^0 karşın $7,3^0$ *CA*) yanma süreci TDC'den sonra, φ=362^0 anından itibaren gerçekleşmiş ve φ =10^o süreci içinde (φ =372-362=10^o) yanma basıncını p_c=45 *bar* değerinden maksimum değerine - p_z=57 *bara* dek yükseltmiştir. Bu durumda ortalama basınç artış oranı $\Delta p/\Delta\varphi$ =(57-45)/12=1,0 $bar/1^0\varphi$ olarak konvansiyonel YO ile mukayesede ~3 kat düşük seviye ($\Delta p/\Delta\varphi$ =2,91'e karşın 1,0 $bar/1^0\varphi$) sergilemiştir. Bu ise "Mach etkisi" ile yanmış ürünlerin sıcaklığının ilaveten yükselmesini önleyerek, NO emisyonunun 1100/302=3,6 kat düşmesine sebep olmuştur.

MR-2 YO'da yanma basıncının konvansiyonel YO ile mukayesede %30 civarında düşmesine rağmen (p_z= 80'ye karşın 57 *bar),* motorun performans verileri kötüleşmemiş, tam tersine, ortalama efektif basınç (p_{me}=0,653'e karşın 0,662 *MPa*) ve duman koyuluğu (k=2,52'ye karşın 2,53 *1/m*) yaklaşık aynı seviyede kalmış, yakıt tüketimi ise %3,7 civarında azalmıştır (b_e =204 karşın 197 *g/BGh*). Bunun esas sebebi, MR-2 yanma odasında nispeten düşük hızda gerçekleşen yanma işlemi, maksimum basıncın TDC'nin φ =10-12^o sonrasına sarkarak, piston-biyel mekanizmasında maksimum momentin oluşması için en uygun zamana denk gelmesidir. Ayrıca, bu zaman içinde piston-biyel mekanizması dikey basınç kuvvetinin düşük değerlerine maruz kaldığı için motorun Gürültü emisyonu ve Mekanik kayıpları da azalmaktadır. Mekanik kayıpların azalması ise motor ömrünün uzanması ile sonuçlanacağı şüphesizdir.

4. MR-Process Yanma Mekanizması ile çalışan Dizel Motorunun Yapısal Değişiklikler Yapılmadan %100 Doğal Gaz Yakıtına dönüştürülmesi

Paragraf 2'de anılan dört supaplı model deney motoru, yüksek Dizel sıkıştırma oranını koruyarak, %100 gaz yakıtlarına dönüştürmek için de kullanılmıştır. Dizel yakıtının kendinden tutuşması için yeterli olan yüksek sıkıştırma oranı (ε =17,5), gaz yakıtlarının (LPG ve CNG) kendinden tutuşması için yeterli olmadığı için Buji Ateşleme sistemini kullanmak ve motoru Otto Çevrimi talepleri ortamında çalıştırmak lüzumu ortaya çıkmıştır.

Şekil 7'de model motorun Otto Çevrimi kullanılmakla gaz yakıtları ile (veya benzinle) çalıştırmak için adapte edilen silindir kafasının 3 boyutlu resmi gösterilmiştir. Buradan görüldüğü gibi, enjektör, çiftleştirilmiş emme portunun sadece bir tarafına, buji ise merkezde yer alan dizel enjektörü yerine bağlanılmıştır. Bunula da aynı konstrüksiyon yapıda motoru hem Dizel, hem de Otto çevrimleri ile çalıştırmak imkânı elde edilmiştir.

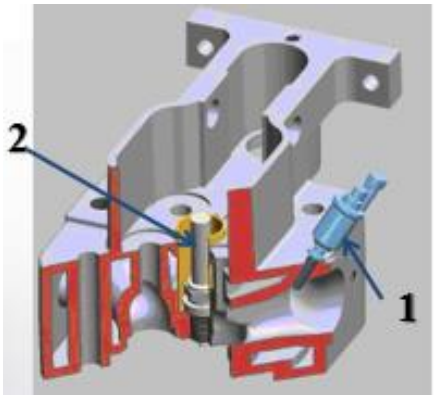

Şekil 7. Tek silindirli model dizel motorun Otto Çevrimi kullanmakla gaz yakıtlarıyla çalıştırmak için adapte edilen silindir kafasının 3 boyutlu resmi
(1- Gaz veya benzin püskürtmek için enjektör, 2- Buji).

Çift Döngülü MR-2 YO tek silindirli deney motorunun Dizel Çevrimi ile çalışması durumunda yapılan deney sonuçları Paragraf 2'de sunulmuştur. Bu Paragrafta ise Otto Çevrimine dönüştürülen aynı motorun Gaz yakıtı kullanılmakla elde edilen bazı deney sonuçlarına yer verilmiştir.

Şekil 8'de motorun konvansiyonel YO ile Dizel Çevrimi ve MR-2 CC ile Otto Çevrimi kullanıldığında çıkarılmış indikatör diyagramları karşılaştırılmıştır. Deneylerde motorun çalışma rejimi olarak n=3000 min^{-1}, sıkıştırma oranı ε =17,5, HFK λ =1,42 ve volumetrik verimi η_v = 0,9 değerlerinde sabit tutulmuştur. Yakıt olarak Dizel versiyonunda EuroDiesel, Otto versiyonunda ise Oktan sayısı 120 civarında olan CNG kullanılmıştır.

Şekilden görüldüğü gibi motor, Dizel Çevrimi ile çalıştığında yanma basıncı p_z=7,7 MPa eşit olan maksimum değerine TCD'den 5^0 ca geçtikten sonra ulaşmıştır. CNG ile çalıştığında ise alevin yayılması bir kadar düşük hızla gerçekleştiği için p_z=6,5 MPa eşit olan maksimum değerine TCD'den 11^0 ca geçtikten sonra ulaşarak, basıncın %15 civarında düşmesine sebep olmuştur. Sıkıştırma oranının yüksek olmasına (ε =17,5) rağmen, CNG ile gerçekleşen yanma süreci, hiçbir vuruntu olayı oluşturmamıştır. Şekil 8'den de gözüktüğü gibi, motor, MR-2 YO ile çalıştığı zaman çıkarılan indikatör diyagramda vuruntu oluşumunun göstergesi olan çalkalanmalar görünmemektedir. Bellidir ki, bu çalkalanmalar, vuruntunun sert gürültü kopartmasına sebep olur. Deney zamanı böyle bir gürültünün fark edilmemesi, motorun vuruntu yapmadan çalıştığını bir daha kanıtlamıştır. Yanma basıncının %15 civarında azalması, motorun verilerini kötüleştirmemiş, tam tersine, yanma basıncın maksimum değerinin TCD'den 11^0 *ca* geçtikten sonra oluşması sayesinde biyelin krank miline maksimum teğet kuvvetle etkisinin en uygun zamana denk gelmesi ile performans ve emisyon verilerini iyileştirmiştir.

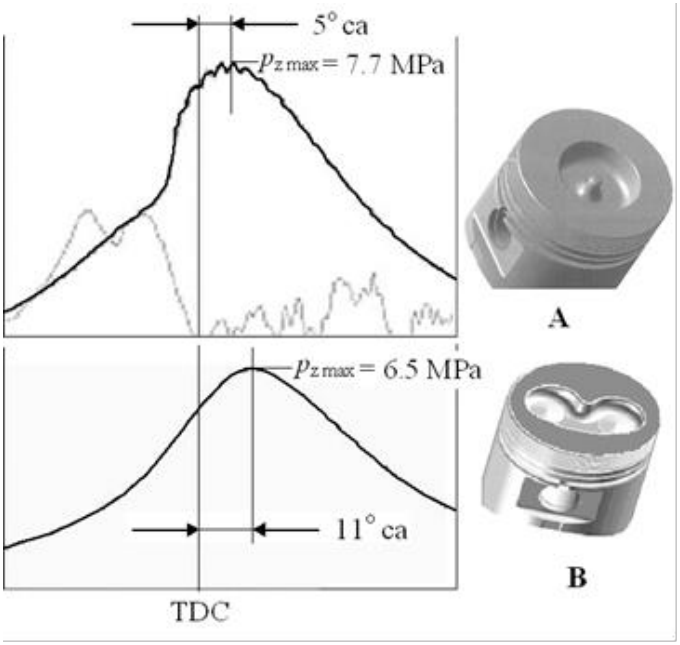

Şekil 8. Tek silindirli model deney motorunun (S/D=95/85) konvansiyonel YO (**A**) ve MR-2 YO (**B**) ile çalıştığında çıkarılan indikatör diyagramların karşılaştırılması.

Tablo 1'de model deney motorun konvansiyonel Dizel YO ve MR-2 YO Otto Çevrimi ile çalıştığında elde edilen test sonuçları karşılaştırılmıştır. Tablodan gözüktüğü gibi, çalışma rejimi parametrelerinin aynı olması durumunda (n=3000 min^{-1}, ε =17,5, λ = 1,42, η_v =0,9), CNG ile çalışan motorda yanma basıncının %15 civarında azalmasına (p_z=7,7 karşın 6,5 *MPa*) rağmen, konvansiyonel dizelle mukayesede motorun ortalama efektif basıncı veya gücü %10 artmış (p_{me} = 0,653 karışın 0,72 *MPa*), efektif verimi ise %8,4 civarında yükselmiştir (η_e =0,306 karışın 0,332). Bunun yanı sıra, Duman koyuluğu *k*=0 olmuş, kirletici *NO* emisyonu ise 403 *ppm* seviyesini aşmayarak, dizelle mukayesede yaklaşık 2,75 kat daha düşük seviye sergilemiştir (*NO*=1100 karışın 403 *ppm*).

MR-Process Yanma Mekanizması kullanılarak, emisyon limit değerleri Stage IIIA Standardına cevap veren 4 silindirli bir traktör dizel motoru (S/D=110/104) Otto Çevrimi ile, dünyada bir ilk olarak, %100 LPG yakıtına dönüştürülmüş ve önemli sonuçlara varılmıştır (Mehdiyev ve diğerleri, 2009) & (Mehdiyev ve diğerleri, 2011). Şekil 9'da bu motorun maksimum tork ürettiği hız rejiminde (n=1500 d/dak) ortalama efektif

basınca (p_{me}) bağlı olarak motor parametre ve emisyonlarının değişme grafikleri gösterilmiştir. Buradan görüldüğü gibi, motor LPG yakıtıyla çalıştığında ortalama efektif

Tablo 1. Deney motorun farklı yanma odaları ile çalıştığında elde edilen test sonuçların karşılaştırılması (n=3000 min^{-1}, ε =17,5, λ =1,42, η_v =0,9).

Yanma Oda ve Çevrim tipleri	***Kullanılan Yakıt***	***p_z, MPa***	***p_{me}, MPa***	***η_e***	***k, 1/m***	***NO, ppm***
Konvansiyonel *YO, Dizel Çevrimi*	EuroDiesel	7,7	0,653	0,306	2,52	1100
MR-2 YO, Otto Çevrimi	CNG	6,5	0,72 (+%10)	0,332 (+%30)	0	403 (-2,75 kat)

basıncın (torkun) maksimum değeri p_{me}=0,85 *MPa,* dizel motorunki ise p_{me}=0,676 *MPa* olmuştur, yani motorun torku veya gücü LPG ile çalıştığında %25 civarında daha fazladır. Fakat p_{me}=0,85 *MPa* değeri hava fazlalık katsayısının □=*1,1* değerinde elde edildiği için (dizel versiyonunda □'nin bu değerinde aşırı duman oluşturulduğundan dolayı kullanılmaz) NOx

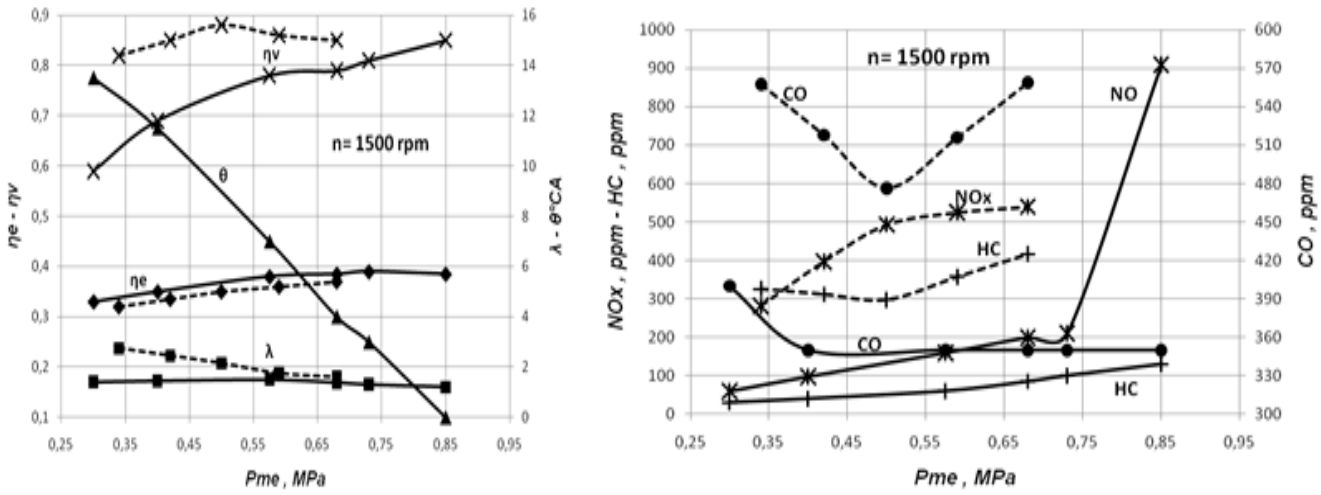

Şekil 9. Motor parametreleri ve Egzoz gaz emisyon değerlerinin karşılaştırılması (MR-2 YO - LPG, Konvansiyonel Dizel YO) (Mehdiyev ve diğerleri, 2011).

emisyonu kabul edilemez seviyeye dek artmış olur. Bu yüzden gaz-hava karışımının maksimum zenginleştirilme oranı λ =1,36 değeri ile sınırlanması gerekmektedir. Bu halde ortalama efektif basıncın maksimum değeri p_{me}=0,735 *MPa* seviyesine düşse bile, yine de dizele göre güç %9 civarında daha yüksek kalmaktadır. Bu durumda tüm yük rejimlerinde Otto Çevrimi ile çalışan LPG'li motor, dizele göre daha verimli çalışarak (η_e yüksektir), çok daha az kirletici maddeler (NO_x, *HC* ve *CO*) üretmektedir.

Şekil 9'dan görüldüğü gibi, Stage IIIA (Tier 3) Standardına cevap veren dizelle mukayesede LPG'li motorun emisyon değerleri, duman emisyonunun da sıfır olduğunu göz önüne aldığımızda (Tablo 1'e bak.), Stage IIIB (Tier 4- Interim), hatta Stage IV (Tier 4– Final) standardına uyacağı şüphe doğurmamaktadır.

Böylece, MR-Process yanma mekanizmasının uygulanması ile dizel motorunun %100 CNG veya LPG yakıtıyla yüksek performanslı ve verimli çalıştırılmasının yanı sıra, hiçbir ek emisyon düşürücü sistemleri kullanmaksızın, güncel emisyon standartlarına cevap vermek mümkün olacaktır.

5. TÜLOMSAŞ motorların "MR-Process" yanma mekanizması kullanılarak modernizasyon ve doğal gaz yakıtına dönüştürme çalışmaları

Bilindiği üzere 1968 yıldan itibaren Eskişehir TÜLOMSAŞ fabrikasında Fransa S.E.M.T. (Socie'te' d' Etudes de Machines Terminus) Pielstick Firmasının artık süresi bitmiş lisansı ile yerli Lokomotifler için dizel motorları üretilmekte, eski motorların ise revizyonu yapılmaktadır. Türk LOYDU No:TO.DEB, 12-0132/12-2466, 10.04.2013 Sertifikası ile Marine tipi olarak 16 silindirli TLM16V185 motorları Van Gölü ulaşımında da kullanılmaya başlanmıştır. Sertifika bilgilerine göre bu motorların gücü katalog değerinden %5,3 daha az (2400 karşılık 2271 BG), yakıt tüketimi ise yaklaşık % 9 kadar fazladır. Bunun esas sebebi, motorun performans ve verimliliğini, egzoz gaz ve gürültü emisyonlarını belirleyen yanma mekanizması 1940-50'li yıllarında geliştirilen Ön Yanma Oda yöntemiyle gerçekleştirilmesidir (Şekil 10, A). Bundan dolayı revizyona alınan motorların gücü daha düşük, özgül yakıt tüketimi be ≥ 210 g/BGh civarında, egzoz gaz emisyon değerleri ise Faz I (Tier I) Standardı seviyesindedir. Hâlbuki Avrupa Birliğinin (AB) yayınladığı direktiflerle önümüzdeki yıllarda Faz III A ve Faz III B standardına uymayan gemi motorların kullanımı engellenecektir.

Bellidir ki, hâlihazırda ileri teknoloji gibi değerlendirilen yüksek basınçlı Common Rail yakıt besleme sistemini kullanmakta olan bildiğimiz lider konumdaki Otomobil ve Ağır Dizel Üreten Firmalar (Volkswagen, Wartsila, MAN vb.) motorun optimum rejim kontrolü açısından avantaj kazanmış olsalar bile, Azot Oksit (NOx) Emisyonunun limit değerlerini aşırı derecede aşma sorunu ile karşı karşıya kalmış, diğer taraftan ekonomik ve pratiklik (servis, onarım, tamir) açısından hiçbir avantaja sahip olamamışlardır. Zaten bu sebepten de ünlü Japon Firması JFE PRIME MOVERS, 1964 yılından bu yana TÜLOMSAŞ motoru ile aynı olan S.E.M.T.-Pielstick motorlarında klasik - düşük basınçlı hidrolik pompa – enjektör kullanarak, hiçbir köklü değişiklik yapmaksızın, Japon ve Asya bölgelerinin gemi ve jeneratör pazarında önemli bir konum edinmiştir. Hâlihazırda TÜLOMSAŞ motorunun yurtdışı "kardeşleri" olarak ABD, İngiltere, G.Kore, Hindistan, İsveç, Çin ve Finlandiya'da da S.E.M.T. - Pielstick lisansı ile yerli markaya dönüştürülmüş askeri ve sivil gemi, lokomotif ve jeneratör uygulamaları için üretim yapılmakta ve Dünya pazarına sunulmaktadır.

Bu örnekler onu gösterir ki, Yakın ve Orta Doğu'nun geniş coğrafyasında tek Türkiye'nin sahip olduğu TÜLOMSAŞ Lokomotif ve Motor Fabrikasının ürettiği ağır dizel motorlarını da, daha fazla zaman kaybı yaşamadan, modernize ederek yenilikçi ve rekabetçi Milli Markaya dönüştürmemiz, ülkenin ekonomisi ve prestiji açısından önem arz etmektedir. Bu amaçla TÜLOMSAŞ motorunun "MR-Process" yanma mekanizması kullanılarak Modernizasyonu ve Doğal Gaz Yakıtına Dönüştürülmesi konusunda aşağıdaki Üç Dönemli proje çalışmalarının yürütülmesi öngörülmektedir:

I. Dönem Modernizasyon çalışmaları olarak TLM16V185 Dizel Motorunun sadece Pistonu üzerinde Çift Döngülü MR-2 Yanma Odalı yeni imalat pistonları uygulayarak güç ve yakıt tüketiminin %10-15 civarında iyileştirilmesi ve Egzoz Gaz Emisyonlarının Faz IIIA Standardı seviyesine düşürülmesi amaçlanmaktadır.

A B

Şekil 10. TÜLOMSAŞ Motorunun mevcut (A) ve MR-2 (B) yanma odalı pistonları.

Şekil 10'da TÜLOMSAŞ motorunun mevcut (A) ve 8'e benzer MR-2 yanma odalarına sahip pistonları gösterilmiştir. "MR-Process" Yanma Mekanizması ile çalışması öngörülen motorda esas değişiklik sadece pistonu üzerinde Çift Döngülü MR-2 Yanma Odasının dizaynıdır. Ön YO mevcut şeklinde kalmaktadır. Burada değişiklik, onun sadece lülesinde (nozulunda) yapılmıştır; mevcut 4 delikli lüle bazında, iki delikli olarak tasarlanmış ve sıkıştırma sürecinde oluşan Çift Hava Döngülerine teğet olarak yönlendirilmiştir. Bu durumda ön YO'da tutuşan yakıt, basıncı artırarak yanmış ürünleri, yanmamış yakıtı ve oluşmuş İs emisyonunu alev kümesi ile birlikte lülenin deliklerinden hava döngülerine teğet olarak püskürtüp yanma sürecini türbülanslı döngü ortamında gerçekleştirmektedir. Yanma sürecinin birbirinin tersine dönen türbülanslı ortamda gerçekleştirilmesiyle alev cephesi YO'nın sağ ve sol cidarlarından yanmamış karışımı, ön YO'da oluşan İsi sıyırıp odanın merkezine - en sıcak bölgesine sürükleyerek yanma reaksiyonlarının alev sönmesi olmadan devam edebilmesini sağlamaktadır.

Sadece piston üzerinde ana yanma odası olarak yer alan MR-2 YO kullanıldığında elde edilecek sonuçların ilkin değerlendirilmesi için teorik araştırmalar yapılmıştır. Teorik araştırmalar, dizel motorun gerçek çevriminin tarafımızdan geliştirilmiş matematik modeli kullanılarak yapılmıştır. Ayrıntıları (Mehdiyev ve diğerleri, 2009)'da verilmiş bu modelle yanma sürecini hesaplamak için "yanma kanununu" belirleyen Vibe denklemi kullanılmaktadır;

$$x = 1 - \exp\left[-6{,}908(\alpha / \alpha_z)^{m+1}\right],$$

Burada, m - yanma süresi için üs, α_z - krank mili açısı (KMA) olarak yanma süresidir.

Modeldeki Vibe denklemi parametrelerini (m, α_z) mümkün olan değerler arasında değiştirerek motorda istenilen yanma kanununu teorik olarak elde etmek mümkündür. Bu ise yanma süreci ile ilgili deneysel olarak yapılması zor olan optimizasyon çalışmalarını bilgisayar kullanımı ile önemli derecede kolaylaştırarak, TÜLOMSAŞ motorlarının tasarım öncesi gerekli parametre değerlerinin elde edilmesine imkan sağlamaktadır.

Tablo 2'de söz konusu motorun mevcut (konvansiyonel) YO ve MR-2 YO ile çalışma rejimi parametrelerinin aynı olması durumunda (n=1500 min^{-1}, ε =13,5, λ =1,45, η_v =0,9) elde edilen hesap sonuçları, Şekil 11'de ise teorik indikatör diyagramları karşılaştırılmıştır. Buradan görüldüğü gibi, mevcut YO kullanıldığında motorun güç ve özgül yakıt tüketiminin hesap değerleri katalog değerleri ile örtüşmektedir; N_e =2400'e

karşın 2350 BG, b_e=170'e karşın *173* g/BGh, yani kullandığımız hesap yöntemi gerçekliği doğru yansıtmaktadır. İndikatör diyagramların karşılaştırılmasından anlaşıldığı gibi, söz konusu motor, mevcut YO ile çalıştığında yanma basıncı ÜÖN'den 70 geçtikten sonra pmax=15 MPa' ya eşit olan maksimum değerine, MR-2 YO ile çalıştığında ise 130 geçtikten sonra pmax=10,7 MPa değerine (%27

Tablo 2. TLM16V185 motorun farklı yanma odaları ile çalıştığında elde edilen termodinamik hesap sonuçların karşılaştırılması (n=1500 min^{-1}, ε =13,5, λ =1,45, η_v=0,9).

YO tipi	p_{max}, *MPa*	η_e	N_e, *BG*	M_e, *Nm*	b_e, *g/BGh*	*NO, ppm*	*Gürültü, dB(A)*
Mevcut YO	**15**	**0,367**	**2350**	**11007**	**173**	**875**	**93,5**
MR-2 YO	**10,7 (-%29)**	**0,415 (+%13)**	**2423 (+%3)**	**11348 (+%3)**	**150 (20 g/BGh)**	**441 (-2 kat)**	**90,3 (-3,2 *dB*)**

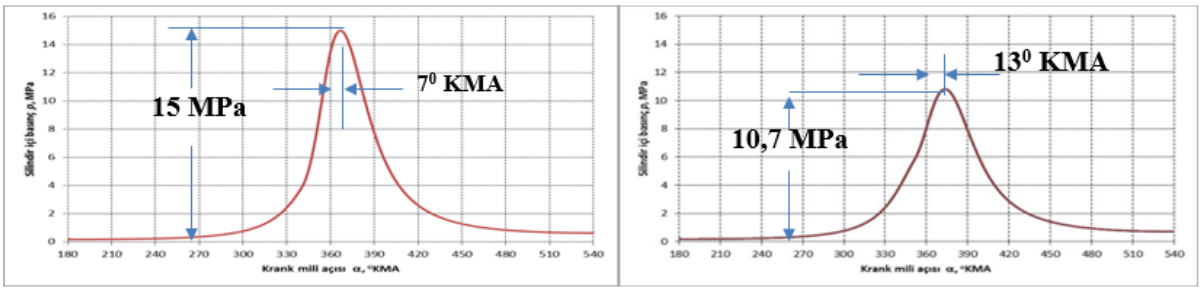

Şekil 11. Motorun mevcut YO (solda) ve MR-2 YO ile çalıştığında teorik indikatör diyagramları.

daha düşük değere) ulaşmıştır, yani yanma süreci genişleme sürecine kayarak, Çift Türbülanslı Döngü ortamında optimum yanma sürecinin gerçekleşmesi mümkün olmuştur. Sonuçta, Tablo 2'den göründüğü gibi, motorun performans ve emisyon verileri iyileşmiştir; güç *%3* ve efektif verim *%13* civarında yükselmiş (N_e *=2350'*e karşın *2423 BG*, η_v *=0,367* karşın *0,415*), özgül yakıt tüketimi *20 g/BGh* azalmış (b_e*=170'*e karşın *150 g/BGh*), NOx emisyonu 2 kat kadar (*NOx= 875* karşın *441 ppm*), gürültü ise *3,2 dB* (*93,5'* karşın *90,3* dB(A) düşmüştür.

Bu karşılaştırmadan anlaşıldığı gibi, torik olarak elde edilen bu bilgiler, Paragraf 2 ve 3'te sunulan tek silindirli model deney düzeneği üzerinde yapılan test sonuçları ile yüksek seviyede örtüşmektedir. Bu ise MR-Process yanma mekanizmasının uygulanması ile fazla zaman ve yatırım harcamadan TLM16V185 motorunu en güncel seviyede modernizasyonunun mümkün olduğunu kanıtlamaktadır.

II. Dönem çalışmaları ile modernizasyonu yapılmış TLM16V185 motorun Çift Yakıt (Duel Fuel) Sistemi ile kısmen CNG yakıtına (%80 CNG ve %20 motorin) dönüştürülmesi öngörülmektedir.

Klasik Lokomotif, Gemi ve Jeneratör motorları Çift Yakıt ("Dual Fuel") Sistemi adlandırılan yöntemle kısmen CNG yakıtına dönüşümü çoktan beri gerçekleştirilmektedir. Bu yöntemle motoru CNG yakıtına dönüştürmek basit konstrüksiyon değişiklikler içerdiği için daha az zaman ve maliyetle uygulanabilir. Gaz

yakıtı silindirlere mevcut emme manifoldun vasıtasıyla paylaşıldığı için ufak değişikliler, sadece bu manifold üzerine gaz yakıt ekipmanlarını (gaz karıştırıcı veya enjektörleri) monte etmek için gerçekleştirilmektedir.

Bellidir ki, Çift Yakıt Sisteminin klasik yanma odasına sahip dizel motorlarında kullanımı vuruntu olayı, kontrol, bakım ve onarım bakımından birçok zorluluklar oluşturmaktadır. Ayrıca, günümüzde limit değerleri düşük olan Egzoz Gaz Emisyon Standartlarının devreye girmesi, bu Sistemle CNG'ın kullanım miktarının motorin yakıta oranla %30-35'i aşmamasını talep etmektedir. Aksi halde vuruntu olayını önlemek, NOx ve HC emisyonlarını düşürmek gibi zorluluklar meydana çıkmaktadır. Bahsedilen az miktarda CNG'ın kullanımı ise ekonomik açıdan kazanımların yetersiz olduğunu göstermektedir.

Modernize olunmuş TLM16V185 motorunda Çift Döngülü MR-2 ana YO kullanıldığı için (Şekil 10, B) ön YO'dan çıkan alev kümesi ile tutuşturulan gaz-hava karışımının yanma süreci Çift Türbülanslı Döngü ortamında gerçekleşmesi sağlanmaktadır. Bu durumda, yukarıda anlatıldığı gibi, vuruntu olayı meydana çıkmamakta ve soğuk cidarlarda alev sönmesi önlendiği için tam yanma gerçekleşmektedir. Bundan dolayı NOx ve HC emisyonlarını yükseltmeden silindirlere verilen CNG miktarını %70-80'e kadar artırmak mümkündür. Bu sebepten söz konusu yöntemle TÜLOMSAŞ motorunun kısmen Doğal Gaz yakıtına dönüşümü hem ekonomik (CNG'nın sadece fiyat farkından dolayı %25-%30 az maliyet), hem de kirletici gaz emisyonların (özel olarak İs – Partikül Madde ve kükürtlü gaz - SO_2) düşürülmesi açısından faydalı olacağı şüphe doğurmamaktadır.

III. Dönem çalışmaları esnasında "MR-Process" Yanma Mekanizmasının Direkt Enjeksiyonlu Dizel sürümünün kullanımı ile TLM16V185 motorun karakteristiklerinin bir kadar da iyileştirilmesi ve aynı konstrüksiyon yapıda %100 NG (CNG veya LNG) gaz yakıtının kullanımı ile Ötto Çevrimine dönüştürülerek performans, verim ve emisyon açısından, hiçbir ek emisyon düşürücü sistem ve olanak kullanmaksızın, güncel Uluslararası Standartların karşılaması öngörülmektedir.

Bellidir ki, söz konusu motorda ön YO'nın kullanımı ile düşük basınçlı (<250 *bar*) yakıt püskürtme imkânı avantajın olmasının yanı sıra, bir taraftan motorun soğutma sisteminde kaybolan ısı enerjisinin yüksek olması, diğer taraftan hızlı gaz akışının önce silindirden ön YO'sına, sonra ise ters yönde gerçekleşmesi ile gaz-dinamik kayıpların kaçınılmaz olması motor veriminin en az %5÷%8 civarında düşmesine sebep olmaktadır.

Anılan dezavantajları göz önünde bulundurarak, motorda mevcut olan ön YO'sının kaldırılması ile "MR-Process" Yanma Mekanizmasının Şekil 4'te gösterilen şemaya uygun direkt enjeksiyonlu sürümü ile gerçekleştirilmesinin daha avantajlı olacağı şüphe doğurmamaktadır. Lakin bu sürümde, Şekil 4'de gösterildiği gibi, iki delikli enjektörden 125 ÷ 200 bar basınçla püskürtülen yakıt demetinin duvara sıvanarak buharlaşabilmesi için Çift Hava Döngülerinin açısal hızı $\omega \geq (5 \div 10)*\pi*n/30$ *1/s* (n, motorun dakikadaki devir sayısı) seviyelerinde olması gerekmektedir. Gerekli hız seviyesini elde etmek için, Şekil 12'de gösterildiği gibi, silindir kafasında birbirinin tersi yönünde yerleştirilmiş iki helisel emme portu dizaynı yapılmalıdır. Paragraf 2'de anlatıldığı gibi, bu durumda direkt enjeksiyonlu motorun performans ve verimini %5÷10 civarında iyileştirmenin yanı sıra, egzoz gaz emisyonların limit değerlerini Faz IIIB (Tier 3) Standardı seviyesine düşürmek mümkün olacaktır.

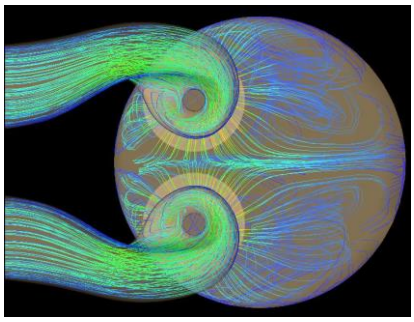

Şekil 12. Silindir başlığında birbirinin tersine yerleştirilmiş iki helisel emme portlarının yardımıyla silindirde çift hava döngülerinin oluşturulma şeması.

Paragraf 3'te sunulan örnekte olduğu gibi, birbirinin tersi yönünde Çift Helisel Emme Portlarına ve MR-2 YO'sına sahip dizel motorunu, hiçbir yapısal değişiklikler yapılmaksızın, %100 Doğal Gaz yakıtına dönüştürülmesi de mümkündür.

Doğal Gaz yakıtına dönüşümünde, yüksek dizel sıkıştırma oranını (>13,5:1) korumak şartıyla, sadece dizel enjektörünün yerine buji, gaz enjektörünü ise Çift Helisel Emme portlarının herhangi birisine bağlanması gerekmektedir. Bu durumda emme sürecinde 8'e benzer MR-2 YO'sının bir yarısına Gaz yakıtının %100'ü, havanın ise %50'si, diğer yarısına ise havanın %50'i dolacaktır. Yukarıda anıldığı gibi, emme ve sıkıştırma süreçlerinde YO'nın oyuklarında oluşan türbülanslı döngü hareketleri aynı hız ve momentuma sahip olduklarından dolayı birbirine karışmayarak buji ateşleme anına kadar YO'nın bir bölgesinde HFK λ =0,6...0,9 arasında değişen zengin karışım, diğer bölgesinde ise sadece hava yer alacaktır. YO'nın merkezinde yer alan buji, zengin gaz-hava karışımı döngüsüyle hava döngüsünün birbirine temas ettiği yerde olduğu için genel HFK'sını geniş aralıkta değiştirerek (λ =1,2…2,5) motorun esas yük rejimlerini elde etmek mümkündür. Genel HFK'nın değiştirilmesi emilen havayı sabit tutarak, sadece gönderilen Gaz yakıtı miktarını değiştirerek gerçekleştirilebildiği için klasik gaz yakıtına dönüştürülmüş motorlardaki gibi hava miktarını değiştiren gaz kelebeğine ihtiyaç kalmamaktadır. Bu durum %100 Gaz yakıtıyla çalışan motorun Elektronik Kontrol Ünitesinin (EKÜ) karmaşık yazılımla donatılmasını gerektirmediği için EKÜ'nün kalibrasyonu ile ilgili deneysel çalışmaları minimuma indirecektir. Böylece, söz konusu dizel motorların %100 Doğal Gaz yakıtına dönüştürülmesi ile Yüksek Verimli ($\eta_e \geq 0,46$) ve Çevreye Duyarlı Yeşil Motor teknolojisinin Sanayi Uygulaması neticesinde TÜLOMSAŞ'a Dünyada bir İlk olarak ulusal ve uluslararası pazarda rekabetçi ve yenilikçi bir ürün sağlanacaktır.

6. SONUÇLAR

1. TÜLOMSAŞ Motorunun mevcut yanma mekanizması 20. Yüzyılın 40-50'li yıllarında geliştirilmiş olan Ön Yanma Oda yöntemiyle gerçekleştirildiğinden dolayı günümüz ağır dizel motorların performans, verim, egzoz gaz ve gürültü emisyonları değerleri ile mukayesede çok geride kalmaktadır. Yapılan bir dizi teorik ve deneysel araştırmalarla tespit edilmiştir ki, başlangıç I. Dönem - fizibilite çalışması olarak 16 Silindirli TLM16V185 Motorunun sadece pistonu üzerinde MR-Process yanma mekanizmasını gerçekleştiren Çift Döngülü MR-2 Yanma Odasını uygulayarak motor gücünü %5÷10 kadar artırmak, egzoz gaz emisyonu limit değerlerini ise Faz 3 A (Tier III) Standardı seviyesine düşürmek mümkündür. Eğer bu teknoloji ile yılda 70 motor revize edilirse toplam yıllık tasarruf 25.200 ton dizel yakıtı veya yaklaşık 60-70 milyon TL seviyesinde olacaktır.

2. Tasarruf edilen miktarın sadece yarısından az bir kısmını harcayarak II. ve III. Dönem çalışmaları ile motorun daha kapsamlı modernizasyonunu gerçekleştirmek ve hiçbir yapısal değişiklik yapılmadan, Dünyada bir ilk olarak motor, %100 Doğal gaz yakıtına dönüştürülebilecektir. Bununla da geliştirilmiş TÜLOMSAŞ motorları yenilikçiliği ve rekabetçiliği ile Pielstick lisansı esasında hâlihazırda üretilmekte olan yurtdışı "kardeşlerinden" üstün bir farklılık sergilemiş olacaktır.

3. TÜLOMSAŞ A.Ş., süresi bitmiş Pielstick lisansı esasında 6, 8 ve 12 silindirli motor üretim olanakları ve kapasiteye de sahiptir. Bu durumda MR-Process yanma mekanizması temel alınarak, Sivil ve Askeri amaçlı gemiler, lokomotifler, iş makineleri, jeneratörler ve enerji santralleri için gücü 500 - 2800 kW arasında değişen, 6-8-12-16 silindirli Yenilikçi ve Rekabetçi Yerli Marka motorların seri üretimini gerçekleştirerek dışa bağımlılık ortadan kaldırılmış olacaktır.

KAYNAKLAR

Dinc, C., Arslan, H. and Mehdiyev, R. (2009). CO2 Emission Reduction Using Stratified Charge in Spark Ignition Engines, Energy & Fuels, 23 (4), 1781-1785.
http://pubs.acs.org/doi/abs/10.1021/ef800349x

Mehdiyev, R.I. ve Wolanski, P. (2000). Bi-Modal Combustion Chamber for a Stratifield Charge Engine Advances in Combustion, SAE-2000-01-0196, p.p.53-61.

Mehdiyev, R., Ogun, K., Derbentli,T., Arslan, H., Ozcan, E. (2009). Development of a Turbo Diesel Engine by a New Combustion Process for Heavy Duty Vehicles and Tractors 09ICE-0048 Copyright © SAE International, p.12. http://mech-ing.com/journal/3-2011.html

Mehdiyev, R. I., Karpov, V. P., Wolanski, P. (1978). Flame Spreading And Evaluation of Toxic Substances During the Stratified Charge Combustion, Archives of Termodynamics And Combustion, vol. 9, No.4, Warszawa, p.p. 645-660.

Mehdiyev R.I. (1983). İYM'da NO ve CH emisyonları oluşumunun özellikleri ve düşürülme yöntemleri (Rus dilinde), SSCB Bilim Akademisinin «Yanma ve Patlamanın Fiziği» -"Fizika Goreniya i Vzrıva" Dergisi No:5, sayfa 70-73.

Mehdiyev, R., Ogun, K., Babaoglu, O. Vb., (2011). "The Twin Swirl "MR-Process" Combustion Mechanism and Conversion of Diesel Engines to Operate with Gaseous Fuels", 10th International Conference on Engines & Vehicles ICE2011, September 11-15, Capri-Napoli / ITALY, Proceedings DVD_2011-24-0066.pdf, Book of Abstracts pp. 90, SAE 2011-24-0066, doi:10.4271/2011-24-0066. http://papers.sae.org/2011-24-0066

Vestergård, J. (2014). Wärtsilä NOx Reducer, Wärtsilä NOx Reducer SCR solution from Wärtsilä, İstanbul.

Resistance Reduction Studies by Means of Increasing the Beam with Waterline Parabolization

Devrim Bülent Danışman[1]*, Ömer Gören[1] and Sander Çalışal[2]

bulent.danisman@itu.edu.tr

[1] *Department of Naval Architecture and Marine Engineering, Faculty of Naval Architecture and Ocean Engineering, Istanbul Technical University, Istanbul, Turkey*

[2] *University of British Columbia, Vancouver, Canada and Piri Reis University, Istanbul, Turkey*

Abstract

It has been more than a decade since Calisal et al. (2002) proposed the concept of reduction of the resistance by increasing the beam. Although this is a controversial concept compared to the traditional approach which adopts that the coefficients of residual resistance vary with the beam to the power of 2. The authors, during the course of resistance reduction studies, have disclosed that the new present concept has the ability to reduce the resistance for the Froude number interval of 0.2 – 0.4. Accordingly, a review of the authors' previous work is presented here from the resistance point of view as well as from the seakeeping point of view. Moreover, the production cost due to increasing the beam is also examined and explained. The studies presented include mathematical, computational and experimental results.

Keywords: Hull form optimization, beam increment, waterline parabolization, wave resistance, cost analysis.

1. Introduction

Kent (1919) was the first one who focused on the relationship between the resistance and the beam together with parallel body length. Weinblum (1950) studied the relationship between wave resistance and beam and gave an empirical value of 1.6 to the power of the beam as a significant physical parameter relater with the wave resistance. Wehausen et al. (1961) calculated this power of beam as 1.8 by making use of Taylor Standard Series. It has been then become a general understanding among naval architects that the coefficients of residual resistance vary with the beam to the power of 2 within experimental error. But most of these and related studies, on which this understanding/conclusion is based, are for relatively slow-speed ships with Froude numbers less than 0.21.

In contrast to the common understanding mentioned above, Çalışal, Gören and Danışman (2002) discusses, for the first time, the resistance reduction potential of increasing the beam while smoothing the shoulders of ships for moderate and relatively higher Froude numbers. The variation of ship

resistance for Froude numbers less than 0.2 with beam decrements was already confirmed mathematically by Çalısal et al. (2002). Nevertheless, the same study, which bases its mathematical justification on Michell's integral, shows that the new concept of parabolization of waterlines by increasing the beam (which leads to a decrease in parallel middle-body) decreases the wave resistance in the Froude number region, approximately, 0.2< Fn < 0.4. Here Gotman's (1998) work, which shows that ships with a mid-ship bulb have the least wave resistance, can also be cited as a support to the present concept.

This paper aims to show that the present concept is not a hull form dependent approach and to clearly identify the techniques and to describe the tools for proper applications of the present concept. A generalized analytical and numerical justification of the concept of increasing the beam is presented. One cross-channel passenger ferry, one heavy-lifter container ship and one Ro-Ro ferry are studied additionally for this purpose, and numerical results and experimental measurements –where available – are presented. Possible construction cost increase due to the beam increment is also examined and explained.

2. Theoretical background

During the preliminary steps of developing the present concept, we investigated mathematically the effect of the beam increment on the wave resistance by means of Michell's integral. Two numerical models were considered for this purpose and a simplification was made by adopting a wall-sided model #1 with a parallel middle-body in the interval –L/4 < x < L/4 with parabolic bow and stern waterlines. On the other hand, wall-sided model #2 has parabolic waterlines along the complete length of the hull. One form of Michell's integral can be given as:

$$R = \frac{4\rho g^2}{\pi c^2}\int_1^\infty \frac{\lambda^2}{\sqrt{\lambda^2-1}}[P^2(\lambda)+Q^2(\lambda)]d\lambda \qquad (1)$$

where

$$P(\lambda) = \iint f_x(x,y)\exp\left(\frac{g\lambda^2}{c^2}y\right)\cos\left(\frac{g\lambda}{c^2}x\right)dxdy \qquad (2)$$

$$Q(\lambda) = \iint f_x(x,y)\exp\left(\frac{g\lambda^2}{c^2}y\right)\sin\left(\frac{g\lambda}{c^2}x\right)dxdy \qquad (3)$$

The details of this formulation can be found in Wehausen and Laitone (1960). Here, c is the ship's speed, ρ is the water density and g is the gravitational acceleration. Since the waterlines are symmetric about the amidships in our numerical model, studying the effect of Q(λ) is adequate. Let Q(λ) be expressed as Q_1 and Q_2 for models #1 and #2, respectively. We assumed shallow draft to reduce the effect of the exponential term in P and Q functions. Q function includes the integrals for the bow and stern regions, but no contribution from the parallel middle-body of the model #1. Q_2, in addition to the integrals of the bow and stern regions, includes the integration, Q_{12}, along the parabolized mid-body at about the half-length for model #2. We then write:

$Q_2 = Q_1 + Q_{12}$, and thus;

$$Q_2^2 = Q_1^2 + 2Q_1Q_{12} + Q_{12}^2 \qquad (4)$$

It is clear that, depending on the sign of Q_1Q_{12}, wave resistance may either increase or decrease with the

addition of parabolic waterlines which in turn increase the beam as compared to model #1 with a parallel middle-body. For various values of λ; Q_{12} is negative, causing the wave resistance to decrease. For this simplified numerical model, it was shown (Çalışal et al., 2002) that a decrease in wave resistance was obtained in the Froude number range of $0.2 < Fr < 0.5$.

Thereafter, a series of studies were carried out to establish the validity of the present concept for various displacement type ships. The first attempt to show the effectiveness of the proposed concept was tested on a coaster tanker which indicates around 10 % of reduction in EHP. As a sequel study, Calisal et al. (2009) made a systematic investigation of ship resistance reduction by beam increments for a fishing vessel (UBC Series Hull). In this study, the beam was increased by 10 to 15 % of the beam by the step-by-step approach using add-on side-bulbs. The approach was controlled and evaluated first by Michell's integral and then by systematic experiments in the BC towing tank. The best alternative showed nearly 15 % reduction in total resistance in the targeted speed range of $0.3 < Fr < 0.4$. Moreover, the vessel's carrying capacity and static stability were also improved. The present parabolization concept was subsequently extended to a high speed NPL trimaran to determine whether resistance reduction using parabolic retrofitted side-bulbs could be achieved for a slender multi-hull vessel (Calisal et al., 2009). The Rankine source-panel method employing Dawson's (1977) algorithm was used to predict wave-making characteristics, an integral boundary layer solver and a RANS solver were used to calculate the viscous drag in the study in which a parametric search varying the size and the location of the bulbs was performed. Experimental validation of the results followed and 6 % reduction in total resistance is recorded. To provide a profound basis for the implementation of the present concept, Calisal et al. (2009) introduced a non-linear optimization technique to find the optimum shape and location of mid-ship bulbs. A Ro-Ro ferry hull is used as the baseline hull in this study and the optimization process studied achieved a reduction in total resistance around 10 %, as validated by the experiments. Both the resistance and seakeeping aspects of the concept were studied by Gould et al. (2010) using the same Ro-Ro hull form considered in the previous study. Although the advantages of the beam increment accompanied by the parabolization of waterlines are very obvious in terms of the resistance, it is not clear enough at this point to set an order of merit depending on seakeeping experiments, because the differences in seakeeping characteristics of the hulls in consideration remain within experimental error particularly for added resistance among the waves.

3. Computational study

Beam increasing design study basically requires 3 computational tools: i) a potential flow solver for calculating wave resistance characteristics, ii) a boundary layer flow solver or a viscous flow solver to check form factor variation, iii) a mathematical programming routine to determine the optimal position of the maximum beam increment.

3.1. Potential flow solver for wave resistance

In order to determine the wave resistance characteristics – such as wave resistance itself, wave elevations, dynamic trim and sinkage, pressure distribution on the wetted hull surface – a flow solver which is based on Dawson's (1977) algorithm is used. According to the present code, ITU-Dawson, the Rankine source distribution is made over the panels which represent the wetted surface area (WSA) of the ship hull under the loaded waterline (LWL) as well as on a portion of the free surface around the hull.

Impermeability condition is applied at the WSA of the ship. The free surface condition proposed by Dawson, quadratic in double-model potential and linear in perturbation potential, is imposed on the discretized free surface around the ship. The differentiation of the velocities in the free surface condition along the streamlines is performed by Dawson's 4-point backward differentiation scheme which numerically satisfies radiation condition within the free surface area around the ship. Wave resistance is then calculated by means of pressure integration over the WSA in the present study.

a. Boundary layer flow solver to check form factor variation

It is recommended that it is necessary to examine the viscous resistance of the parent and improved hulls to determine if there are form drag penalties due to the addition of a mid-ship bulb or due to an increase in the beam. Integral Boundary Layer (IBL) solvers are available and are more versatile in obtaining form factors as compared to the viscous (RANS) solvers. A commercially available IBL solver is used in the present design studies. RANS and IBL solvers predicted lower frictional drag than the ITTC correlation line and both solvers predicted approximately 1% increase in frictional resistance coefficient for the parabolized hull, (Calisal et al., 2009). This is an expected result caused by the growth of boundary layer thickness due to an increase in the fullness of the parabolized hull.

b. Mathematical programming routine

In the present approach, wave resistance is taken as the objective function. An unfavorable increase in the form drag is treated as a penalty in the optimization procedure. There are many general-purpose, gradient-based packages available to solve this shape optimization problem for minimum wave resistance. As for the geometric modeling; a rectangular patch is defined on the wetted surface of the hull on which the optimal position of the maximum beam increment is searched, (Calisal et al., 2009). Indeed, geometric modeling requires intricate work and in some cases a systematic search might be preferred to figure out the favorable position of the amidships bulb or of the position of maximum beam increment on the hull. Recently, an attempt by Gören et al. was made on determining the optimal shape of the design waterline by allowing an increase in the beam of ship based on mathematical programming.

4. Additional work

The present paper aims to show that the present concept is not a hull form-dependent approach. Thus, one cross-channel passenger ferry, one heavy-lifter container ship and a Ro-Ro ferry hull forms are additionally studied within the frame of the present concept for this purpose and the results are presented in the following. The possibility of a beam increase by a retrofit and the cost analysis was also discussed in the following chapters.

4.1. Passenger ferry (PF)

First, the PF is taken into account (due to a project given by Istanbul Deniz Otobüsleri (IDO)), which is a cross-channel passenger ferry employed in the public marine transportation by IDO in Istanbul, (see Fig. 1 and Table 1 for cross-sections and main particulars, respectively). Despite the fact that the PF hull form has not a parallel middle-body, a beam increment is studied by the potential flow solver for

minimum wave resistance by systematic search under the given design constraints. It is understood from the wave resistance analysis that about 5 % increment made to the beam (see Figure 2) acts like a (mid-ship) bulb and results in nearly 25 % reduction in wave resistance, Figure 3. This is confirmed by tow-tank experiments which point out around 12 % effective power reduction at the service speed of 15 kn, Fig. 4.

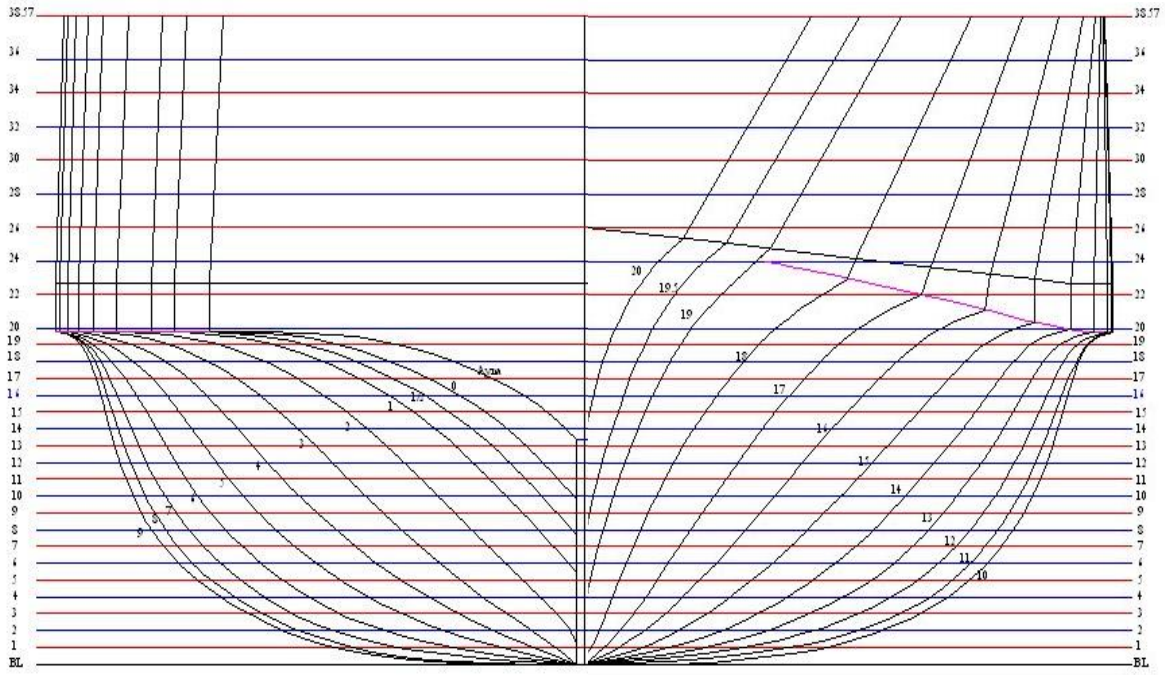

Figure 1. PF cross-sections.

Table 1. Main particulars of PF

Length between perp.	L_{BP} (m)	52.80
Length on waterline	L_{WL} (m)	55.02
Beam	B (m)	10.94
Draught (midship)	T (m)	2.35
Draught (AP)	T_A (m)	2.60
Draught (FP)	T_F (m)	2.10
Displacement Volume	∇ (m^3)	603.17
Service Speed	V (knot)	15

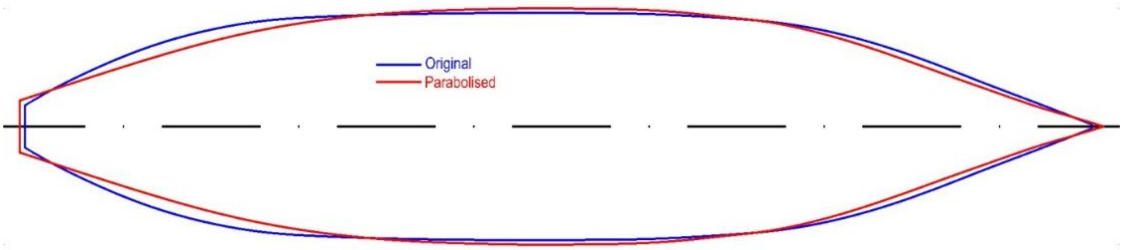

Figure 2. Beam increment at the loaded waterline.

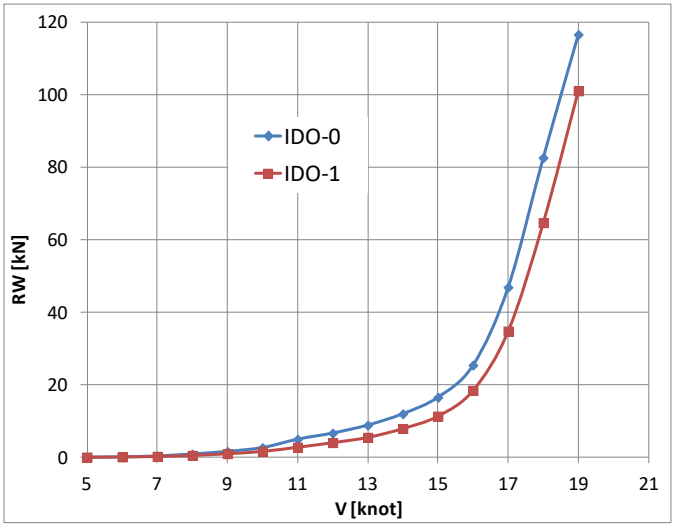

Figure 3. Computed wave resistances (Rw) for original (IDO-0) and for optimized (IDO-1) hulls.

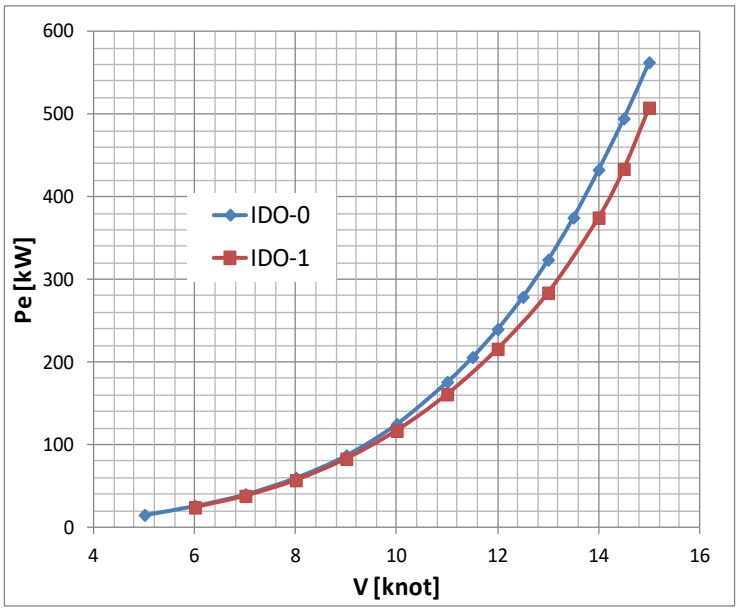

Figure 4. Experimental results for effective powers of the hulls.

4.2. Heavy-Lifter containership (HLC)

The owner and his designer of this HLC is faced with a stability problem due to the heavy gears which are to be installed on the deck of the ship. Thus, the problem turns out to be an ideal application of the present concept, since the owner/designer would like to resolve the stability problem by increasing the beam while not having a penalty from the resistance. Meantime, a new bulbous bow optimization is performed in addition to the beam increasing study. The potential flow solver for wave resistance and the boundary layer flow solver to figure out the change in the form factor are employed in the present hull form improvement study. The improved hull form – with a 6 % increase in the beam and a slight decrease in parallel midbody which allows the smoothing of the shoulders – as compared to the initial hull form is given in cross-sections in Fig. 5. The beam increment shows its effect after 13.5 knots (F_n = 0.26) which additionally reduces the wave resistance 12 % (at the design speed of 14.5 kn) as compared to the hull form with the new bulb design, Fig. 6. The effect of the beam increment accompanied by the smoothing of the shoulders can also be observed in Fig. 7 by comparing the wave elevations around the hull. It should be noted here that considerable percentage of the gain in wave resistance due to the increased beam is lost by a slight increase in wetted surface area and in turn by the frictional resistance and by a slight increase in the form factor as computational studies point out. But there is still a small amount of gain around 2 % in total resistance, according to the computational analysis, due to the increased beam with smoothed shoulders together with other advantages such as considerable gains in stability and in payload capacity.

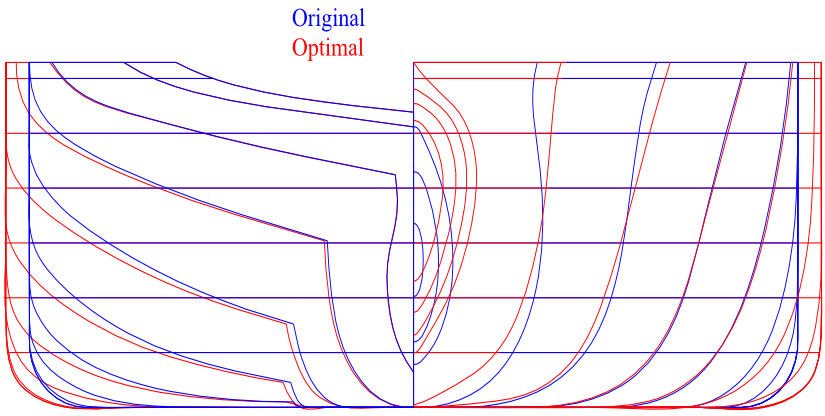

Figure 5. Cross-sections of the original (blue) and the widened/optimal (red) hulls.

4.3.BC Ro-Ro ferry

The present work on British Columbia's Ro-Ro hull is a continuation of the previous work of Calisal et al. (2009). Both the potential flow solver and the viscous flow solver is utilized in connection with the Sequential Programming algorithm to optimize the position and geometry of the side bulb. The original form and the improved form obtained by increasing the beam can be compared in Fig. 8. Table 2 gives the main particulars of both forms for comparison. Note that as a design requirement the displacement is kept constant for the fixed draft. Comparison of the free surface wave deformations caused by the parent and by the optimized (with amidships bulb) hulls given in Fig. 9 pinpoints the relative

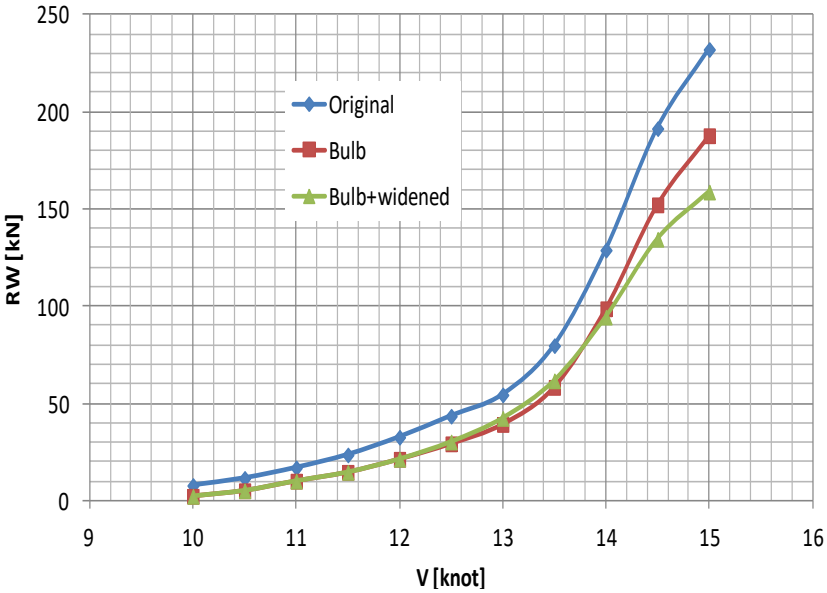

Figure 6. Computational wave resistances of the original and of the improved hulls.

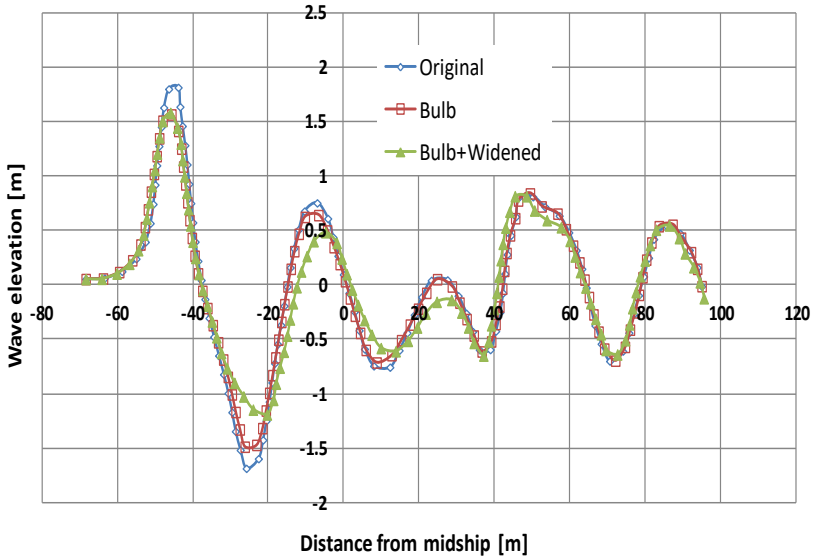

Figure 7. Wave elevations around the hull (V = 14.5 kn).

resistance reduction performance of the improved (optimized) hull with a mid-ship bulb. In Fig. 10, one can observe the wave resistance reduction capacity of the optimized hull (with mid-ship bulb) which is able to reduce the wave resistance (coefficient) by 18 % according to the computational results and by 20 % according to the experimental results. Computed form factors, (1+k), for the parent hull and for the optimized hull are found to be 1.305 and 1.290 (at Reynolds number of 5.35×10^6), respectively. Form factors obtained from the experiments are 1.28 and 1.24 for the parent and for the optimized hulls, respectively. The decrease in the form factor may be attributed to the finer entrance and run of the optimized hull to keep the displacement constant despite an increase in the beam. Thus the resultant reduction in total resistance according to the experimental analysis at Fr = 0. 33 is about 11%.

A recent study of Gören et al., which aims to base the present design concept fully on mathematical

programming, shows computationally and experimentally that the methodology presented is capable of obtaining very favourable wave resistance characteristics. In this respect, Fig. 11 comperatively pinpoints the drastic cancellation of the wave system accomplished by the optimal hull which comprises a beam increment determined by mathematical programming.

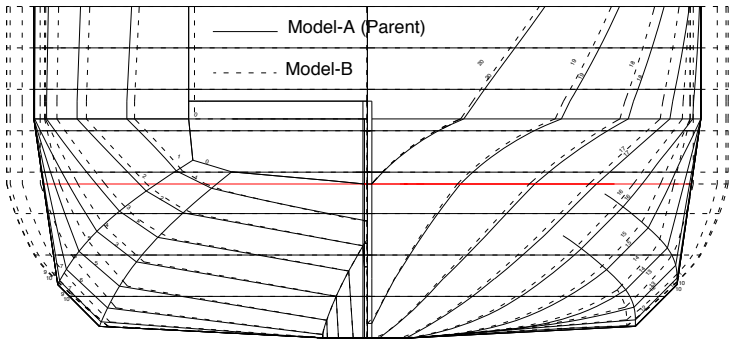

Figure 8. The parent form (Model-A) and the improved (widened) form (Model-B).

Table 2. Main particulars of the forms.

	Form (M318-A)	Optimized Form (M318-B)
L_{WL} (m)	38.75	38.75
B (m)	10.886	12.116
T (m)	2.6	2.6
WSA (m^2)	450.29	437.108
Displacement (ton)	679	679
C_B	0.602	0.534
C_P	0.659	0.626

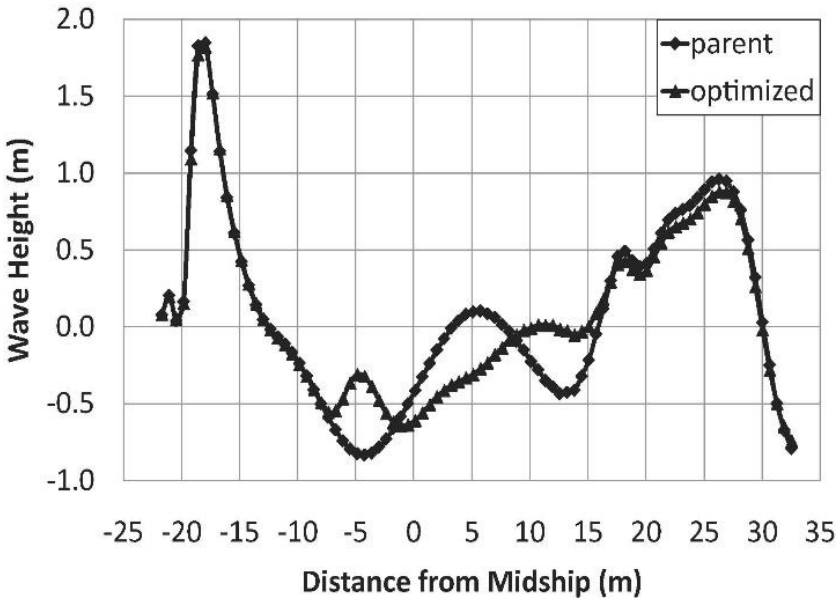

Figure 9. Comparative wave deformations around the hulls (V=13kn).

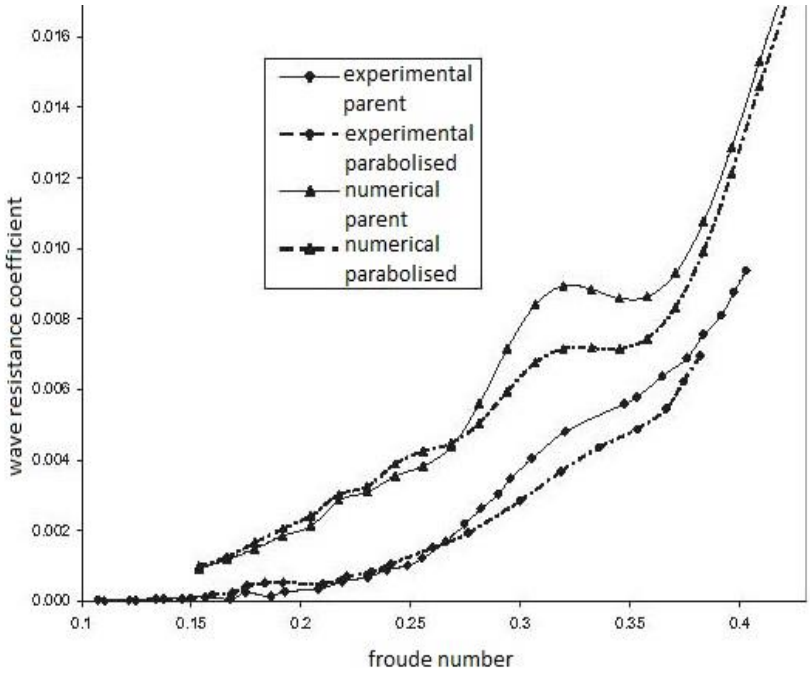

Figure 10. Computational and experimental coefficients of wave resistance for the both parent and parabolised hull forms

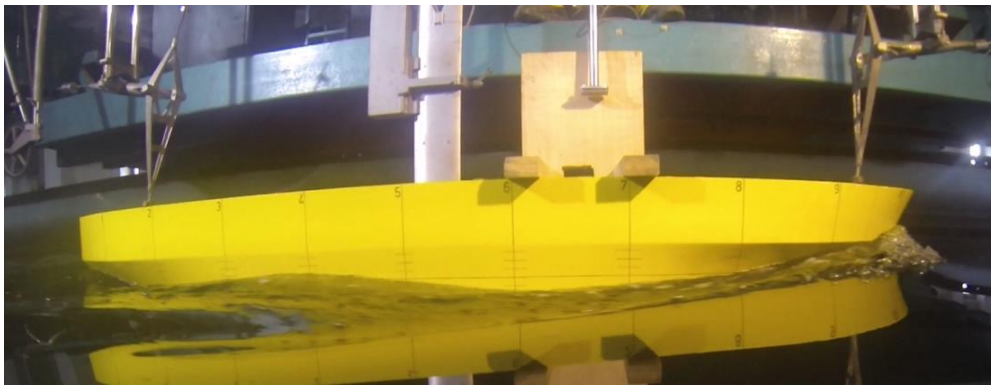

(a)

(b)

Figure 11. Wave elevation around the periphery of the original form (a) and of the optimized form (b) at Fr = 0.33 (BC Ferry Hull), Gören et al.

5. Additional construction cost of beam increase by a retrofit

The above given studies and calculations proved that it is possible to reduce the resistance up to 10% and sometimes more than 10 % by the beam increase. Such a considerable amount of saving may pave the way to apply beam increase on a working ship hull. Deli et al. (2016) studied a platform support vessel and obtained around 6 % reduction in the total resistance. They also conduct a cost analysis for a retrofit application. For PODAC (Product Oriented Design and Construction) cost modelling used in the preliminary design, the price of the total ship is taken as a function of displacement, speed and a complexity factor. A complexity factor is necessary to normalize the data and achieve better equations, because the cost data available to the IPT (Insurance Premium Tax) changes as the ship type changes. For the complexity factor, the IPT used is derived from a Size Factor and Ship Type Factor (STF) (see; Ennis et al., 1997).

For the platform supply vessel in consideration, the values of an oceangoing naval tug are taken into account and accordingly ship type factor is taken as 1.00. Fig. 12 shows the savings data for 60 months of the time period with different ship type factors.

Figure 12. The savings data for 60 months of time period with different ship type factors (Deli et al., 2016).

6. Conclusion and discussion

It has been shown that the systematic application of the waterline parabolization concept, in which the parallel middle-body of the vessel is expanded outward with locally parabolic waterlines, is able to reduce the wave resistance of displacement type ships at moderate Froude numbers. The promising capacity of this concept or of the "increased beam" or the side bulb in reducing effective power requirements for small craft at moderate and relatively higher speeds was proposed in Calisal et al. (2009). This paper provides evidence of the existing potential in reducing the fuel consumption of a large class of ships such as fishing vessels, yachts, ferry boats, container ships, etc. The numerical and experimental evidence given in this paper suggests that the parabolization concept can be applied successfully, as a retrofit or in original designs for significant fuel savings for different types of ships. During the application of the concept, the main focus of attention was the wave resistance first. Subsequently, attention was also directed to the changes in form factor for viscous resistance, to the impact of parabolization on seakeeping, added resistance, etc. The attempt in here is to share the design experience and experimental evidence collected at the Istanbul Technical University and the University of British Columbia to design more fuel efficient ships and to encourage the application of the concept.

During the course of the studies of the present concept, the authors also took into account the two issues. One of them is the question of how the beam increments affect the viscous resistance and in particular form resistance. For the cases reported in this paper or studied by the authors, no major increase in the viscous resistance was observed.

The second concern was on the possible increase in the construction cost of the ship frames for parabolized hulls. Of course, with the inclusion of parallel middle body there exists substantial savings in

the construction cost of the frames and plates. A recent case study by Deli et al. (2016) on a platform supply vessel showed that the extra investment for an increase in the beam covers itself within shorter than 9 to 16 months of operation at the given conditions which is very reasonable.

The general hull form optimization methods usually suggested that the beam of the ship was to be kept constant or less than a maximum value as the expectation was that the ship-wave resistance was to increase with the square of the beam value. The experience gained and published earlier by the authors suggest that, in the formulation of the hull form optimization the beam of the ship should be a free variable within the concept of parabolization as described above. This new formulation is expected to provide hull forms with less fuel consumption or lower energy efficiency design indices EEDI of IMO.

Acknowledgements

The major portion of the reported experimental work was done in Ata Nutku Ship Model Testing Laboratory at Istanbul Technical University. Thanks are due to the staff and members of this organization who carefully built and modified the ship models and tested them with care.

References

Calisal, S.M., Vyselaar, D., Klaptocz, V. and Goren, O. (2009). “A resistance reduction study of a trimaran using waterline parabolization”, Marine Technology, Vol. 46, No. 2, 91-98.

Calisal S., Tan, J., Sireli, M. and Goren. O. (2009). “A systematic investigation of ship resistance reduction by beam increment for small craft”, The Journal of Ocean Technology, Vol. 4, No 3, 57-72.

Calisal, S.M., Danisman, D.B., Goren, O., Gould, K., Maurice, P. and Klaptocz, V. (2009). “Reduction of wave resistance of displacement vessels by waterline parabolization”, SNAME Annual Meeting, Providence, Paper No. 2009-053.

Calisal, S.M., Goren, O. and Danisman, D.B. (2002). “Resistance reduction by increased beam for displacement-type ships”, Journal of Ship Research, Vol. 46, No. 3, 208-213.

Dawson, C.W. (1977). “A practical computer method for solving ship-wave problems”, Proceedings, 2nd Int. Conf. on Numerical Ship Hydrodynamics, Berkeley, 30-38.

Deli, O., Goren, O., Calisal, S. (2016). “Parabolization and Structural Integrity of Side Bulb Applied Platform Supply Vessel Hull Form”, Proceedings of PRADS2016, 4th – 8th September, Copenhagen, Denmark.

Ennis, K. J., Dougherty, J. J., Lamb, T., Greenwell, C. R., Zimmermann, R. (1997). “Product-Oriented Design and Construction Cost Model”, SNAME Ship Production Symposium, April 21-23, New Orleans, Louisiana.

Goren, O., Calisal, S.M. and Danisman, D.B. “Mathematical programming basis for ship resistance reduction through the optimization of design waterline”, submitted for publication to the Journal of MS&T.

Gotman, A. (1998). “The comparative criterion in deciding on the ship hull form with least wave resistance”, Proceedings, Colloquium EUROMECH 374, Poitiers, 277-284.

Gould, K., Calisal, S.M., Mikkelsen, J., Goren, O., Okan, B. and Kim, Y-T. (2010). “Powering and seakeeping

characteristics of a displacement hull form with waterline parabolization", Proceedings, ASME 29th Int. Conf. on Ocean & Arctic Eng. (OMAE), Shangai, Paper No. 2010-20951.

Kent, J.L. (1919). "Model experiments on the effect of the beam on the resistance of mercantile ship forms", Transactions, Institute of Naval Architects, Vol. LXI, 311-319.

Weinblum, G.P. (1950). "Analysis of wave resistance", Davit W. Taylor Model Basin, TMB Report 710, Washington, 27.

Wehausen, J.V., Reichtert,G. and Gauthey, J.R. (1961). "On the resistance of ships", Institute of Engineering Research Series, Series 82, Issue #21, iii+55.

Wehausen, J.V. and Laitone, E.V. (1960). "Surface Waves", Handbuch der Physik, W. Flugge, (Ed.), Vol. 9, SpringerVerlag, Berlin, 446-778.

NOT: